CHARACTERIZATION AND MODIFICATION OF GENETICALLY ENCODED INDICATORS TO MONITOR NEURAL ACTIVITY IN *DROSOPHILA MELANOGASTER*

Dissertation

zur Erlangung des Doktorgrades der Naturwissenschaften

an der Fakultät für Biologie
der Ludwig-Maximilians-Universität München

Alexandra Ihring

München, 2006

Erstgutachter: Prof. Dr. Alexander Borst

Zweitgutachter: Prof. Dr. Rainer Uhl

Tag der mündlichen Prüfung: 18.Juli 2006

Table of Contents

Table of Figures

Abbreviations

A	adenine
aa	aminoacid
AM	acetoxymethyl
AMPA	α-amino-3-hydroxy-5-methyl-4-isoxazole propionic acid
BBS	BES-buffered saline
BES	N,N-bis[2-hydroxyethyl]-2-aminoethanesulfonic acid
BFP	blue mutant of GFP
BSA	bovine serum albumin
C	cytosine
CaM	calmodulin
Camg	Camgaroo
CCD	charge-coupled device
CFP	cyan fluorescent protein
CLSM	confocal laser scanning microscopy
CNS	central nervous system
DMSO	dimethyl sulfoxide
DNA	deoxyribonucleic acid
DsRed	red fluorescent protein from Discosoma sp.
EDTA	ethylenediamine tetraacetic acid
EGFP	"enhanced" version of GFP
EGTA	ethylene glycol-bis[β-amino-ethyl ether] N,N,N',N'-tetraacetic acid
ER	endoplasmatic reticulum
F	fluorescence light intensity
FCS	fetal calf serum
FRET	fluorescence resonance energy transfer
G	guanine
Gal	galactose
GFP	green fluorescent protein
HBSS	Hanks' balanced salt solution
HEPES	N-(2-hydroxyethyl)piperazine-N'-(2-ethanesulfonic acid)

IP	Inverse Pericam
kb	kilo base pair
K_d	dissociation constant
koff	dissociation rate constant
kon	association rate constant
mRNA	messenger RNA
ms	millisecond
NGS	normal goat serum
NMJ	neuromuscular junction
OD	optical density
PBS	phosphate-buffered saline
PBT	phosphate-buffered saline with Triton X-100
PCR	polymerase chain reaction
PFA	paraformaldehyde
R	ratio; fluorescence intensity of acceptor emission over donor emission
Rmax	ratio R at highest ligand concentration
Rmin	ratio R in ligand-free conditions
s	second
SEM	Standard error of mean
SNR	Signal-to-Noise-Ratio
SpH	Synaptophluorin
τ	time constant
T	thymine
TAE	tris-acetate-EDTA electrophoresis buffer
TE	tris-EDTA buffer
Tn	troponin
UAS	upstream activating sequence
WT	wildtype
YC	Yellow Cameleon
YFP	yellow fluorescent protein
$\Delta F/F$	fractional change in fluorescent light intensity
$\Delta R/R$	relative changes in the fluorescence ratio

X

1 Abstract

Genetically encoded fluorescent indicators of neural activity represent promising tools for systems neuroscience. In the first part of my thesis, a comparative *in vivo* analysis of ten different genetically encoded calcium indicators as well as the pH-sensitive SynaptopHluorin is presented. The calcium indicators are either based on a single chromophore (GCaMP variants, Camgaroo variants, Pericam variants) or on two chromophores (Yellow Cameleon variants, Troponeon variants). I expressed these indicators in the cytosol of presynaptic boutons of the *Drosophila* larval neuromuscular junction and analyzed their fluorescence changes upon stimulation. GCaMP 1.3, GCaMP 1.6, Yellow Cameleon 2.0, 2.3, and 3.3, Inverse-Pericam, the troponin C-based calcium sensor TNL 15 and SynaptopHluorin allowed reliable detection of presynaptic fluorescence changes at the level of individual boutons. However, the response characteristics of all of these indicators differed considerably from each other. TNL 15 exhibited the most stable and fastest rising signals at lower activity rates, whereas GCaMP 1.6 produced the fastest signals at high rates of nerve activity with largest fluorescence changes. GCaMP 1.6 and GCaMP 1.3 signals, however, were complicated by bleaching, as was the case for Inverse Pericam. The fluorescence signals of the double-chromophore indicators were in general smaller but more photostable and reproducible. Camgaroo-1 and Camgaroo-2 showed little or no response, and Flash Pericam did not result in any detectable fluorescence. GCaMP 1.3 and YC 3.3 revealed fairly linear fluorescence changes and a corresponding linear increase in the signal-to-noise ratio (SNR) over an expanded range of neural activity. As expected, the expression level of the indicator had an influence on the signal kinetics and the SNR, whereas the signal amplitude was independent.

In the second part of my thesis work I fused several genetically encoded calcium indicators to different signal sequences. The targeting of the indicators to distinct parts of the cell such as the membrane, vesicles or ion channels allows detection of calcium ions before they disperse in the cytosol. Specific signals can be extracted more efficiently and in a more relevant physiological context. Tagging of YC 2.3, GCaMP 1.6 and TNL 15 to transmembrane domains or proteins involved in the synaptic vesicle cycle did not result in functional targeting. TN XL fused to the transmembrane

domain mCD8 at the N-terminus and eight amino acids from a calcium channel subunit at the C-terminus resulted in membrane association at the NMJ. Fractional fluorescence changes up to 6.5 % were recorded upon stimulation. In cells of the fly visual system scattered fluorescent puncta were observed. This fusion protein has the potential for monitoring calcium dynamics in close proximity of ion influx.

The presented data will be useful for *in vivo* experiments with respect to the selection of an appropriate indicator, as well as for the correct interpretation of optical signals.

2 Introduction

2.1 General

Studies in neurobiology often rely on recordings of neural membrane potential by means of intracellular and extracellular electrodes. Despite its unmatched directness and temporal resolution, this method offers limited spatial resolution and introduces a bias toward larger neurons. These disadvantages were overcome with the implementation of synthetic optical probes for neural activity reporting membrane potential (Cohen et al., 1978) or intracellular calcium (Grynkiewicz et al., 1985). When applied by intracellular injection or as membrane permeable AM-ester (Stosiek et al., 2003), a spatially resolved recording of neuronal activity in single cells (Borst and Egelhaaf, 1992; Tank et al., 1988; Svoboda et al., 1997) or in multiple neurons simultaneously can be achieved. The use of synthetic dyes is invasive, however, and does not allow for targeting to specific neuronal populations. Genetically encoded indicators based on the green fluorescent protein (GFP) (Miyawaki et al., 1997; Persechini et al., 1997; Romoser et al., 1997) offer a solution to this problem (see 2.4). Formed from amino acids, they can bypass the limitations of synthetic dye application by biosynthesis *in situ*. This provides some advantages compared to synthetic dyes. On the one hand organic dyes have to be loaded into cells by bath application or direct injection. Genetically encoded indicators instead can be expressed in cells or tissues of choice and the protein remains there for the time of imaging procedures. Another disadvantage of synthetic dyes is that it is difficult to design indicators for more complex ligands like nucleotides and peptides. However, indicators based on proteins can be modified genetically to respond to more complex processes in the cell such as phosphorylation and enzyme activation.

A promising feature of genetically determined molecules is their ability to be targeted to distinct parts of a cell by molecular construction of fusion proteins without loss of Ca^{2+}-dependent fluorescence changes. As mechanisms of Ca^{2+}-dependence and fluorescence emission vary between different genetic indicator molecules we work on different targeting strategies and on different indicator molecules. Targeting them close to ion channels, for example, would allow detection of ions before they dilute and disperse in the intracellular space. In small microdomains close to channels ion

concentrations are high and can be detected by indicators that have a K_d in a micromolar range. As they can be targeted for example to pre- or postsynaptic structures in neurons, i.e. ion channels subunits or vesicle proteins, they might be able to constitute a link to functional anatomy and cellular organization.

In general the approach of using genetically encoded indicators offers the possibility of uncovering the identity and relationships of neurons. Due to the small size of some neurons, they have escaped almost completely from physiological analysis so far. The possibility to specifically direct the expression of genetic indicators to the entire nervous system, cell populations and even single-cell clones offers huge potential to identify elements that are involved in neural processes.

The establishment of specific expression techniques is one important demand for these experiments (Brand and Perrimon, 1993; Lee and O'Dowd, 1999; Wong et al., 2002). Directed expression in functional classes of neurons can be achieved by fusion of genetic probes to distinct promoters (Hasan et al., 2004). Other approaches use the GAL4-UAS system in *Drosophila* that allows gene expression in specific tissues (Brand and Perrimon, 1993) (see 2.6). Different techniques have been applied to tag them to subcellular compartments (Miyawaki et al., 1997; Heim and Griesbeck, 2004; Guerrero et al., 2005).

Only a few indicators have been applied to neurons of living animals in a limited number of preparations: *Caenorhabditis elegans* (Kerr et al., 2000; Shyn et al., 2003; Kimura et al., 2004), *Drosophila* (Fiala et al., 2002; Reiff et al., 2002; Liu et al., 2003; Wang et al., 2003; Yu et al., 2003; Wang et al., 2004), and zebrafish (Higashijima et al., 2003). Direct comparison of the indicator properties was not possible so far as they were used in different animals and cell types. Many of the presently available indicators have not been used *in vivo* at all. Only recently, three different indicators were tested in mice and fish (Hasan et al., 2004) and analyzed in transfected mammalian brain slices (Pologruto et al., 2004). This emphasizes the need to analyze the fluorescence properties of the various indicators *in vivo* under reproducible and well controlled conditions (see 2.7.1).

To characterize different genetic indicators and their derivative fusion molecules the *Drosophila melanogaster* NMJ can be used as a test system. The known physiology and easy accessibility for optical and electrical recordings makes this preparation an

ideal model system to study potential physiological effects and indicator performance in an *in vivo* situation (see 2.7.1).

2.2 Green Fluorescencent Protein

A tremendous milestone for the field of fluorescent imaging was the discovery of the green fluorescent protein (GFP) from the Pacific Northwest jellyfish *Aequoria victoria* in 1962 by Shimomura and his colleagues when they were characterizing aequorin, a luminescent protein from the same jellyfish (Shimomura et al., 1962).

It was the first and is now the best-known of all fluorescent proteins. Its structure was solved in 1996 by Yang et al. (1996) and Ormo et al. (1996). It consists of a β-barrel and has the shape of a cylinder. The diameter is about 25 Å and the length about 40 Å. The name "β-barrel" comes from the eleven β-sheets that form the body of the cylinder. In the middle of the cylinder, there is an α-helix that forms the scaffold containing the chromophore. The chromophore consists of two aromatic rings and derives from a Serine-Tyrosine-Glycine sequence that undergoes several biochemical postprocessing steps in wildtype GFP (Figure 1, yellow structure).
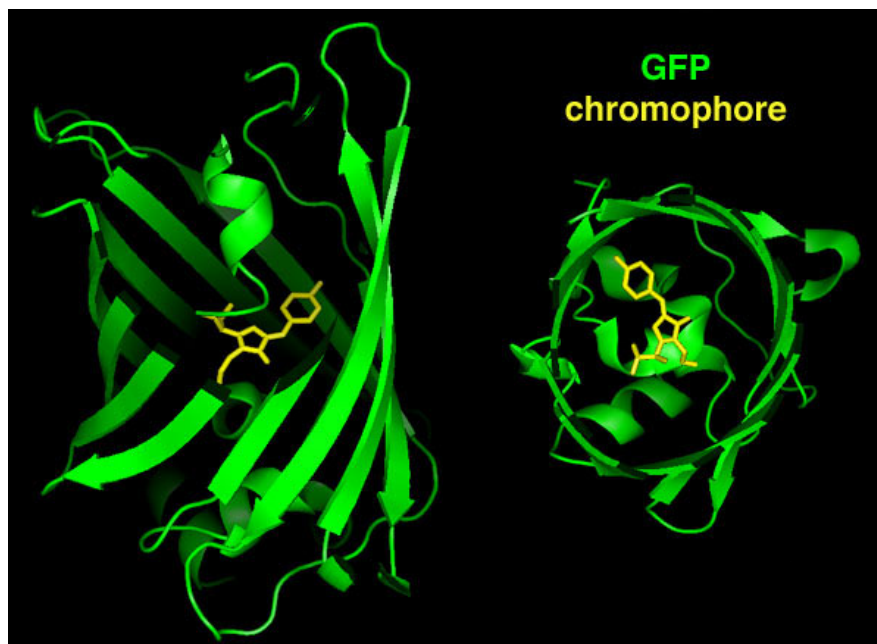
Figure 1: Crystal structure of GFP with a Ser-Tyr-Gly sequence forming the chromophore. Side view (left) and top view (right) of the β-barrel. Some amino acids were deleted to allow a better view on the fluorophore (yellow). Picture from http://www.mekentosj.com/science/fret/gfp.html.

Since the chromophore formation proceeds in an autocatalytic manner without external cofactors, GFP is an ideal tool for intracellular applications. This feature is rarely observed in other protein species.

The wildtype GFP sequence has been mutated to improve its physical properties (Tsien, 1998). Different mutations in and around the chromophore lead to shifts in excitation and emission spectra. Several GFP variants, such as cyan fluorescent protein (CFP), yellow fluorescent protein (YFP), blue fluorescent protein (BFP) and Sapphire, a UV-excitable GFP variant, derive from these mutations.

Other mutations were made to deal with problems such as pH and Cl^- sensitivity, low photostability, low expression levels and slow folding. Two mutated fluorescent proteins that show several improvements can be highlighted: the enhanced variant of CFP (ECFP) (Heim and Tsien, 1996) and Citrine, a protein variant from YFP (Griesbeck et al., 2001).

Fluorescent proteins do not only originate from *Aequoria victoria*. Others were found in Anthozoan species, for example Cop-Green from *Copepoda* and Phi-Yellow from *Hydrozoa* (Shagin et al., 2004). However, all these proteins suffer from the same problems as early GFPs: they are not very bright, fold poorly at 37 °C and tend to form dimers and tetramers which makes them unsuitable for sensing protein-protein interactions and trafficking. Amongst them, the best-known protein is DsRed from a *Discosoma* coral which emits red light and is therefore an important complement to the blue, green and yellow emitting *Aequoria* proteins (Matz et al., 1999). This tetrameric protein has already been turned into monomeric forms. The protein's brightness is much higher, it is more stable and it does not form complexes with other fluorescent proteins (Shaner et al., 2004).

These fluorescent proteins have been expressed as functional transgenes in a variety of living species, such as bacteria, yeast, plants, *Drosophila*, zebrafish and mammals. They have enormous potential as tools for visualization of cellular dynamics, developmental processes and molecular activity (Amsterdam et al., 1995; Chalfie et al., 1994; Prasher, 1995; Yeh et al., 1995).

As stressed before an important advantage of fluorescent proteins is that they can be used as non-invasive markers in living cells as they do not have to be injected. It has already been reported in many studies that fusion of GFP to a protein, for example, does not disturb the protein's activity (Estes et al., 2000). GFP can be therefore used

to monitor protein localization, gene expression or protein-protein interactions (Lippincott-Schwartz and Patterson, 2003).

2.3 Fluorescence and FRET

Fluorescence microscopy allows the detection of even low levels of emitted light that originates from fluorescent probes like synthetic fluorescent dyes or expressed fluorescent proteins.

Fluorescence is a three-stage process. The Jablonski diagram displays the electronic states that lead to fluorescence (Figure 2). The first stage is called excitation. A photon of energy hv_A is supplied by an external light source like a lamp or a laser. The fluorescent molecule is converted from the ground state S0 to an excited singlet state S1 by absorbing a photon of a specific wavelength. The excited-state lifetime, that is the average time between its excitation and the return to the ground state, has a duration of 1–10 nanoseconds. In the second stage, the fluorophore undergoes conformational changes and can interact with its molecular environment. The excited fluorophore relaxes to the lowest energy level of the excited state during which the subsequent fluorescence emission emerges.

The fluorescence quantum yield, which is the ratio of the number of fluorescence photons emitted to the number of photons absorbed during excitation, represents the amount of radiative and non-radiative decay. In a last stage, the fluorophore returns to its ground state S0 by emission of a photon of energy hv_{em}.

As the energy of the emitted photon is lower than that of the excitation photon, hv_{em} emission occurs at a longer wavelength than excitation. The difference in energy or $hv_{ex} - hv_{em}$ is called Stokes' shift. The Stokes' shift allows emission photons to be detected at another wavelength than excitation photons.

But not all electrons that were initially excited return to the ground state S0 by fluorescence emission. Non-radiative decay can occur as well: internal conversion (IC), intersystem crossing (ISC) and vibrational relaxation. Examples of the first two can be seen in the diagram (Figure 2). Internal conversion is the radiationless transition between energy states of the same spin state. Intersystem crossing is a radiationless transition between different spin states. Vibrational relaxation, the most common of the three-for most molecules, occurs very quickly ($<1 \times 10^{-12}$ seconds)

and is enhanced by physical contact of an excited molecule with other particles. Energy, in the form of vibrations and rotations, can be transferred through collisions.
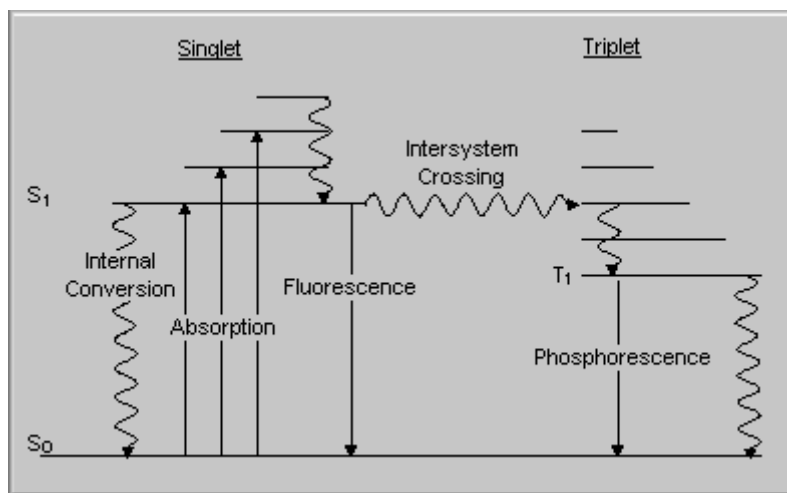
Figure 2: Jablonski diagram of the three main stages of fluorescence. The fluorescent molecule is converted from the ground state S0 to an excited singlet state by absorbing energy. By releasing some of the absorbed energy the molecule goes to a more relaxed singlet state, S1. In a third step the molecule will return to its ground energy state by releasing the remaining energy.

One problem that appears in fluorescence microscopy is photobleaching. It is the irreversible destruction of the excited fluorophore with high-intensity illumination. The rate of bleaching depends on the photolability of the fluorophore and is enhanced by the presence of reactive molecules like oxygen.

The environmental sensitivity of the fluorophore is another problem occurring in fluorescence microscopy. Intensity of fluorescence can be decreased by different quenching processes caused by either fluorophore-fluorophore interactions or between fluorophore and other molecules in the environment. This environmental sensitivity of fluorescent dyes can be a useful characteristic when dyes are used as reporters of environmental changes such as pH or ion concentration.

The advantage of ratiometric measurements is the reduction of data distortions caused by sample motion artefacts, instrumental failures and other external factors. Ratioing therefore leads to a more stable signal output (Figure 3) (Helmchen, 2000).
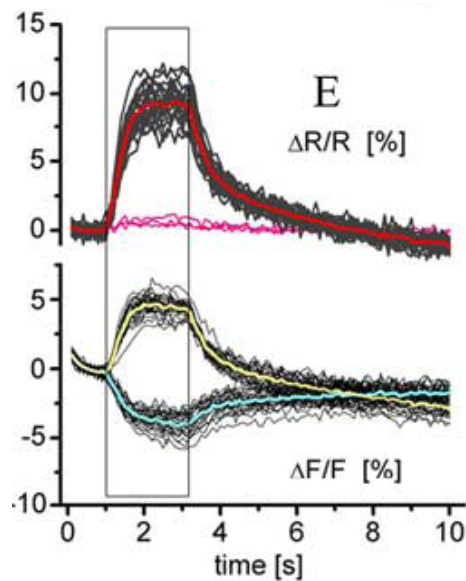
Figure 3: Benefits of dual-wavelength ratiometric measurements of a fluorescent probe. Even though the two emission intensities decrease over time due to internal and external factors such as bleaching and quenching (lower part of the figure), the ratioed signal of acceptor intensity/donor intensity in the upper part of the figure remains stable before and after stimulation (box). Thin black traces represent signals from individual boutons, and mean ΔF/F calculated for CFP and YFP is plotted in cyan and yellow, respectively. The mean ΔR/R is shown in red. Signals from background regions are represented by pink traces. Figure from Reiff et al. (2005).

One phenomenon that is used by one type of fluorescent dyes is termed 'fluorescence resonance energy transfer' (FRET). It is a quantum-mechanical transfer of energy from the excited state of the donor fluorophore to the ground state of a neighboring (fluorescent or non-fluorescent) acceptor molecule, without emission of a photon. Important for FRET is the overlap of the absorption spectrum of the acceptor and the fluorescence emission spectrum of the donor. As FRET is dependent on distance and orientation, the two molecules must be in close proximity to each other (around 50 Å) (Patterson et al., 2000).

One application that harnessed FRET is the design of genetically encoded ratiometric indicators (Figure 4). They change their FRET efficiency in response to biochemical signals. A linker that attaches both GFP variants undergoes a conformational change upon binding a specific ligand. This change alters the distance and the orientation of the two fluorophores relative to each other and leads to a change in FRET. When FRET occurs, the donor transfers some energy to the acceptor molecule. The acceptor in turn emits the transferred energy with its fluorescence at higher wavelength. Thus intensity changes can be detected both in the donor and the acceptor emission.

9
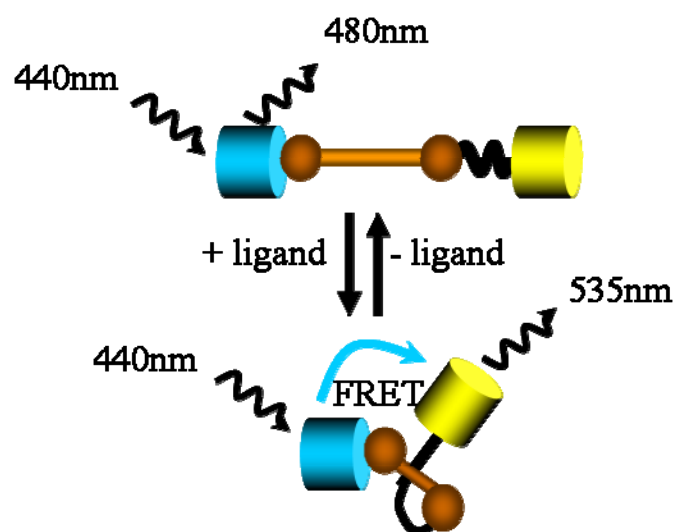
Figure 4: Schematic representation of FRET occurring in a ratiometric indicator consisting of two fluorescent proteins with a ligand binding linker protein in between. Ligand binding to the linker peptide leads to a conformational change in the whole macromolecule, thereby enhancing the fluorescence resonance energy transfer (FRET) from the donor to the acceptor. The illumination wavelength is chosen so as to excite only the donor, and the ensuing donor and acceptor emissions are monitored at their respective wavelengths.

Fluorescent dyes can be used not only as visible markers, but turned into very sensitive and selective reporters to a variety of specific stimuli. The use of these indicators allows the examination of cellular dynamics, analysis of processing elements and investigation of organizations of networks in real-time imaging experiments.

2.4 Genetically Encoded Indicators

Different genetically encoded indicators have been designed to report changes in membrane potential, intracellular calcium concentrations, the number of synaptic vesicles released or second messengers such as cAMP or cGMP. Their chromophores consist almost exclusively of GFP variants.

2.4.1 Voltage Sensors

Insertion of GFP after the sixth transmembrane domain of a nonconducting mutant of the Shaker potassium channel of *Drosophila* has led to the generation of a sensor for

voltage changes, called FlaSh (Siegel and Isacoff, 1997). The voltage-driven rearrangement of the channel is converted into a change in fluorescence intensity of GFP. It has slow kinetics (the time constant for decay is higher than 85 ms) and folds poorly at 37 ºC.

In the meantime, FlaSh has been significantly improved by Guerrero and colleagues (Guerrero et al., 2002). They substituted various GFP variants and mutated the channel domain resulting in probes with faster kinetics, improved folding at 37 ºC and an altered dynamic range enabling efficient detection of voltage changes around -60 to -70 mV. To date this construct has been reported to be functional only in oocytes. One explanation is that its subunits could aggregate with endogenous potassium channels that are missing in oocytes and disrupt the function of the channels or the construct itself.

A similar approach has been applied to create another genetically encoded voltage probe using a different channel. The sensor called SPARC (sodium channel protein based activity reporting construct) contains a wild type GFP inserted into an intracellular loop of a reversibly non-conducting form of a voltage-gated sodium channel (Ataka and Pieribone, 2002). In oocytes it can detect depolarizing pulses as short as 2 ms without inactivating during extended depolarizations.

A different approach to develop a voltage sensor uses FRET between cyan and yellow emitting fluorescent proteins (CFP and YFP). The two GFP variants are linked together and fused to the C-terminus of the voltage sensing S4 segment of a K^+ channel (VSFP1, Sakai et al., 2001). Membrane depolarization leads to movement of S4. This structural change alters the angle between the dipole moments of CFP and YFP and leads to a change in the FRET signal. When expressed in human embryonic kidney (HEK293) cells, the YFP signal is changed by 1.5% during a depolarization step between - 80 and - 20 mV, with a time constant of 0.7 ms.

2.4.2 Sensor for Vesicle Release: SynaptopHluorin

The chromophore of a GFP type protein is surrounded by a hydrogen-bond network within the β-barrel. It can become pH-sensitive when this network is affected by external protons. Wild type GFP exhibits pH-insensitive fluorescence. Yellow-emitting variants of Aequorea GFP and their circularly permuted constructs, however, show pH sensitivity. Miesenbock and colleagues developed pH-sensitive mutants of

green fluorescent protein with the aim to utilize the acidic pH inside secretory vesicles to monitor vesicle exocytosis and recycling (SpH, Miesenbock et al., 1998). The chromophore is expressed in the lumen of synaptic vesicles by fusion to the transmembrane domain of synaptobrevin. Fusion of the acidified vesicle to the plasma membrane leads to an exchange of its interior with the extracellular fluid and causes an instantaneous rise of pH from ~ 5 to 7.4. SpH reflects this pH change by a change in its excitation spectrum.

Several *in vivo* studies reported SpH as a reliable indicator of neural activity (Ng et al., 2002; Bozza et al., 2004). SpH positive synapses *in vivo* were fluorescent even under resting conditions. *In vitro*, the main source of baseline fluorescence is a small SpH pool that is constitutively present at the cell surface (Sankaranarayanan and Ryan, 2000); *in vivo*, SpH that appears at the surface as a result of spontaneous synaptic activity may contribute in addition.

2.4.3   Calcium Indicators

Probes responding to changes in intracellular calcium concentration were amongst the first genetically encoded indicators. In 1997 Miyawaki et al. and Romoser et al. designed an indicator based on FRET that consists of two GFP variants linked by a calcium sensitive protein (Miyawaki et al., 1997; Romoser et al., 1997). The construct designed by Miyawaki et al. was called Yellow Cameleon 2.0 and consisted of a BFP and a GFP protein. As the BFP showed poor photo-physical properties, low brightness and an intense sensitivity for photobleaching, this pair was replaced by CFP and YFP. A calmodulin protein was fused in between the two fluorescent proteins as the calcium binding moiety. The calmodulin itself, however, did not induce enough conformational change to get an adequate FRET response. Therefore, the authors fused an additional calmodulin binding domain of myosin light chain kinase (M13) to the C-terminus of the calmodulin to turn this calcium indicator into a functional system. The additional protein should also help to reduce interactions of the calmodulin with different cellular targets by binding it preferentially.

One problem that occurs when dealing with FRET-based ratiometric indicators is that CFP emission and YFP emission spectra overlap and are therefore hard to separate completely, even with narrow bandpass filters (Figure 5). As CFP emission has a

broad emission range it shows up in the YFP emission channel. FRET probes with a larger Stokes' shift could eliminate these drawbacks by further separating the emission wavelengths.
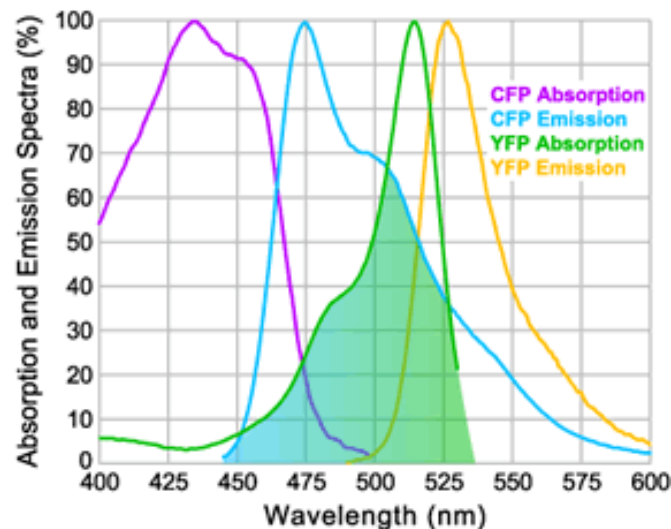
Figure 5: Excitation and emission spectra of CFP and YFP. Magenta and green lines are the excitation of CFP and YFP, respectively; cyan and yellow lines the emission spectra of the two proteins. The green area shows the wavelengths at which CFP emission and YFP excitation overlap. Figure from www.semrock.com.

A further problem is that the YFP protein is sensitive to pH, interferes with chloride, and shows poor photostability and poor expression at 37 °C.

Improvements of fluorophores led to the creation of better probes. More stable and brighter YFP variants were made. Citrine, for example, leads to a more stable FRET signal, when substituted for YFP (Griesbeck et al., 2001). Different ratiometric indicators are composed of an enhanced CFP as donor and Citrine as acceptor. Sapphire or EGFP, replacements for GFP, show improved folding properties that is especially appropriate when expressed within organelles or as a fusion tag. Its absorption spectrum is pH-stable making it highly resistant to pH perturbation inside the cell (Zapata-Hommer and Griesbeck, 2003; Erickson et al., 2001). The improved version of YC 2.0, YC 2.3, still consists of four calcium binding domains, while YC 3.3 exhibits a mutation in the calcium binding site (Q104E) and has therefore lower affinity to calcium (Griesbeck et al., 2001).

Ratiometric Cameleon indicators seem to perform sometimes poorly in mammals. Experiments in a transgenic mouse line expressing Yellow Cameleon 3.60 in neurons

under control of the β-actin promoter showed that even tetanic stimulation led to only a 3 % ratio change in hippocampal brain slices (Nagai et al., 2004). For creation of YC 3.60 the relative orientation of the two chromophores was optimized by fusing YFP at different angles. They also generated circularly permuted YFPs (cpYFPs) that showed efficient maturation and acid stability. These cp proteins consist of two halves of a GFP that were cut at position 145 and exchanged in their order with a short linker peptide. The M13 is fused to the N-terminus and the Xenopus calmodulin is linked to the C-terminal end.

Other indicators were generated that are based on a single chromophore including a circular permuted variant. It turned out that the GFP protein allows insertions of other proteins at various sites of the molecule. Thus, calcium binding domains such as calmodulin could be fused into specific sites. Therefore new indicators were created that respond to calcium with fluorescence intensity changes. Many of these single fluorescent protein probes have higher and faster signals than the FRET based ones.

Single chromophore indicators like Camgaroo-1 (Baird et al., 1999) and Camgaroo-2 (Griesbeck et al., 2001) were made that are composed of YFP or Citrine and lack the calmodulin binding domain M13. The Ca^{2+} binding site calmodulin is inserted at amino acid residue 145. Fluorescence increases result from calcium-induced deprotonation of the EYFP chromophore. Their *in vitro* K_d is much higher than in other single chromophore indicators (Table 1).

Other single GFP indicators based on one chromophore are composed of calmodulin and its binding partner M13 and a cp version of GFP. These indicators are named GCaMP variants (based on GFP) and Pericam variants (based on YFP) (Nakai et al., 2001; Nagai et al., 2001). They have a much higher affinity (lower K_d) to calcium compared to the Camgaroo variants (Table 1).

A disadvantage that appears when using single-chromophore indicators is that they code the signal just by changing the fluorescence intensity. External factors, for example movement of the specimen, may have additional negative effects on signal detection (Rudolf et al., 2003).

FRET-based and single-GFP calcium indicators have been expressed in living cells, tissue culture and transgenic animals. Even the earliest published Cameleon YC 2.0

was successfully expressed in cell culture, and calcium imaging was possible in the cytosol, the endoplasmatic reticulum and the nucleus (Miyawaki et al., 1997).

Several transgenic animals have been created in recent years. The first successful calcium imaging experiments in transgenic organisms were done in *C. elegans* (Kerr et al., 2000), *Drosophila* (Fiala et al., 2002; Reiff et al., 2002), zebrafish (Higashijima et al., 2003), and mice (Ji et al., 2004; Hasan et al., 2004). Calcium indicators were not only expressed in the cytosol but also targeted to various organelles within the cell. It turned out that not all of these experiments were successful. Some versions of Cameleon indicators lost their functionality when fused to the cell membrane or to synaptic proteins and receptor domains.

Most of the calcium indicators use the combination calmodulin-M13 as the calcium binding domain. Because of problems encountered in the experiments, i.e. loss of functionality, it was considered that the calmodulin could be responsible for the inactivation or modification of the indicators. Calmodulin is a central signaling molecule in the cell. It is bound by a variety of proteins and has a large number of phosphorylation sites (Jurado et al., 1999). The group around Griesbeck addressed that problem by replacing the calmodulin by troponin C (TnC) from chicken skeletal muscle, keeping the functionality and dynamic range as convenient as possible and at the same time being less sensitive to interaction with cellular components (Heim and Griesbeck, 2004; Mank et al., 2006). These indicators named TNL 15 (containing Citrine) and TN XL (containing a cp variant of Citrine) are both based on the FRET principle and show *in vitro* changes of 140 and over 400 % ΔR/R, respectively. The authors report that TNL 15 worked in targetings in which other indicators failed and should be more compatible with transgenic expression within whole organisms (Heim and Griesbeck, 2004). TN XL exhibited the fastest kinetics of all indicators (τ_{rise} = 430 ms and τ_{decay} = 240 ms) when stimulated with 40 Hz at the neuromuscular junction (NMJ) of *Drosophila melanogaster* (Mank et al., 2006).

The indicators used in this study represent almost all currently known designs of genetic calcium indicators (Tsien and Miyawaki, 1998; Guerrero and Isacoff, 2001; Zhang et al., 2002; Miyawaki, 2003a; Miyawaki, 2003b; Rudolf et al., 2003; Griesbeck, 2004; Heim and Griesbeck, 2004; Mank et al., 2006). An overview of these indicators is presented in Figure 6.
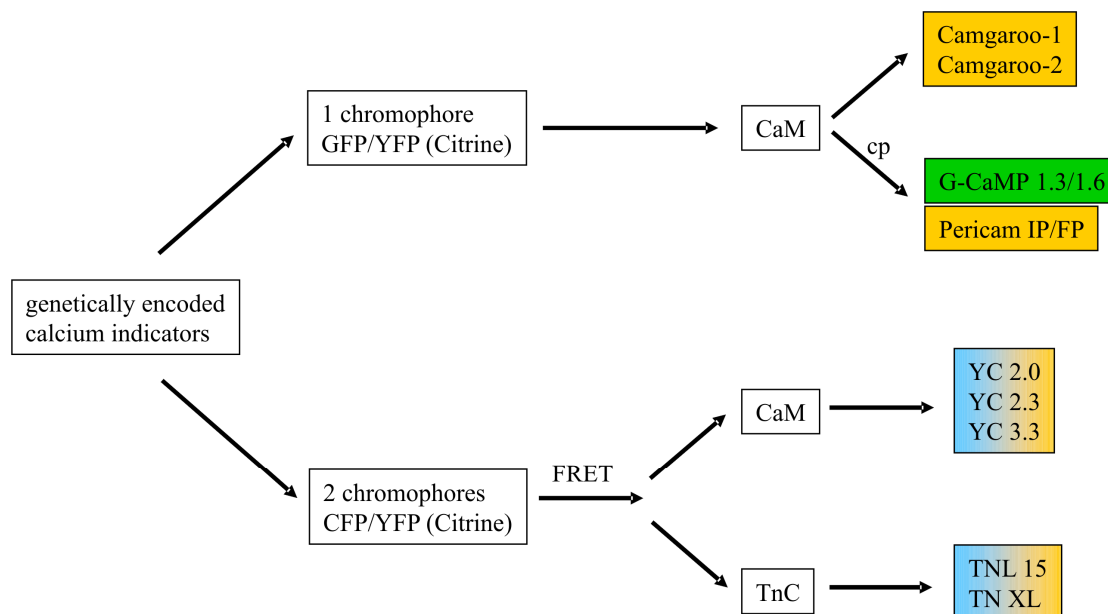
Figure 6: Overview of genetically encoded calcium indicators based on fluorescent proteins to visualize neural activity used in the study. They either consist of one or two chromophores. The calcium binding domain is calmodulin (CaM) or troponin C (TnC). IP: Inverse Pericam, FP: Flash Pericam, YC: Yellow Cameleon.

The design, the working principle and the *in vitro* data of all indicators used in the study is summarized in Table 1.

indicator	design	Ca^{2+} sensor	working principle	*in vitro* p_{Ka}[#]	*in vitro* K_d (µM)	*in vitro* change (%)
YC 2.0	ECFP/EYFP	CaM	FRET	6.9	0.1 11.0	100
YC 2.3	ECFP/Citrine	CaM	FRET	5.7	0.1 4.3	100
YC 3.3	ECFP/Citrine	CaM	FRET	5.7	1.5	100
TNL 15	ECFP/Citrine	Tpn C	FRET	5.7	1.2	140
Camg-1	split EYFP	CaM	Ca-induced p_{Ka} change	~ 7	7.0	700
Camg-2	split Citrine	CaM	Ca-induced p_{Ka} change	~ 7	5.3	700
FP	cpEYFP	CaM	Ca-induced p_{Ka} change	~ 7	0.7	800
IP	cpEYFP	CaM	Ca-induced p_{Ka} change	~ 7	0.2	down to 15

16

GCaMP 1.3	cpEGFP	CaM	Ca-induced p_{Ka} change	~ 7	0.235	450
GCaMP 1.6	cpEGFP	CaM	Ca-induced p_{Ka} change	~ 8.5	0.146	480
SpH	EGFP		p_{Ka}	~ 6		600

Table 1: Design and *in vitro* properties of genetically encoded probes of neural activity. The components, the calcium binding domain, the dissociation constant K_d, the pH sensitivity and the relative fluorescence changes *in vitro* were summarized. #: in double chromophore probes, the relevant p_{Ka} of the longer wavelength chromophore.

2.5 *Drosophila melanogaster*

Drosophila melanogaster is one of the best analyzed model organisms in the world. It was first described in 1830 and used as an experimental animal in 1901 for studying the effect of inbreeding by W.E. Castle. The same year, T.H. Morgan started to breed fruit flies in the laboratory and discovered that genes lie on the chromosome sequentially and identified their order and distance. His results were summarized in so called genetic maps. Since that time lots of geneticists have gathered essential knowledge about the function of genes in the genome of the fly.

2.5.1 *D. melanogaster* Life Cycle
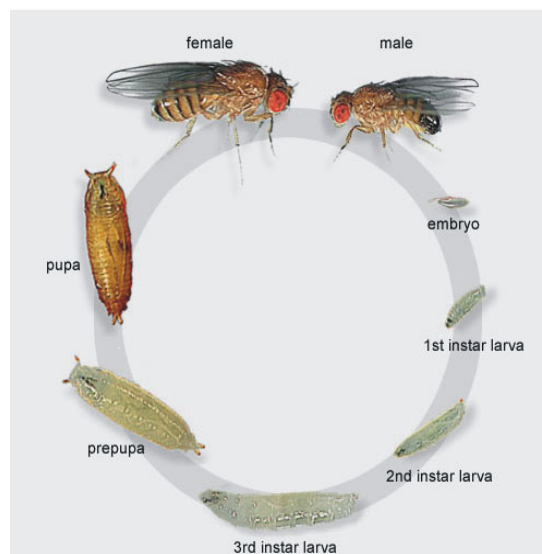
Figure 7: Life cycle of *Drosophila melanogaster*. Picture from http://flymove.uni-muenster.de.

During a lifetime, females lay about 400 0.5 mm long eggs coated by the chorion and a vitelline membrane. Development depends on the temperature in the environment. From about 7 days at 29 ^{o}C it can be prolonged to 19 days at 18 ^{o}C.

At 25 °C embryogenesis takes about one day. After passing through three larval stages, the first and second last for two days and the third for another two, the animal reaches the pupa stage and hatches four days later. After 11 days the life cycle is completed.

One big advantage of this model organism is that it does not take much effort to breed a large number of flies. It is also advantageous that its genome consists of only four chromosome pairs and phenotypical abnormalities from wildtype often can be detected by eye. Many known markers help to visualize genetically manipulated animals. To prevent mutant chromosomes from recombining with wild type chromosomes, so-called 'balancer chromosomes' are often used. These chromosomes carry multiple inversions with one or more dominant markers for easy detection of their presence. Homozygous flies for balancer chromosomes are lethal.

2.5.2 The *D. melanogaster* Genome

As mentioned above, *Drosophila* has four pairs of chromosomes. The genome contains 3 pairs of autosomal chromosomes ("2 right arm, 2 left arm, 3 right arm, 3 left arm, 4 right arm and 4 left arm"), and the sex chromosomes X/Y. The whole genome consists of about 180 million bases and estimated 14000 genes. Each *Drosophila* gene contains on average 4 exons of approximately 750 base pairs in length. Intron size is highly variable and can range from 40 base pairs to more than 70000 base pairs. The genome has been sequenced almost to completion in 2000 and published by Venter and colleagues (Adams et al., 2000).

2.6 GAL4 -UAS System

The yeast transcriptional activator GAL4 is a positive regulator of gene expression for galactose-induced genes (Laughon and Gesteland, 1982). These genes encode enzymes which convert galactose to glucose. GAL4 recognizes a 17 base-pair long palindromic sequence in the upstream activating sequence (UAS) and activates transcription (Giniger et al., 1985).
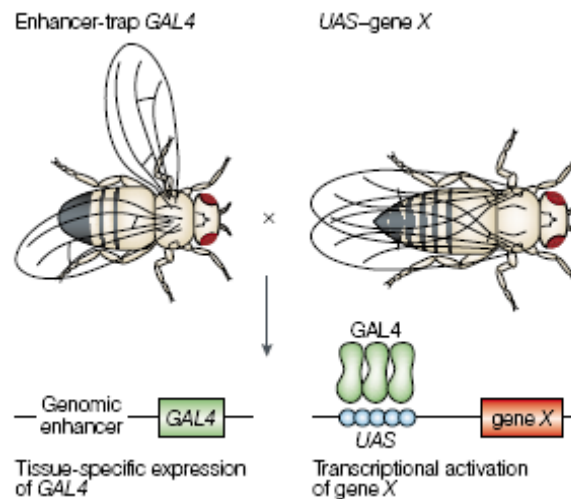
Figure 8: The GAL4-UAS System. The enhancer trap line allows expression of GAL4 in a tissue specific manner. By crossing the GAL4 line to a fly line comprising UAS and a gene of interest GAL4 activates the transcription of gene X. Picture from Brand and Perrimon (1993).

The GAL4-UAS-system can be used to direct gene expression to specific tissues. For this purpose, two different lines of flies are needed. One line expresses the gene GAL4 under control of a genomic enhancer. This line is obtained by inserting a mobile DNA element, usually a P element that contains the *GAL4* gene, randomly in the genome of the fly close to an endogenous enhancer of gene expression (so called 'enhancer trap line'). By screening various lines, distinct patterns can be identified and used for different tasks. In the other fly line the gene of interest (X) is inserted downstream of an upstream activating sequence (UAS). By crossing the two of them GAL4 binds to the UAS and allows expression of gene X in cells where the selected enhancer is active (combinatorial system). Choosing the appropriate GAL4 enhancer trap line therefore allows selective and specific expression in different tissues or even single cells (Brand and Perrimon, 1993).

2.7 *Analysis of Genetically Encoded Indicators*

2.7.1 The *Drosophila* Neuromuscular Junction

The *Drosophila* neuromuscular junction (NMJ) is an excellent model system for studying the cellular and molecular mechanisms of synaptic development and neurotransmission. The advantages of small invertebrate systems, where individual cells can be examined with single-cell resolution, can be combined with the powerful

techniques of patch-clamp analysis and molecular genetics (Keshishian et al., 1996). The anatomy of the *Drosophila* neuromuscular junction is well known and the synapses can be readily accessed for electrophysiology and easily imaged in a semi-intact preparation. The postsynaptic site, in this case the muscle, is free of fluorescence and leads to an almost negligible background. That increases the signal to noise ratio and makes it an ideal system to test the properties of genetically encoded probes.

This system shares important structural and molecular features with CNS synapses in mammals. It exhibits bilaterally symmetric organization that is repeated in every segment. Thirty distinct muscles are innervated by motoneuron axons that are grouped into six major nerve branches: ISN (intersegmental nerve branch), SNa (segmental nerve branch a), SNb (segmental nerve branch b), SNc (segmental nerve branch c), SNd (segmental nerve branch d) and TN (transverse nerve) (Figure 9).
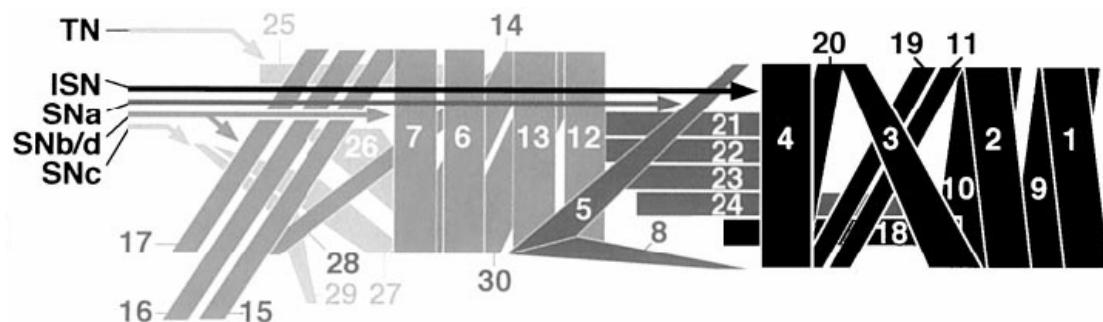
Figure 9: Schematic of the dorsal view of a dissected third instar larva. The thirty muscles (1 – 30) in each half segment are innervated by the motoneurons through the six nerve branches TN, ISN, SNa, SNb, SNc, and SNd. Cartoon from Hoang and Chiba (2001).

The *Drosophila* NMJ is a glutamatergic synapse and its postsynaptic receptors are related to vertebrate AMPA and kainate receptors. Five muscle receptors have been identified which differ in their physiological properties (Petersen et al., 1997; DiAntonio et al., 1999; Davis et al., 1998). The presynaptic active zones and the postsynaptic specializations are organized via PDZ domains, very similar to the situation in mammalian synapses. The NMJ also shows functional and structural plasticity. The group of Chiba has shown that only one motoneuron axon of a given bouton type innervates a single muscle, while up to four motoneuron axons of different bouton types can innervate the same muscle (Hoang and Chiba, 2001).
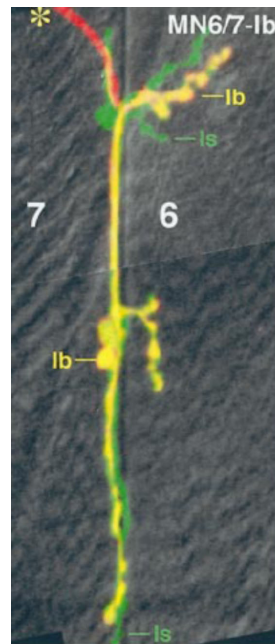
Figure 10: The *Drosophila* neuromuscular junction between muscle 6 and 7. The junction consists of Ib and Is boutons. Picture from Hoang and Chiba (2001).

In Figure 10 motoneurons between muscles 6 and 7 are shown. The boutons that innervate these muscles are either Ib (big) or Is (small) boutons.

For optical imaging, a gene of interest can be expressed in the presynaptic boutons by using the GAL4-UAS system (2.6). Defined stimulation paradigms controlling the experiments and the high reproducibility of experiments in this system allow the direct comparison of different indicators in an *in vivo* situation.

NMJ can be stimulated in accord with the reported average length of motoneuron patterns during fictive larval locomotion (~ 80 Hz / 80 action potentials) (Barclay et al., 2002). When fast synthetic dyes were used, steady-state fluorescence signals with linear relationship to the stimulus frequency were observed in the same preparation (Macleod et al., 2002; 2004).

Similar results were reported from presynaptic terminals at the crayfish NMJ in which the underlying calcium dynamics were described by a single compartment model. In this model, calcium quickly reaches a plateau when influx and efflux/sequestration are in balance (Tank et al., 1995). A rather low endogenous buffer capacity and a fast extrusion of calcium after stimulation were described. Thus, time to achieve steady state, amplitude, deviation, and time to return to baseline of the fluorescence can

mostly be assigned to the intrinsic properties of the cell, the expression level of the indicator, and its dissociation constant.

Using rather low concentrations of Oregon-Green-BAPTA with a K_d of ~ 500 nM, (Macleod et al., 2002; 2004) showed that the decay in calcium after a single AP as well as after long stimulus trains was ~ 60 ms in type Ib boutons of muscle 6/7 *Drosophila* NMJs. Thus, 60 ms is likely to correspond to an intrinsic calcium extrusion rate of the motoneuron of about 17 Hz.

So far, direct comparison of genetically encoded indicators was not possible as they were used in different animals and cell types. Most of them have not been analyzed *in vivo* at all. To solve this problem, we created transgenic flies expressing fluorescent indicators and determined the performance in presynaptic boutons of the NMJ under reproducible and well controlled conditions.

3 Material and Methods

3.1 Laboratory Animals and Preparations

3.1.1 Fly Strains

Animals used in this work were designed by our group unless stated otherwise. The following table shows all fly strains that I used in my thesis.

Fly strain	Provider and engineering
WT Bayreuth w$^-$	provided by C. Lehner, University of Bayreuth (Germany)
elav^{C155}- GAL4	provided by C. S. Goodman, University of California Berkeley, Berkeley (USA) (Lin and Goodman, 1994)
DB331- GAL4	provided by R. Stocker, University of Fribourg (Switzerland)
3A- GAL4	provided by M. Heisenberg, University of Wuerzburg (Germany)
UAS-CD8-GFP	provided by L. Luo, Stanford University, Stanford (USA) (Lee and Luo, 1999)
UAS-YellowCameleon 2.0	provided by C. Schuster, University of Heidelberg, (Germany) (Reiff et al., 2002)
UAS-YellowCameleon 2.3	generated by A. Ihring and D.F. Reiff 2002, MPI of Neurobiology, Martinsried (Germany) cDNA provided by O. Griesbeck, MPI of Neurobiology, Martinsried (Germany) (Griesbeck et al., 2001)
UAS-YellowCameleon 3.3	generated by A. Ihring and D.F. Reiff 2002, MPI of Neurobiology, Martinsried

	(Germany)
	cDNA provided by O. Griesbeck, MPI of Neurobiology, Martinsried (Germany) (Griesbeck et al., 2001)
UAS-YellowCameleon 4.3er	generated by A. Ihring and D.F. Reiff 2002, MPI of Neurobiology, Martinsried (Germany)
	cDNA provided by O. Griesbeck, MPI of Neurobiology, Martinsried (Germany)
UAS-GCaMP 1.3	generated by A. Ihring and D.F. Reiff 2002, MPI of Neurobiology, Martinsried (Germany)
	cDNA provided by Y. Nakai, RIKEN Brain Science Institute, Wako City (Japan)
	(Nakai et al., 2001)
	additional line provided by Y. Wang, Cold Spring Harbor Laboratory, Cold Spring Harbor (USA)
UAS-GCaMP 1.6	generated by A. Ihring and D.F. Reiff 2002, MPI of Neurobiology, Martinsried (Germany)
	cDNA provided by Y. Nakai, RIKEN Brain Science Institute, Wako City (Japan)
	(Ohkura et al., 2005)
UAS-Camgaroo-1	generated by A. Ihring and D.F. Reiff 2002, MPI of Neurobiology, Martinsried (Germany)
	cDNA provided by R. Y. Tsien, University of California, San Diego (USA)
	(Baird et al., 1999)

UAS-Camgaroo-2	generated by A. Ihring and D.F. Reiff 2002, MPI of Neurobiology, Martinsried (Germany) cDNA provided by O. Griesbeck, MPI of Neurobiology, Martinsried (Germany) (Griesbeck et al., 2001)
UAS-Inverse Pericam	generated by A. Ihring and D.F. Reiff 2002, MPI of Neurobiology, Martinsried (Germany) cDNA provided by A. Miyawaki, RIKEN Brain Science Institute, Wako City (Japan) (Nagai et al., 2001)
UAS-Flash Pericam	generated by A. Ihring and D.F. Reiff 2002, MPI of Neurobiology, Martinsried (Germany) cDNA provided by A. Miyawaki, RIKEN Brain Science Institute, Wako City (Japan) (Nagai et al., 2001)
UAS-SynaptoPhluorin	provided by G. Miesenbock, Yale University School of Medicine, New Haven (USA) (Miesenbock et al., 1998)
UAS-TNL 15	generated by A. Ihring and D.F. Reiff 2002, MPI of Neurobiology, Martinsried (Germany) cDNA provided by O. Griesbeck, MPI of Neurobiology, Martinsried (Germany) (Griesbeck et al., 2001)
UAS-mCD8-GCaMP 1.6	generated by A. Ihring 2004, MPI of Neurobiology, Martinsried (Germany) mCD8 cDNA provided by L. Luo,

	Stanford University, Stanford (USA) (Lee and Luo, 2001) GCaMP 1.6 cDNA provided by Y. Nakai, RIKEN Brain Science Institute, Wako City (Japan) (Ohkura et al., 2005)
UAS-TNL 15-ras	generated by A. Ihring 2004, MPI of Neurobiology, Martinsried (Germany) TNL 15 cDNA provided by O. Griesbeck, MPI of Neurobiology, Martinsried (Germany) (Griesbeck et al., 2001) ras: (Aronheim et al., 1994)
UAS-TNL 15-ras 8aa	generated by A. Ihring 2004, MPI of Neurobiology, Martinsried (Germany) TNL 15 cDNA provided by O. Griesbeck, MPI of Neurobiology, Martinsried (Germany) (Griesbeck et al., 2001) ras: (Aronheim et al., 1994) 8aa-tag: (Maximov and Bezprozvanny, 2002)
UAS-8aa TNL 15-ras	generated by A. Ihring 2004, MPI of Neurobiology, Martinsried (Germany) TNL 15 cDNA provided by O. Griesbeck, MPI of Neurobiology, Martinsried (Germany) (Griesbeck et al., 2001) ras: (Aronheim et al., 1994) 8aa-tag: (Maximov and Bezprozvanny, 2002)
UAS-Syx-YC 2.3	generated by A. Ihring 2004, MPI of Neurobiology, Martinsried (Germany)

	YC 2.3 cDNA provided by O. Griesbeck, MPI of Neurobiology, Martinsried (Germany)
	(Griesbeck et al., 2001)
	Syx cDNA provided by H. Bellen, Howard Hughes Medical Institute, Houston (USA)
	(Schulze et al., 1995)
UAS-n-syb YC 2.3	generated by A. Ihring 2003, MPI of Neurobiology, Martinsried (Germany)
	YC 2.3 cDNA provided by O. Griesbeck, MPI of Neurobiology, Martinsried (Germany)
	(Griesbeck et al., 2001)
	n-syb cDNA provided by T. Schwarz, Children's Hospital, Boston (USA)
	(Deitcher et al., 1998)
UAS-mCD8 TN XL 8aa	generated by A. Ihring 2005, MPI of Neurobiology, Martinsried (Germany)
	TN XL cDNA provided by O. Griesbeck, MPI of Neurobiology, Martinsried (Germany)
	(Mank et al., 2006)
	mCD8 cDNA provided by L. Luo, Stanford University, Stanford (USA)
	(Lee and Luo, 2001)
	8aa-tag: (Maximov and Bezprozvanny, 2002)

Table 2: Fly lines used in this study.

3.1.2 Driver Lines

The elav[C155]- GAL4 and elav- GAL4 driver lines allow expression of the indicators in the whole nervous system. In the line elav[C155]- GAL4 the elav promoter fused to GAL4 is located on the X-chromosome.

Crossing UAS reporter to DB331- GAL4 flies, expression is visible in some of the lobula plate tangential cells, namely VS and HS cells, some cells that give input to these cells (T4, T5, Shamprasad, personal communication) and numerous unidentified cells. The 3A-promoter expresses GAL4 in VS and HS cells of the lobula plate (Scott et al., 2002).

3.1.3 Fly Food

3.1.3.1 Appleagar Dishes

200 ml apple juice (Rio D`Oro, Aldi) were warmed up in the microwave for approx. 2 minutes and mixed with 3 g Select Agar. After reheating, the solution could be poured into petri dishes.

3.1.3.2 Drosophila Food

Ingredients: see Media, Buffer and Solutions

Soy flour, corn flour, and dry yeast were mixed in one liter of cold water. Agar was soaked before cooking in another liter of cold water. Three liters were heated to 98º C and the agar was added. After one additional hour of agitation, malcine, treacle and the flour mash were mixed with the boiling water. The solution was then filled up to five liters and cooled down to 65 ºC. At this temperature Propionic acid was added. The food was filled into plastic vials.

3.1.4 Breeding

About 5 female and 5 male flies were collected in vials containing food (see 2.1.2.2) and yeast. Generation time (from egg to adult) takes approximately seven days at 29 ºC, nine days at 25 ºC, eleven days at 22 ºC, or 19 days at 18 ºC (source: Bloomington stock center).

3.1.5 Engineering of Transgenic Flies

3.1.5.1 *Spin Dialysis*

The DNA has to be cleaned by spin dialysis before injection. Little columns were prepared by cutting the lids of plastic tubes and poking a hole in the bottom with a very thin needle. The tube (A) was filled with 25 µl glass beads (300 µm diameter) and put in another tube (B). This was filled with 10x Sepharose CL6B and centrifuged at 3000 rpm for 3 minutes. After discarding tube B, tube A was put in a new tube (C). DNA was incubated at 65 ºC for 10 minutes and applied carefully onto the glass beads and centrifuged at 3000 rpm for another 3 minutes.

3.1.5.2 *DNA-Precipitation and Injection Mix*

Spin dialysed DNA (approx. 6 µg) and spin dialysed Δ2-3 (transposase source, approx. 2 µg) were diluted in 100 µl H_2O. For precipitating the DNA mix 1/10 % vol. of 3 M Na-Acetat was added to the solution. After mixing, 2.5 x 100 % EtOH was added and the sample was incubated in a freezer at – 70 ºC for 30 minutes and centrifuged at 15 000 rpm for 30 minutes. The supernatant was discarded and the sample washed with 100 µl 70 % EtOH. After centrifuging again at 15 000 rpm for 30 minutes, the supernatant was discarded again and the DNA was dried exposed to air. The DNA was diluted in 20 µl 1x injection buffer. For analysing the sample 0.5 -1 µl was run on an agarose gel.

3.1.5.3 *Injection of Fly Embryos with DNA*

WT flies were collected in a collection tube placed on apple agar plates and held overnight at room temperature with light. The apple agar plate was changed every 30 minutes and the eggs laid onto it were collected. After washing the eggs with PBT, they were put in Klorix for 3 minutes to remove the chorion. Then they were washed again with PBT and lined up on a piece of apple agar. A coverslip coated with custom made glue based on tape and heptan was pressed on the eggs to pick them up.

A glass electrode (GB150F-10) was filled with Voltalef 3S oil and the injection mix was sucked in. The embryos were dried in silica gel, covered with Voltalef 10S oil and put under the microscope. Small amounts of injection mix were injected into the dorsal part of the eggs by exerting pressure on the syringe. The DNA was inserted in the genome of the germ line cells by p-element mediated transfection (Spradling and

Rubin, 1982). After injection the embryos were placed on apple agar plates and incubated at 18 ºC until the embryos developed to larvae. The larvae were collected and put in a vial containing food until the flies hatched.

3.1.5.4   Generation of Transgenic Fly Stocks

Every male fly that hatched from the injected embryos was crossed to 10 wild type virgins. The progeny were screened for colored eyes (a marker for successful insertion into the fly genome) and single flies were crossed to the balancer line rl/Sm6Tm6 that carries the two markers 'curly wings' and 'tubby larvae' on a fused 2nd and 3rd chromosome. These flies were transferred into a new vial to breed a new fly stock.

3.1.6   Crossing for GAL4-UAS flies

5 to 10 virgin female GAL4-driver flies were crossed to three male flies carrying UAS and a gene of interest. They were put in a vial containing fly food and yeast. Because *D. melanogaster* adults do not mate for about 10 hours after eclosion, virgin females can be obtained by collecting them within 8-10 hours after the vial has been cleared from adults.

3.2   Material

3.2.1   Chemicals

Material	Supplier
Adenosine Triphosphate (ATP), Sodium	Sigma, St. Louis (USA)
Agar	Sigma, St. Louis (USA)
Ammonium Acetate	Merck, Darmstadt (Germany)
Ampicillin Sodium Salt	Roth, Karlsruhe (Germany)
ATP (see adenosine triphosphate)	Sigma, St. Louis (USA)
Bactopeptone	Becton Dickinson GmbH, Heidelberg (Germany)

BES	Roth, Karlsruhe (Germany)
Bovine Serum Albumin (BSA)	Sigma, St. Louis (USA)
Bovine Serum Albumin (BSA)	New England Biolabs, Beverly (USA)
Buffer P1 resuspension buffer	Qiagen, Hilden (Germany)
Calcium Chloride, dihydrate	Sigma, St. Louis (USA)
Deoxyribonuclease	Sigma, St. Louis (USA)
DMSO (Dimethylsulfoxide)	Sigma, St. Louis (USA)
D-Trehalose Dihydrate	Sigma, St. Louis (USA)
EGTA (Ethylene glycol bis (beta-amino ethyl ether tetra-acetic acid)	Sigma, St. Louis (USA)
Fetal Bovine Serum	Biochrom AG, Berlin, Germany
Glucose (D-(+)-Glucose anhydrous, min 99%)	Sigma, St. Louis (USA)
Glycine	Merck, Darmstadt (Germany)
HEPES free acid	Sigma, St. Louis (USA)
Insulin	Sigma, St. Louis (USA)
Ionomycin, calcium salt	Sigma, St. Louis (USA)
L-Glutamic Acid	Roth, Karlsruhe (Germany)
Magnesium Chloride Hexahydrate	Merck, Darmstadt (Germany)
Normal Goat Serum (NGS)	Sigma, St. Louis (USA)
Pfu Polymerase	Stratagene, La Jolla (USA)
Poly-L-lysine Hydrobromide	Sigma, St. Louis (USA)
Potassium Chloride	Merck, Darmstadt (Germany
Ribonuclease A	Sigma, St. Louis (USA)
Saccharose	Merck, Darmstadt (Germany)

Sepharose CL6B	Sigma, St. Louis (USA)
Shields and Sang M3 insect medium	Sigma, St. Louis (USA)
Sodium Bicarbonate	Sigma, St. Louis (USA)
Sodium Chloride	Sigma, St. Louis (USA)
Sodium Phosphate Monobasic, Anhydrous	Sigma, St. Louis (USA)
Streptomycin-Penicillin solution	Sigma, St. Louis (USA)
T4-Ligase	New England Biolabs, Beverly (USA)
Triton	Sigma, St. Louis (USA)
Trizma Base	Sigma, St. Louis (USA)
Trypsin EDTA	Invitrogen, Karlsruhe (Germany)
Vectashield mounting medium	Vector Laboratories, Burlingham (USA)
Vent polymerase	New England Biolabs, Beverly (USA)
Voltalef 10S oil	Lehmann & Voss & Co., Hamburg (Germany)
Voltalef 3S oil	Lehmann & Voss & Co., Hamburg (Germany)
Yeast extract	Sigma, St. Louis (USA)

3.2.2 Instruments

3.2.2.1 Imaging Setup

Name	Supplier
60 x water immersion objective	LumPlanFL; Olympus Optical, Tokyo, (Japan)
analog-to-digital converter	DAS-1602/12; Computerboards, Middleboro (USA)
CCD camera Cool Snap HQ	Visitron Systems, Puchheim, Germany
Custom experiment controlling software	Delphi, Borland, Scotts Valley (USA),
Dicroic mirrors (455 DCLP, 515 DCLP, 490 DCLP)	Chroma Technologym, Rockingham (USA)
Optical filters (Q 480 LP, HQ 535 / 50 BP)	Chroma Technologym, Rockingham (USA)
Dissecting Microscope (50 x)	Leitz, Stuttgart (Germany)
Dyad DNA Engine Peltier Thermal Cycler	MJ Research Inc., Waltham (USA)
Focus drive	Luigs & Neumann Ratingen (Germany)
MetaView software	Visitron Systems, Puchheim, Germany
Microscope Axioskop	Zeiss, Oberkochen (Germany)
Microscope Axiovert 35M	Zeiss, Oberkochen (Germany)
Micropipette Puller Model P-97	Sutter Instrument Co.
Multispec Viewer	Optical Insights Tucson (USA)
Polychrome IV	T.I.L.L. Photonics, Martinsried (Germany)
Stimulator	Iso-Stim 01-D; NPI Electronics, Tamm (Germany)

3.2.2.2 Confocal Microscopy

Name	Supplier
Leitz DM RBE microscope	Leica, Wetzlar (Germany)
Leica TCS NT confocal	Leica, Wetzlar (Germany)
HBO 50W fluorescent lamp	Leica, Wetzlar (Germany)
TCS NT Vers.1.6.587 program	Leica, Wetzlar (Germany)
Objective HC PL APO 10x/0.40 IMM	Leica, Wetzlar (Germany)
Objective HC PL APO 20x/0.70 IMM CORR	Leica, Wetzlar (Germany)
Objective PL APO 40x/1.25 oil Ph3	Leica, Wetzlar (Germany)
Objective PL APO 63x/1.32 oil Ph3	Leica, Wetzlar (Germany)

3.2.3 Consumables

Name	Supplier
Tube	Eppendorf, Hamburg (Germany)
PCR Tube	Eppendorf, Hamburg (Germany)
Falcon 50ml tube	Becton Dickinson, Franklin Lakes (USA)
Falcon 15ml tube	Becton Dickinson, Franklin Lakes (USA)
Falcon Tissue Culture Plate, 12 Well	Becton Dickinson, Franklin Lakes (USA)
QIAquick Miniprep Kit	Qiagen, Hilden (Germany)
QIAquick Midiprep Kit	Qiagen, Hilden (Germany)
QIAquick Gel Extraction Kit	Qiagen, Hilden (Germany)
QIAquick PCR Purification Kit	Qiagen, Hilden (Germany)
Needle 27GX3/4", 0,4X20 TERUMO	VWR, Vienna (Austria)

Glass pipette GB150F-10	Science Products GmbH, Hofheim (Germany)
Glass pipette GB100F-10	Science Products GmbH, Hofheim (Germany)

3.2.4 Antibodies

Antibody	Supplier
α-GFP linked to Alexa 488	Molecular Probes, Karlsruhe (Germany)
Alexa 594	Molecular Probes, Karlsruhe (Germany)
Alexa 488	Molecular Probes, Karlsruhe (Germany)
α-synapsin	E. Buchner, Würzburg, (Germany)
α-cysteine string protein	E. Buchner, Würzburg (Germany)
α-nc82	E. Buchner, Würzburg (Germany)

3.2.5 Plasmids

Plasmid	Supplier
pcDNA3 (5,4 kb)	Invitrogen, Carlsbad (USA)
pMT (3,5 kb)	Invitrogen, Carlsbad (USA)
pUAST (9,5 kb)	*Drosophila* Genomics Resource Center, Indiana (USA)
pRSETb (3,3 kb)	Invitrogen, Carlsbad (USA)

3.2.6 Enzymes

Enzyme Name	Cutting Sequence	Supplier
BamHI	GGATCC	New England Biolabs GmbH, Frankfurt (Germany)
DpnI	GATC	New England Biolabs GmbH, Frankfurt (Germany)
EcoRI	GAATTC	New England Biolabs GmbH, Frankfurt (Germany)
NotI	GCGGCCGC	New England Biolabs GmbH, Frankfurt (Germany)
SacI	GAGCTC	New England Biolabs GmbH, Frankfurt (Germany)
SpHI	GCATGC	New England Biolabs GmbH, Frankfurt (Germany)
XbaI	TCTAGA	New England Biolabs GmbH, Frankfurt (Germany)

3.2.7 Oligonucleotides

Primer Name	Primer Sequence
Bam_Not_8aa_CFP_for	CGG GAT CCG CGG CCG CCA CCA TGT GTT GGG ATG AAG AAG ATG GCG GCA TGG TGA GCA GGG CGG AGG AGC TG
Bam_Not_CFP_for	CGG GAT CCG CGG CCG CCA CCA TGG TGA GCA GGG CGG AGG AGC TG
BGH reverse	TAG AAG GCA CAG TCG AGG
BglII_mCD8_for	GAA GAT CTA TGG CCT CAC CGT TGA CCC GC
BglII_Syx_for	GAA GAT CTG ACT AAG ACA

	GAT TAG CCG CTC TCC
CaM_SacI_rev	CGA GCT CGG AGA TCT TCT TGAACC GGT TGG C
Eco_Xba_8aa_ras_rev	GGA ATT CTC TAG ATT AAC ACC AAT CTT CTT CAT CGC CGC CGC TCA GCA CGC ACT TGC AGC T
EcoRI_CD4_forw	GGA ATT CCG CCA CCA TGA ACC GGG GAG TCC CTT TTA GG
EcoRI_LAPTM_for	GGA ATT CAT GTT TAG GAT CCA CCT CAA GAT GGG TCC C
EcoRI_mCD8_for	GGA ATT CAT GGC CTC ACC GTT GAC CCG C
EcoRI_n-syb_for	GGA ATT CAA CAT GGC GGA CGC TGC ACC AGC TGG C
EcoRI_Syt_for	GGA ATT CAT GCC GCC AAA TGC AAA ATC G
EcoRI_XbaI_ras_rev	GGA ATT CTC TAG ATT AGC TCA GCA CGC ACT TGC AGC T
GCaMP 1.6_mid_rev	GCC ATC ATT GTC AGG AAC TCA GGG
G-CaMP 1.6+8_C_for G-CaMP 1.6_for	ATA AGA ATG CGG CCG CCA CCA TGG CAC ACC ATC ACC ACC ATC ACT C
G-CaMP 1.6+8_C_rev	GCT CTA GAT CAA CAC CAA TCT TCT TCA TCG CCG CCC TTC GCT GTC ATC ATT TGT ACA AAC TC
G-CaMP 1.6+8_N_for	ATA AGA ATG CGG CCG CCA CCA TGT GTT GGG ATG AAG AAG ATG GCG GCA TGG CAC ACC ATC ACC ACC ATC ACT C
G-CaMP 1.6+8_N_rev	GCT CTA GAT CAC TTC GCT GTC ATC ATT TGT ACA AAC TC

GFP_5`_rev	GTT TAC GTC GCC GTC CAG CTC GAC
GFP_mid_rev	GCG GCT GAA GCA CTG CAC GCC CCA GGT CAG
mCD8_middle_forw	CAA GAT AAC GTG GGA CGA GAA GC
MT forward	CAT CTC AGT GCA ACT AAA
Not_CFP_for	ATA AGA ATG CGG CCG CCA CCA TGG TGA GC
NotI_CD4_rev	ATA AGA ATG CGG CCG CGG GGC TAC ATG TCT TCT GAA AC
NotI_LAPTM_rev	ATA AGA ATG CGG CCG CAG CCT GGC TTT CGT CGC GTC C
NotI_mCD8_for	ATA AGA ATG CGG CCG CCA CCA TGG CCT CAC CGT TGA CCC GC
NotI_mCD8_rev	ATA AGA ATG CGG CCG CGC GGC TGT GGT AGC AGA TGA G
NotI_n-syb_rev	ATA AGA ATG CGG CCG CCA CGC CGC CGT GAT CGC CAG C
NotI_Syt_rev	ATA AGA ATG CGG CCG CCT TCA TGT TCT TCA GGA TCT C
NotI_Syx_for	ATA AGA ATG CGG CCG CCA CCA TGA CTA AAG ACA GAT TAG CCG CT
NotI_Syx_rev	ATA AGA ATG CGG CCG CCA TGA AAT AAC TGC TAA CAT ATG AGG CCG C
pMT_mutXba_forw	CAA CTA AAG GGG GGA TCT CGA TCG GGG TAC CTA CTA
pMT_mutXba_rev	CTA GTA GGT ACC CCG ATC GAG ATC CCC CCT TTA GTT G
pUAST_for_new	CAA TCT GCA GTA AAG TGC AAG

pUAST_rev_new	CTC TGT AGG TAG TTT GTC AA
SacI_TnC_rev	GCG AGC TCC TGC ACA CCC TCC ATC ATC TTC
SacI_YFP_for	CGA GCT CAT GGT GAG CAA GGG CGA GGA GCT G
SpHI_CaM_for	CGC ATG CAT GAC CAA CTG ACA GAA GAG CAG
SpHI_CFP_rev	ACA TGC ATG CGG GCG GCG GTC ACG AAC TCC AGC
SpHI_Tp_for	ACA TGC ATG CTC AGC GAG GAG ATG ATT GCT AGA T
XbaI_8aa_cp-cit_rev	GCT CTA GAT TAA CAC CAA TCT TCT TCA TCG CCG CCG TCC TCG ATG TTG TGG CGG ATC TT
YC 2.3_C_for	ATA AGA ATG CGG CCG CCA CCA TGG TGA GCA AGG GCG AGG AGC TG
YC 2.3_N_rev	GCT CTA GAT TAC TTG TAC AGC TCG TCC ATG CCG AG
YC 2.3+8_C_rev	GCT CTA GAT TAA CAC CAA TCT TCT TCA TCG CCG CCC TTG TAC AGC TCG TCC ATG CCG AG
YC 2.3+8_N_for	ATA AGA ATG CGG CCG CCA CCA TGT GTT GGG ATG AAG AAG ATG GCG GCA TGG TGA GCA AGG GCG AGG AGC TG

3.2.8 Antibiotics

Antibiotic	Working solution
Ampicillin	50 µg/ml
Kanamycin	50 µg/ml
Streptomycin-Penicillin solution	20 µl/ml

3.3 Media, Buffer and Solutions

Medium	Recipe
LB (Luria-Bertani) medium pH 7,0	20 g/l LB broth base in ddH$_2$0
LB Agar	LB Medium 15 g Agar in 1 liter ddH$_2$O
PBS (Phosphate buffered salt solution, 1 x) pH 7,4	137 mM NaCl 2.7 mM KCl 80.9 mM Na$_2$HPO$_4$ 1.5 mM KH$_2$PO$_4$ in ddH$_2$O
Paraformaldehyde solution (PFA) (4 %)	4 % (w/v) Paraformaldehyde in 1x PBS, pH 7.4
Saline (isotonic)	0.9 % (w/v) NaCl in ddH$_2$0
TAE (10 x)	48.4 g Tris base 11.4 ml glacial acetic acid 20 ml of 0.5 M EDTA, pH 8.0 add H$_2$O to 1 liter
TBE (10 x)	450 mM Tris base 440 mM Borsäure 10 mM EDTA

	in ddH$_2$0
Triton X-100 (0.1 % / 0.5 %)	0.1 % / 0.5 % (v/v) Triton X-100 in 1 x PBS
Fly Food	5 l ddH$_2$O 28 g fiber agar 110 g treacle 400 g Malzin 400 g Corn-based flour 50 g Soja-based flour 90 g dry yeast 31,5 ml Propionic acid
HL6.1 (Macleod et al., 2003) pH 7,2	15,0 mM MgCl$_2$ 24,8 mM KCl 23,7 mM NaCl 10,0 mM NaHCO$_3$ 13,8 mM Isethionic acid (Na$^+$) 5,0 mM BES 80,0 mM Trehalose x 2H$_2$O 5,7 mM L-Alanine 2,0 mM L-Arginine HCl 14,5 mM Glycine 11,0 mM L-Histidine 1,7 mM L-Methionine 13,0 mM L-Proline 2,3 mM L-Serine 2,5 mM L-Threonine 1,4 mM L-Tyrosine 1,0 mM L-Valine
Na-Acetat (3 M) pH 5-5.2	24.61 g Na-Acetat in 100 ml H$_2$O
KCl (1 M)	7.455 g KCl in 100 ml H$_2$O
0,5 M "NaPi" pH 6.8-7	a) 44.5 g Na$_2$HPO$_4$x2H$_2$O to 500 mlH$_2$O

	b) 34.5 g $NaH_2PO_4xH_2O$ to 500 mlH_2O
	mix a) and b) (approx.5:2), to pH 7
10x injection buffer pH 6,8	0,2 ml 0,5M NaPi
	5 ml 1 M KCl
	94,8 ml ddH_2O
Phosphate Buffered Saline (PBS) (10x)	100 mM Na_2HPO_4, pH 7.4
	20 mM KH_2PO_4
	1.37 M NaCl
	27 mM KCl
Triton X-100 10 %	10 ml Triton X-100
	90 ml H_2O
Phosphate Buffered Saline containing Triton X (PBT) (1x)	0.05 % Triton X-100
	in 1x PBS
Klorix 50 %	50 ml Klorix
	50 ml H_2O
Glue (based on heptan)	Tape (Tesa) in 50 ml n-Heptan
Sepharose-solution	2 Vol. Sepharose CL6B in 1 Vol. 1 x TE
1M Tris-Cl pH 7,5	121,1 g Tris
	65 ml HCl_{conc}
	add ddH_2O to 1 liter
TE (1 x)	10 mM Tris-Cl
	1 mM EDTA
Cell culture media for neuronal cells	900 ml M3 Sang and Shields
	1.25 g bactopeptone
	0.5 g yeast extract
	10 % FBS
	10 mg Insulin
BBS (2 x)	50 mM BES (acid), pH 6.96
	280 mM NaCl
	1.5 mM Na_2HPO_4
$CaCl_2$ solution for phosphate transfection	250 mM $CaCl_2$ in H_2O
DNA Gel Loading Buffer (10 x)	100 mM Tris/HCl, pH 7.5
	10 mM EDTA

	50 % Glycerol
	1 % Orange G
HBSS	25 mM HEPES pH 7.4
	140 mM NaCl
	5 mM KCl
	1 mM CaCl$_2$
	1 mM MgCl$_2$
	1 mM Glucose
	0.25 % BSA
HBSS with 80 mM KCl	25 mM HEPES, pH 7.4
	40 mM NaCl
	100 mM KCl
	1 mM CaCl$_2$
	1 mM MgCl$_2$
	1 mM Glucose
	0.25 % BSA

3.4 Molecular Methods

3.4.1 Spectrometric Determination of DNA Concentration

Double-stranded DNA has an absorption maximum at 260 nm; by measuring the absorption of DNA diluted in water in a 1 cm quartz cuvette, the DNA concentration of the sample could be calculated using the following formula:

DNA [µg/ml] = OD$_{260}$ * 50 * dilution factor

3.4.2 DNA Amplification using Polymerase Chain Reaction

Primer-annealing temperatures varied in different reactions and were chosen according to the predicted primer melting temperature which correlates to the GC content of the primers' overlapping regions.

PCR reaction mix:

50-60 ng plasmid DNA as reaction template

1 µl dNTP solution (12.5 mM)

2 µl primer No. 1 (50 µM)

2 µl primer No. 2 (50 µM)

5 µl polymerase buffer (10 x, provided by manufacturer)

38 µl H$_2$O

1 µl (2 U) Vent polymerase.

Reaction cycles:

5 min heating to 95°C;

30 amplification cycles:

30 sec 95°C: melting of double-stranded DNA

30 sec annealing of primers; temperatures varying from 52-62°C

2 min 72°C: DNA synthesis

After cycle completion: 3 min 72°C; reaction termination by cooling to 4°C

3.4.3 Restriction site cleavage of DNA

DNA restriction was used to generate a vector or insert fragments necessary for DNA cloning. Insert and vector were cut with either one or two restriction enzymes at a time. 0.5 - 1 µg DNA for analytical purposes or about 10 µg DNA for larger preparations were cut with 1 – 5 U restriction enzymes per µg DNA. Buffers were used according to the manufacturer's protocols. To avoid unspecific cutting, the volume of each reaction was raised to a minimum of 10 x the amount of restriction enzymes used. Incubation times were at least 2 hours. The efficiency of the restriction was controlled by running a test sample on an agarose gel.

3.4.4 Ligation of DNA Fragments

In DNA ligations, the ratio of insert to vector should be at least 3:1; DNA concentrations were determined by spectrometric measurements. The ligation reaction mix was incubated overnight at 16°C or at room temperature for 2 h.

Ligation approach:

60 ng vector DNA

180 ng insert DNA

1 µl ligase buffer (10 x)

1 µl (400 U) T4 DNA Ligase

ad 10 µl with H_2O

3.4.5 Transformation of Chemically Competent E. coli

Chemically competent *E. coli* cells kept in 50 µl aliquots at -80 °C were thawed on ice, mixed with the desired DNA plasmid and incubated on ice for about 20 minutes. A heat shock was applied to the cells by transferring them into a 42 °C water bath for 1 minute, and afterwards they were again incubated on ice for about 2 minutes. The cells were then diluted in 150 µl LB medium, shaken in a 37 °C incubator for 45 minutes and plated onto LB agarose plates containing the appropriate antibiotic for selection.

3.4.6 Isolation of Nucleic Acids

3.4.6.1 Small-scale Plasmid Isolation from E. coli (Miniprep)

3 ml LB/Amp-Medium (100 µg/ml ampicillin) was inoculated with a single colony and incubated overnight at 37 °C with constant agitation. Cultures were transferred into 2 ml Eppendorf tubes and cells were centrifuged (14000 g, 1 min, RT). Plasmids were isolated from bacterial cells using anion exchange columns (Qiagen) according to the manufacturer's protocol. DNA was eluted from the columns by addition of 50 µl ddH_2O with centrifugation (14000 g, 2 min, RT).

3.4.6.2 Large-scale Plasmid Isolation from E. coli (Midiprep)

A single colony was inoculated in 3 ml LB/Amp-Medium and shaken for 3 hours at 37 °C. This preculture was poured into 200 ml LB/Amp-Medium and incubated overnight at 37 °C with constant agitation. Cultures were transferred into centrifugation tubes and spun at 14000 g for 30 minutes at 4 °C to harvest the cells.

3.4.7 Agarose Gel Electrophoresis

The efficiency of restrictions was evaluated by running samples on an 0.5 – 2 % agarose gel. Therefore agarose was diluted in TAE buffer in a suitable amount. After

pouring the solution in a gel chamber, 20 µl Ethidiumbromide was added. The samples were applied singly.

3.4.8 Site-directed Mutagenesis by PCR

The original vector pMT/V5-His contains two XbaI restriction sites. In order to get rid of one site, primers were designed that introduce a point mutation in the desired place. The mutagenic primer pair contains the DNA sequence with a mutated base located in the middle with about 10 – 15 bases of the original DNA sequence on both sides. The length of the primer was chosen so that a melting temperature of about 74 °C is achieved (based on the formula: $Tm = (2 °C)(A+T) + (4 °C)(G+C)$). The primers should have a minimum GC content of 40% and should terminate with G or C. Primer extension time was set to 2 minutes per 1000 base pairs, leading to a total extension time of 8 minutes for the 3.5 kb long pMT.

PCR Reaction Mix

50 ng plasmid-DNA as reaction template (pMT/V5-HisA)

0.8 µl dNTP solution (12.5 mM)

1.1 µl primer pMT_mutXba_forw (10 µM)

1.1 µl primer pMT_mutXba_rev (10 µM)

5 µl Pfu polymerase buffer (10 x)

40.5 µl H_2O

1 µl (2.5 U) Pfu polymerase

Reaction Cycles

30 sec heating to 95°C

16 amplification cycles:

30 sec 95°C: melting of double-stranded DNA

1 min 55°C: annealing of primers

8 min 68°C: DNA extension

Reaction termination by cooling to 4°C

After the PCR reaction the sample was incubated for 2 hours at 37 °C with 1 µl (20 U) DpnI to get rid of the unmutated template DNA. DpnI cuts the unwanted methylated

plasmid DNA and leaves the newly synthesized mutated DNA. 1 - 2 µl of this restriction assay were used for transformation in bacteria.

3.5 Cell culture

3.5.1 Maintenance of *Drosophila* Neuronal Cell Culture

3.5.1.1 Media

3.5.1.1.1 Heat inactivated Fetal Bovine Serum

Frozen fetal bovine serum was thawed on a shaker at 2 - 8 ºC overnight. After pre-heating a water bath to a temperature of 56 ºC the serum was heated for 30 minutes. Before adding to cells the serum has to be cooled at room temperature.

3.5.1.1.2 M3 / BPYE / 10 % FBS / Insulin

0.5 g yeast extract and 1.25 g bactopeptone were added to 450 ml Shields and Sang M3 insect medium and stirred until the powder was dissolved. The medium was filter-sterilized, using a 0.2 µm filter, and dispensed into sterile bottles. 50 ml of the heat-inactivated fetal bovine serum and 10 µg/ml Insulin were added to the prepared medium. It was stored at 4^oC.

3.5.1.2 Splitting Cells

Cells were maintained in a 25 cm^2 flask and kept at 26 ºC without CO_2. For splitting the cells the medium was removed and about 1 ml Trypsin-EDTA was added. After one minute of incubation at room temperature cells have lost their attachment to the plastic and to each other. New medium containing M3, 10 % FBS and Insulin was added and the cells were resuspended by pipetting. New flasks with new unconditioned medium were prepared and the cell suspension was transferred in a proportion of 1 : 1.

3.5.2 Transfection of *Drosophila* Neuronal Cells

For transfection of a dish (diameter: 35 mm) 100 µl of $CaCl_2$ solution were mixed thoroughly with 10 µg DNA. 100 µl 2 x BBS was added; the solution was mixed

carefully and incubated for 40 minutes. 200 µl of the transfection mix were put in small droplets onto the cell layers and the dishes were incubated at 26 °C for 3 - 5 hours. In order to remove as much of the $CaPO_4$ precipitate as possible, the dishes were carefully rinsed 2 - 3 times with PBS, and afterwards supplied with 2 ml fresh M3 medium. Depending on the promoter efficiency, protein expression could be detected 24 - 48 hours after transfection and lasted for several days.

3.6 Histology and Immunohistochemistry

3.6.1 Antibody Staining of Larvae

3.6.1.1 Antibody Staining with Primary and Secondary Antibodies

Localization of targeted indicators was confirmed by co-visualization of fluorescent protein expression and antibody staining of presynaptic proteins (anti-synapsin/anti-CSP/anti-nc82).

Late third instar larvae were pinned down on a sylgard covered dish, covered with HL6.1 and guts, salivary gland and the brain were removed. After fixation with PFA for 5 minutes the filets were washed in PBT and collected in tubes containing PBT. For saturation of unspecific binding sites PBT containing 10 % NGS was added. The sample was incubated for 45 minutes at room temperature. The primary monoclonal mouse antibody against the *Drosophila* proteins synapsin, CSP or nc82 was applied. After incubation for 1 hour at room temperature the solution was removed by washing the filets three times in PBT for 20 minutes. The Alexa 594-labelled secondary goat anti-mouse antibody was added in PBT / 10 % NGS and incubated overnight at 4 °C. The first washing procedure was repeated and the filets were equilibrated 70 % Glycerol / PBS overnight at 4 °C. The immunostained filets were mounted on glass slides, covered with Vectashield mounting medium and a coverslip.

3.6.1.2 Antibody Staining with α-GFP Alexa Fluor488

For visualization of GFP in animals with low expression level, an anti-GFP Alexa Fluor® 488 conjugate antibody staining was used. For that purpose the larvae were prepared as described in 3.6.1.1, incubated with the anti-GFP antibody for 1 hour at room temperature or overnight at 4 °C and mounted after the washing procedure described above.

3.6.2 Dissection of *Drosophila* Brains

Some indicators were tested for localization in the central brain of the fly. In particular the lobula plate tangential cells, important interneurons in motion detection, were analyzed. For that purpose, flies carrying the desired construct were crossed to the GAL4 driver lines DB331 and 3A that allow expression in the lobula plate tangential cells of the vertical system (VS-cells) and the horizontal system (HS). The animals were anesthetized and transferred in 1 x PBT. The head was disconnected from the rest of the body with a sharp scalpel. By removing the chitin carefully with some tweezers, the central brain could be unhinged from its case. Afterwards the trachea were removed. The PBT was replaced with 4 % PFA and the dissected brains were shaken for 30 – 45 minutes at room temperature and washed after this procedure for 1 hour in PBT. If no antibody was applied, the brain was directly mounted on a microscope slide by covering it with Vectashield and a coverslip. The brain could then be analyzed by confocal laser scanning microcopy.

If an antibody was needed for enhancing the signal, it was applied after the wash with PBT. In this case 1 x PBT, a primary antibody and 5 % NGS were added to the brains. They were shaken over night at 4 °C. The next day, the non-bound antibody was washed away by shaking for 1 hour with fresh 1 x PBT. The second antibody was applied following similar rules. It had to be removed by washing the preparations 3 times with 1 x PBT for 1 hour. After this procedure, the brains were mounted as described before.

3.7 Stimulation and Optical Imaging

3.7.1 Larval Preparation

The comparison of 10 different genetically encoded Calcium indicators and the pH-sensitive SynaptopHluorin was performed at the larval neuromuscular junction (NMJ) of *Drosophila melanogaster.*

Late third instar larvae were pinned down on a sylgard covered recording chamber and opened up along the dorsal midline. They were covered with HL6.1 without calcium. Guts, salivary gland and trachea were removed carefully and the segmental nerves were severed (Figure 11).
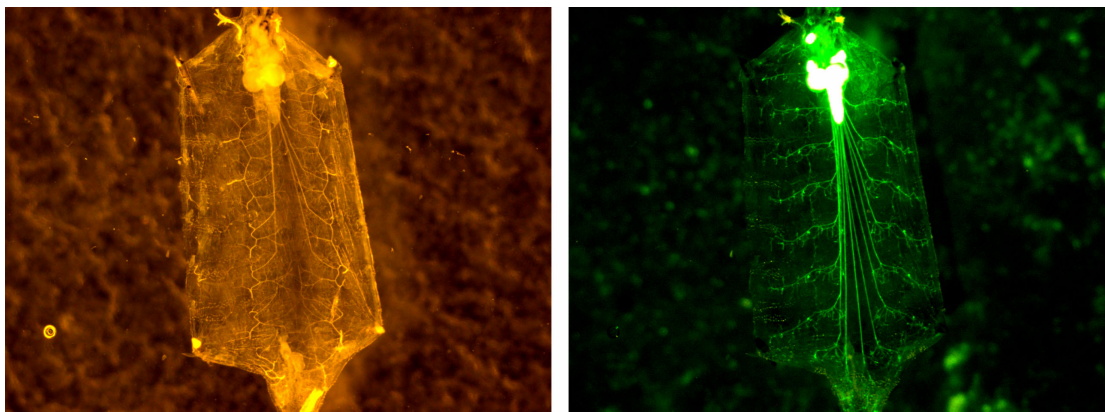
Figure 11: Larval preparation of a third instar larva expressing YC 3.60. The image on the left shows a pinned-down larva in bright field. The corresponding epifluorescence of YC 3.60 is depicted in the right picture. Pictures kindly provided by T. Hendel.

All experiments were performed in HL6 (Macleod et al., 2002) containing 7 mM glutamate and 1.5 mM calcium unless otherwise stated. Glutamate effectively blocked postsynaptic muscle contractions at concentrations >5 mM without influencing presynaptic calcium dynamics (Macleod et al., 2004).

3.7.2 Physiology and Imaging
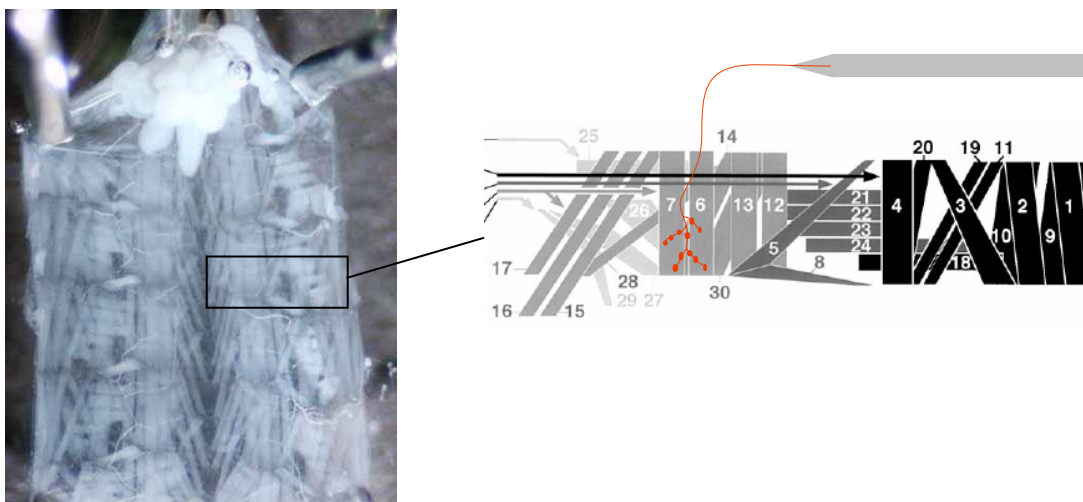
Figure 12: Dissected third instar larva. On the right an expanded cartoon of the muscles from the left picture are shown. The motoneuron innervating muscle 6 and 7 is highlighted in red color. A suction electrode sucks in the cut end of the segmental nerve. Pictures from www.utsc.utoronto.ca and Hoang and Chiba (2001).

Larval NMJs were recorded at muscle 6/7 in abdominal segments 2 or 3 (Figure 12). The cut end of the segmental nerve of the dissected larvae was placed into a suction electrode and stimulated by suprathreshold current pulses while the indicator response was imaged simultaneously on a CCD camera. Stimulus protocols from 0 to 80 Hz, in some cases up to 160 Hz were changed randomly. The experiments were controlled by custom software written by J. Haag in Delphi using an analog to digital converter. A 60 x water immersion objective was used for wide-field epifluorescence detection. Images were acquired at a rate of 10 Hz and 3 x 3 binning of the CCD chip. The imaging of the ratiometric YC variants and TNL 15 was performed by exciting the chromophore at 430 nm using a 455 dichroic long pass (DCLP) and splitting the emission using a multispec viewer with an additional 515 DCLP. The single chromophore indicators SpH, GCaMP 1.3, GCaMP 1.6, Camg 1, and Camg 2 were imaged by excitation at 470 nm using a Q 480 LP and a HQ 535 / 50 bandpass. Inverse Pericam (IP) was excited at 485 nm, and the emission was separated using a 490 DCLP and an HQ 535 / 50 bandpass.

3.7.3 Data Analysis

Data were analyzed using custom software programmed by A. Borst in IDL version 6. Relative changes in fluorescence ($\Delta F/F$) were calculated by subtracting a control image (F_{cntrl}) from each image F of the series and then dividing the difference images by F_{cntrl}. The control image was obtained by averaging the images before stimulus onset. The background was determined within a homogeneous region close to the individual bouton. This fluorescence intensity was subtracted from the raw intensity of the bouton before $\Delta F/F$ was calculated. For two chromophore indicators background subtraction was done by subtracting a background region close to a bouton from the raw intensity in each of the two channels individually. A ratio image sequence was calculated from the enhanced yellow fluorescent protein (EYFP) or Citrine images and the enhanced cyan fluorescent protein (ECFP). Then $\Delta R/R$ was calculated as described above.

3.7.4 Signal-to-Noise-Ratio

For the calculation of the SNR, five time points surrounding the peak of the average response were selected per each individual bouton. The mean and the standard deviation (SD) of the mean were calculated for all boutons. The SNR was calculated by dividing the mean amplitude by the SD (Reiff et al., 2005).

4 Results

4.1 Analyzed Indicators and Transgenic Flies

One main goal of this study was to characterize and compare different genetic indicators of neural activity *in vivo*. The cDNAs encoding nine different indicators were subcloned into the pUAST vector containing a UAS site and the mini white gene (Brand and Perrimon, 1993). Transgenic DNA was inserted into the *Drosophila* genome by P-element-mediated germ-line transfection (Spradling and Rubin, 1982). In addition, three fly lines, UAS-SpH, UAS-YC 2.0, and one additional UAS-GCaMP 1.3 were obtained from other laboratories (see Material and Methods) and included in the analysis.

Transgenic flies were generated that express the single chromophore indicators Camgaroo-1 and Camgaroo-2 (Griesbeck et al., 2001), respectively, and the circular permuted single chromophore indicators GCaMP 1.3 (Nakai et al., 2001), GCaMP 1.6 (Ohkura et al., 2005), Flash Pericam and Inverse Pericam (Nagai et al., 2001). As double chromophore indicators we chose Yellow Cameleon indicators 2.3 and 3.3 (Griesbeck et al., 2001) and compared them to the original Yellow Cameleon 2.0 (Miyawaki et al., 1997) and TNL 15. TNL 15 also contains of two chromophores and has a calcium-binding site that is derived from chicken troponin C (Heim and Griesbeck, 2004).

Direct comparison of these indicators and their properties has not been not possible so far because they were used in different animals and cell types. Three different indicators were tested in mice and fish (Hasan et al., 2004) and rigorously analyzed in transfected mammalian brain slices (Pologruto et al., 2004). Many of the presently available indicators, however, have not been used *in vivo* so far. To determine the fluorescence properties of the various indicators *in vivo* under reproducible and well controlled conditions we analyzed the performance of 10 genetically encoded calcium indicators and SynaptopHluorin in presynaptic boutons of the *Drosophila* larval neuromuscular junction (NMJ).

Indicator expression was achieved by crossing the UAS-indicator lines to the pan neuronal driver line elav[C155]-GAL4 leading to the expression of the indicators in the entire nervous system (Lin and Goodman, 1994). The specificity of the GAL4-driver allowed us to optically isolate structures of interest such as dendrites, axons, and

presynaptic terminals and to characterize the exhibited fluorescence changes of the different indicators on the level of individual boutons *in vivo.*

4.1.1 Expression

In Figure 13, a section of a larval hemisegment of a YC 3.3 expressing animal is shown (Reiff et al., 2005). Two photon imaging reveals the specificity of elav [C155]-GAL4-driven UAS-indicator expression in the larval nervous system. The expression is exclusively directed to axons and NMJs. For each line the expression pattern was verified in the way that larvae were dissected and the expression level of protein was confirmed by fluorescent microscopy.
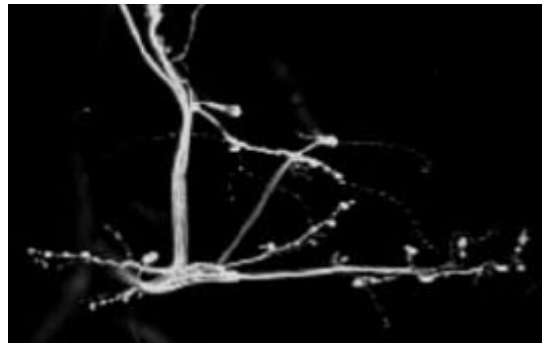
Figure 13: Analysis of the expression level in newly generated UAS-indicator flies. The NMJ of an YC 3.3-expressing larva is shown. Figure from Reiff et al. (2005).

In some indicators, namely GCaMPs and Camgaroos, fluorescence at rest is low and sometimes not visible at all. The most plausible explanation of this result is the complete disruption of the chromophore when no calcium is bound.

The effectiveness of GAL4-driven indicator expression was determined by crossing all newly generated UAS-indicator lines to the GAL4 driver (Lin and Goodman, 1994) and subsequent antibody staining with a fluorescent antibody (Alexa Fluor 488) against GFP (Figure 14, see Material and Methods). The antibody binds to the chromophore and reveals even disrupted GFP molecules. Fly lines that gave rise to sufficiently strong expression were selected for the imaging experiments.

The efficacy of GAL4-driven indicator expression varied strongly between individual lines, presumably depending on the different locations of the P-element on the chromosomes influenced by flanking regions (Spradling and Rubin, 1983). In Figure

14, antibody stainings of three different GCaMP 1.6 fly lines are shown. Several circular permuted indicator lines, however, did not show noteworthy expression at all.
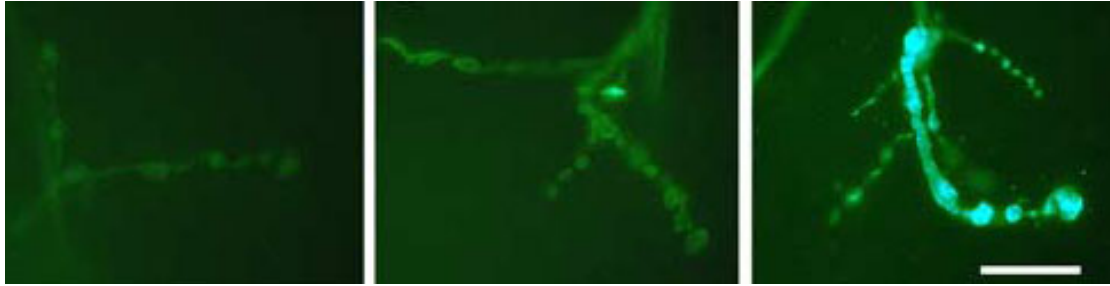

Figure 14: Anti-GFP stainings of three different GCaMP lines at the larval NMJ. Scale bar: 20μm, Figure from Reiff et al. (2005).

For the analysis of the performance of the indicators at the NMJ sufficient fluorescence intensities are required. Indicator expression level could be controlled in many ways: using lines with a single indicator copy but different expression level (Figure 14), using lines with multiple indicator copies or rendering experimental flies heterozygous or homozygous for indicators and/or the *GAL4* gene.

Lines with different expression levels were used to analyze the influence of the amount of indicator protein on the kinetics and the SNR (4.5.2, Figure 30).

4.1.2 Experimental Procedure

Figure 15 shows the analysis of indicator performance in the larval NMJs. Electrical stimulation of up to 80 Hz mimicked the natural activity of this synapse (Barclay et al., 2002). The temporal order of the applied stimulus paradigms at different frequencies was changed randomly (for details see Material and Methods). The stimulus was applied for 2.2 s starting one second after onset of image acquisition and fluorescence excitation. False color images for a ratiometric indicator display changes in ΔR/R that are observed at the junction (Figure 15 D). Only boutons that innervate muscle 6/7 in abdominal segment 2 or 3 were analyzed, allowing data analysis under similar conditions for every indicator (Figure 15 A, C).

During the stimulation period, double chromophore indicators always showed negative fluorescence changes in the CFP channel and positive changes in the YFP or citrine channel, indicating that the observed fluorescence changes were not

attributable to motion, bleaching, or other artifacts (Figure 15 E). The predominant number of the analyzed boutons was located in the central part of the NMJs and showed quite uniform fluorescence changes which is in accordance with a previous study (Reiff et al., 2002). We found ~ 10% signal change when $\Delta R/R$ (Figure 15 E, top graph) was calculated compared with only ~ 5% $\Delta F/F$ in the individual channels (Figure 15 E, bottom graph). The background was free of fluorescence changes (signals from the background regions in Figure 15 A are represented by the pink traces in Figure 15 E) if no out-of-focus presynaptic structures were included. Steady state, the fluorescence change to a static calcium concentration, was reached by most indicators at high stimulations.
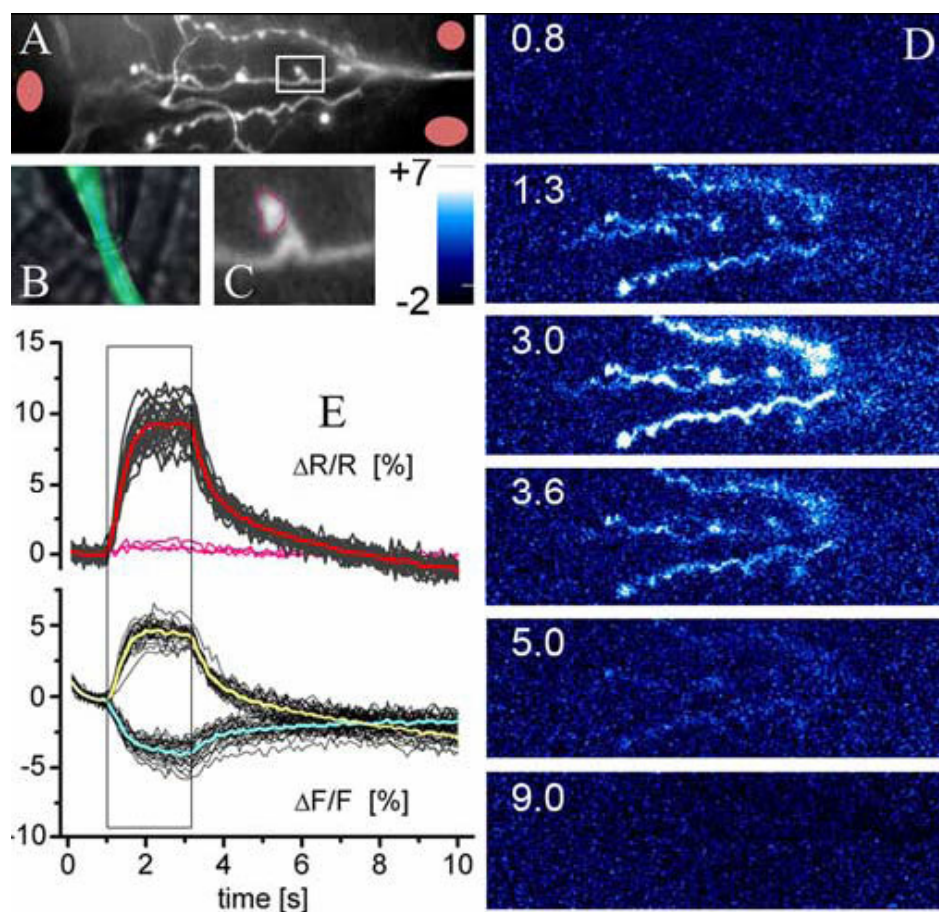
Figure 15: Analysis of indicator performance at the sub cellular level in larval NMJs. A: The raw image of an NMJ at muscle 6/7 shows expression of YC 2.0. B: The segmental nerve that innervates the relevant axon was placed in a stimulation electrode. C: Close-up of the bouton (marked by the white box in A) D: False-color images encoding $\Delta R/R$ during the experiment. The nerve was stimulated at 80 Hz. Active boutons can be detected time-locked to the synaptic stimulation. E: Analysis of the fluorescent changes in individual boutons (black traces). Mean $\Delta F/F$ of CFP and YFP is plotted in cyan and yellow, respectively. Mean $\Delta R/R$ is shown in red. Figure from Reiff et al. (2005).

4.2 In Vivo Measurements of Genetic Calcium Indicators and SpH

Ten different genetically encoded calcium indicators and the pH-dependent indicator of vesicle fusion SpH were analyzed and compared in an *in vivo* situation. At this point, these indicators cover almost the complete set of genetically encoded indicators available. *In vitro* analyses show affinities for calcium from a K_d of ~ 0.1 to ~ 11 µM. All these indicators were expressed in the cytosol of the cell except SpH that is bound to the membrane within vesicles by VAMP-2.

In Table 3 visibility at rest and the *in vivo* performance of the tested genetically encoded indicators are presented. Fluorescence changes at 40 and 80 Hz and the time constants for rise and decay are listed in the table.

indicator	visibility at rest	change at 40 Hz (%)	change at 80 Hz (%)	τ_{rise} at 40 Hz	τ_{decay} at 40 Hz	τ_{rise} at 80 Hz	τ_{decay} at 80 Hz
YC 2.0	high	7.8	11.6	1.52	0.58/2.52	0.53	0.47/3.39
YC 2.3	high	5.5	9.4	0.72	0.53/3.48	0.35	0.53/3.48
YC 3.3	high	5.9	9.6	1.07	0.62/3.02	0.42	0.51/2.84
TNL 15	high	6.9	8.2	0.49	1.29	0.31	1.29
Camg-1	very low	-	-				
Camg-2	moderate	-	-				
FP	none						
IP	high	-6.7 [*]	-8.9 [*]	0.61	0.90	0.28	0.98
GCaMP 1.3	moderate	8.2	16.1	0.84	0.46	0.31	0.48
GCaMP 1.6	high	6.2	17.8	0.56	0.34	0.16	0.35
SpH	moderate	9.1	16.5	4.33	did not return to baseline by the end of experiment	2.49	did not return to baseline by the end of experiment

Table 3: Visibility at rest and the *in vivo* performances of the tested genetically encoded indicators. The fluorescence change at 40 and 80 Hz and the time constants for rise and decay are stated. *: Calculated after subtraction of fluorescence intensities without stimulus (Figure 17).

The results shown in Table 3 are described in detail in the following chapters. Some of these data were measured and analyzed by D. Reiff.

4.3 Superecliptic SpH

SpH allows the measurement presynaptic vesicle fusion based on differences in pH between the intravesicular lumen and extracellular cleft (see Introduction).

SpH is not fluorescent at pH lower six (Miesenbock et al., 1998), it was supposed that fluorescence was not visible at rest. Individual boutons, however, could be identified indicating that a small pool of vesicles releases spontaneously at the *Drosophila* NMJ. Axons were not visible at all.

We found that SpH is a very reliable indicator of neural activity; however, kinetics were slow compared to most genetically encoded calcium indicators. Analyzing boutons revealed 9.1 % ΔF/F at stimulation at 40 Hz and a single exponential time constant for rise of τ_{rise} = 4.3 s. At 80 Hz a fluorescence change of 16.5 % could be detected with a τ_{rise} = 2.5 s. The fluorescence did not reach a plateau during either stimulation procedures. During 10 seconds of imaging SpH fluorescence did not return to baseline suggesting a slow endocytosis of released vesicles (Figure 16). For this experiment three different junctions of three different animals with a total number of 51 boutons were analyzed.
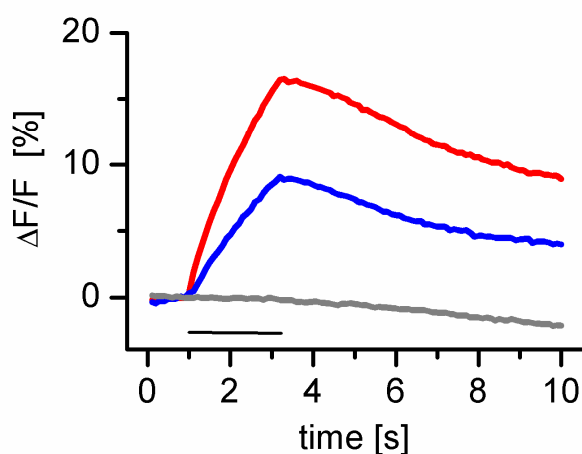

Figure 16: Fractional fluorescence change ΔF/F [%] of SpH. Vesicle fusion was evoked by electrical stimulation at 0 (gray), 40 (blue) and 80 Hz (red). The black bar indicates the stimulation period.

4.4 Calcium Indicators Based on One Chromophore

4.4.1 Inverse Pericam

In contrast to all other indicators tested, Inverse Pericam shows a decrease in fluorescence during calcium binding (Nagai et al., 2001). At resting potential high fluorescence could be detected. With onset of illumination, however, it bleached with a fluorescence loss of 20% $\Delta F/F$ within the first second. Because the initial time course before stimulus onset matched perfectly it was possible to subtract the control movies from the stimulus movies (Figure 17). Then presynaptic activity could be detected more clearly and was time locked to evoked neuronal activity.

From 40 to 80 Hz the maximum $\Delta F/F$ increased from ~ 6.7 to only 8.9 %. At the same time, τ_{rise} was smaller at 80 Hz indicating that the increase of calcium in the presynaptic terminal was sufficient to partially saturate IP (see also Table 3). At 40 Hz stimulation a fast rise could be observed (τ_{rise} = 610 ms) while τ_{decay} was slightly slower (τ_{decay} = 900 ms, see Table 3). Clear saturation of IP is suggested by the reported *in vitro* K_d of 200 nM (Nagai et al., 2001). The moderate saturation found in our measurements is in better accordance with the reported K_d of 900 nM in brain slices (Pologruto et al., 2004).

In total 39 boutons of three different animals were analyzed to obtain these traces.
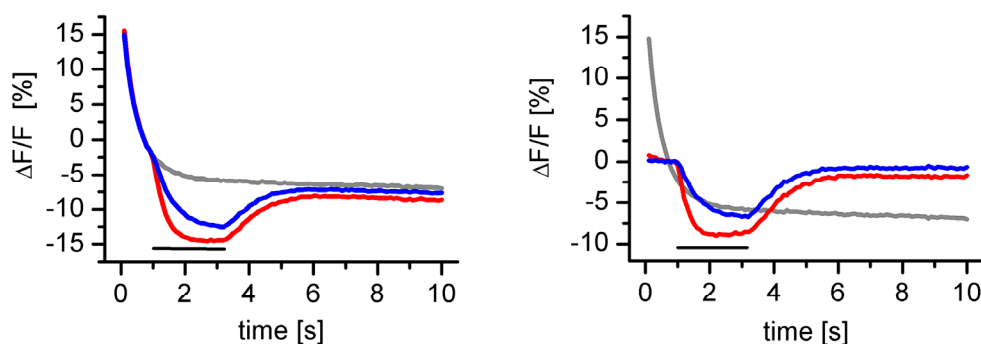

Figure 17: Fractional fluorescence change $\Delta F/F$ [%] of Inverse Pericam. Shown are the mean traces of fluorescence responses with stimulation at 0 (gray), 40 (blue) and 80 Hz (red). Notice the strong bleaching in the beginning with and without stimulation (left) while on the right the mean traces without stimulation were subtracted from the stimulated traces.

4.4.2 Camgaroo Variants

4.4.2.1 Camgaroo-1

Camgaroo-1 fluorescence at rest was almost not detectable. Many animals were examined for the expression level, but only in two animals NMJs could be identified with a total number of 22 boutons. At 40 Hz stimulation no noticeable fluorescence change could be observed whereas at 80 Hz there was evidence of a very low fluorescence increase during the stimulation period (Figure 18). The SNR, however, was too low to allow a reasonable statement about fluorescence changes.
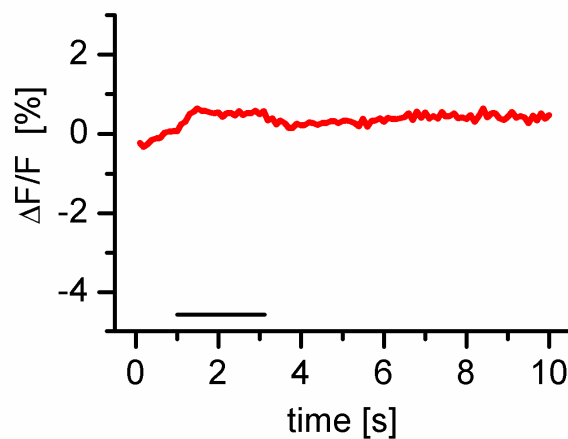
Figure 18: Fractional fluorescence change ΔF/F [%] of Camgaroo-1. Shown is the mean trace of fluorescence responses with stimulation at 80 Hz (red).

4.4.2.2 Camgaroo-2

Camgaroo-2 has a higher fluorescence at rest and was therefore easier to detect than Camgaroo-1 (Griesbeck et al., 2001). However, it did not perform better than Camg-1. This was unexpected as *in vitro* studies of Baird et al. (1999) and Griesbeck et al. (2001) reported a high fluorescence change up to 700 %. The reason could be the high K_d. After raising the calcium in the extracellular solution to 10 mM, however, no higher signals could be detected. Instead, strong degradation of the signal was found (Figure 19, gray trace).
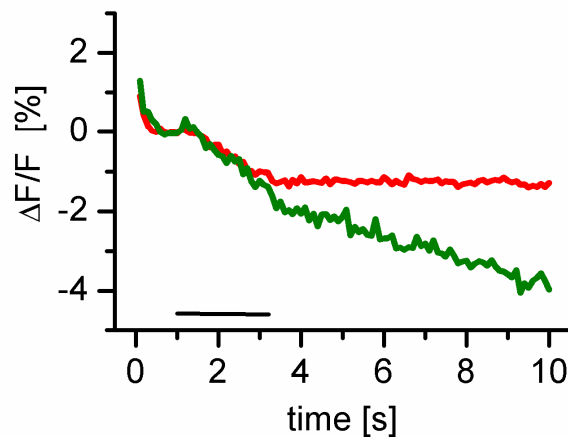
Figure 19: Fractional fluorescence change ΔF/F [%] of Camgaroo-2 with 1.5 mM (red) and 10 mM (green) extracellular Ca^{2+}. Shown are the mean traces of fluorescence responses with stimulation at 80 Hz.

4.4.3 Flash Pericam

In dissected larvae, fluorescence of Flash Pericam (FP) could not be detected at the NMJ at all. After staining with an anti-GFP-Alexa 488 antibody (see Materials and Methods), however, the protein could be visualized (Figure 20). The *in vitro* K_d for calcium is in the range of ~ 700 nM and high fluorescence changes (~ 800 %) were reported by Nagai et al. (2001). In these experiments it was focused to the cleft between muscle 6 and 7 and the nerve was stimulated as usual. No signal and no increase in fluorescence during stimulation could be detected in any of the junctions.

Figure 20: Anti GFP Alexa 488 staining of a NMJ of an animal expressing Flash Pericam (FP).

4.4.4 GCaMP Variants

4.4.4.1 GCaMP 1.3

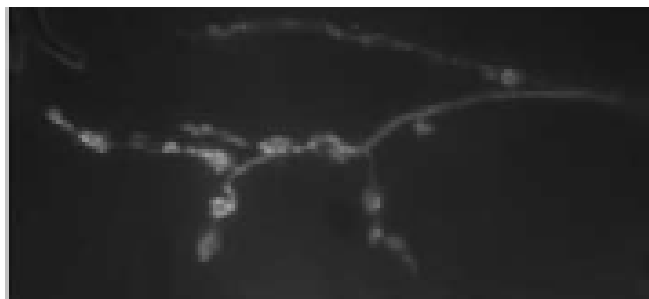For the analysis of GCaMP 1.3, six NMJs from five animals with a total number of 74 boutons were evaluated. In most cases, two copies of UAS-GCaMP 1.3 (on second and third chromosome) had to be used to result in clearly visible NMJs at rest.

Before onset of stimulation strong bleaching was observed (Figure 21). At 80 Hz stimulation the signal exhibited a peak response and did not clearly settle to a steady state, a fact that was still observed after applying a double exponential bleach correction (Figure 22 and Figure 29). This is in contrast to the reported time course of presynaptic calcium in this preparation measured with synthetic dyes during prolonged stimulation periods (Macleod et al., 2002; 2004). At stimulations with 40 Hz no such peak is visible. Looking at both stimulation paradigms, however, a persistent undershoot was noticeable after the offset of the stimulus (Figure 21). This undershoot exceeded the bleaching in the control movies and indicates increased bleaching of the fluorophore in the fluorescent state. From 40 to 80 Hz the maximum $\Delta F/F$ increased from 8 to 16 %, a twofold increase that can also be obtained after background subtraction and bleach correction (Figure 22).

As the K_d for GCaMP 1.3 is 235 nM *in vitro*, saturation of the indicator could be expected in these experiments referring also to the paper from Macleod et al. (2004) where calcium concentrations of nano- to micromoles are assumed in *Drosophila* NMJ boutons under these conditions. Time constants were calculated of $\tau_{rise} = 840$ ms and $\tau_{rise} = 310$ ms and $\tau_{decay} = 460$ ms and $\tau_{decay} = 480$ ms at 40 and 80 Hz, respectively.

Figure 21: Fractional fluorescence changes ΔF/F [%] of GCaMP 1.3. Shown are the mean traces of fluorescence responses with stimulation at 0 (gray), 40 (blue) and 80 Hz (red).

Figure 22: Influence of bleach correction on the fractional fluorescence change ΔF/F [%] of GCaMP 1.3 at different stimulus frequencies. Black traces: ΔF/F [%] after background subtraction. Red traces: double exponential bleach correction by deleting the time of stimulation before fitting. Blue trace: bleach corrected fluorescence change. Figure from Reiff et al. (2005).

4.4.4.2 GCaMP 1.6

GCaMP 1.6 is a derivative of GCaMP 1.3, carrying an additional 64 amino acids at its N terminus and two amino acid changes within the wild-type GFP backbone. These modifications improved visibility at rest (Table 3) with only a single copy of the indicator in the fly genome required (Ohkura et al., 2005). At the stimulation frequency of 40 Hz a maximum fluorescence change of 6 % could be detected whereas 80 Hz stimulation showed an almost threefold increase up to 17 % (Figure 23). In the beginning, before stimulation onset, GCaMP 1.6 showed strong bleaching. During stimulation, a clear peak without steady state appeared and after offset of stimulation a pronounced undershoot could be measured. As shown in Figure 23, the undershoot at 80 Hz stimulation is only slightly more pronounced than at 40 Hz stimulation. Saturation was expected for the GCaMPs in the experiments because calcium changes of many hundred nanomoles up to the micromolar range can be expected in the *Drosophila* boutons under these conditions (Macleod et al., 2004), and K_d values of 235 and 146 nM have been reported for GCaMP 1.3 (Nakai et al., 2001) and GCaMP 1.6, respectively, when measured *in vitro*.

The kinetics of this indicator were fast; we calculated at 40 Hz stimulation $\tau_{rise} = 560$ ms, $\tau_{decay} = 340$ ms and at 80 Hz stimulation $\tau_{rise} = 160$ ms and $\tau_{decay} = 350$ ms (Table 3). In total 54 boutons from four different junctions from three animals were analyzed.

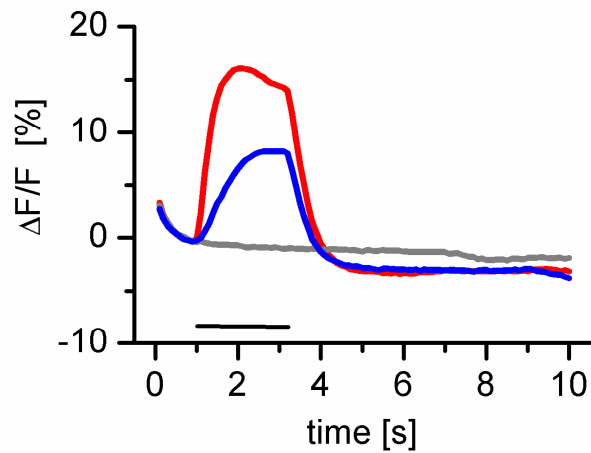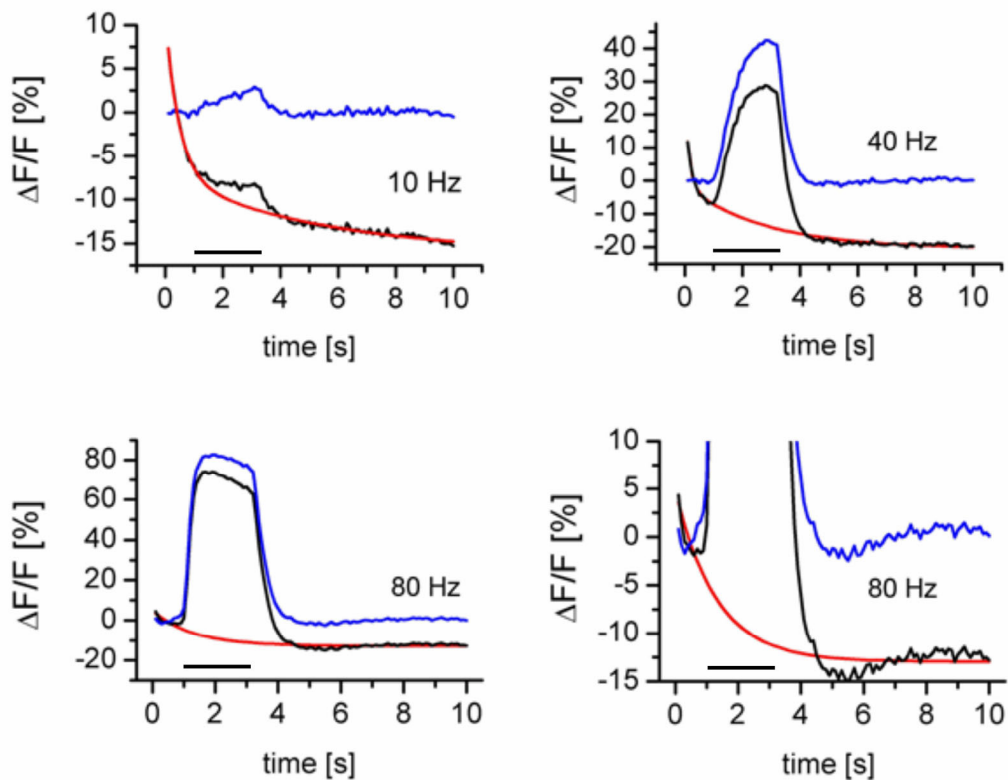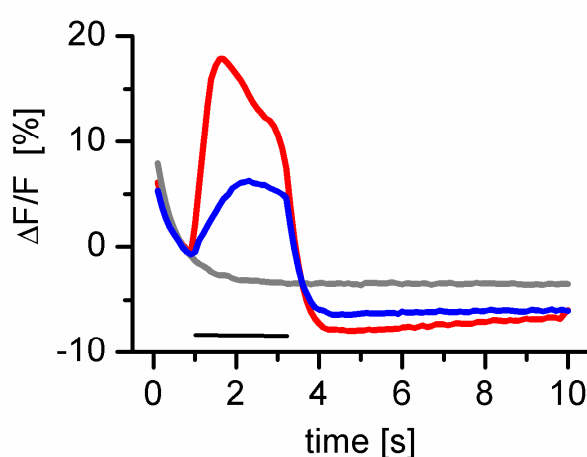**Figure 23: Fractional fluorescence change ΔF/F [%] of GCaMP 1.6.** Shown are the mean traces of fluorescence responses with stimulation at 0 (gray), 40 (blue) and 80 Hz (red).

4.5 Calcium Indicators Based on Two Chromophores

The previous chapters dealt with indicators based on a single chromophore. The following section deals with indicators composed of two chromophores, namely the Yellow Cameleons and the Troponeons.

4.5.1 Yellow Cameleon 2.0

Yellow Cameleon 2.0 (Miyawaki et al., 1997) performed well in the experiments at the larval NMJ. Fluorescence at rest was high and therefore the examinated boutons easily visible. For the experiments 44 boutons of four NMJs in two animals were tested. At 40 Hz stimulation a maximum ratio change of 7.8 % was found whereas at 80 Hz stimulation a maximum $\Delta R/R$ of 11.6 % was reached (Figure 24). No steady state was observed at 40 Hz stimulation. The time constants for YC 2.0 showed $\tau_{rise} = 1520$ ms and $\tau_{decay} = 580$ and 2520 ms. The fluorescence change reached baseline with the mentioned slow time course, namely at the end of recording after 10 seconds. Although YC 2.0 lacks some improvements that were made in YC 2.3 and YC 3.3 (e.g. pH stability and brighter fluorescence (Griesbeck et al., 2001)) no deficits could be observed compared to these indicators. In fact, fluorescence without stimulation was even more stable (Figure 24, light gray line). Also during the time before stimulus onset no significant bleaching was observed.
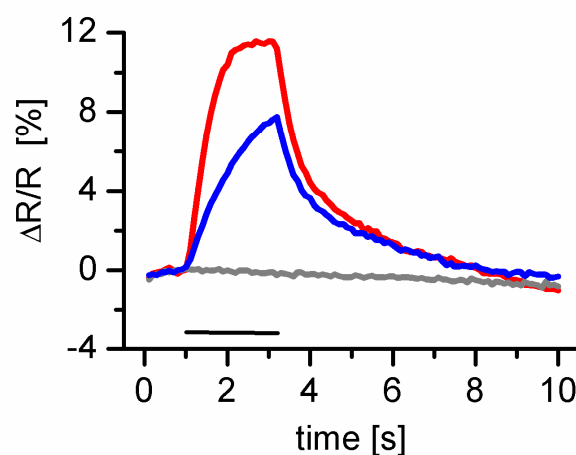

Figure 24: Fractional fluorescence change $\Delta R/R$ [%] of YC 2.0. Shown are the mean traces of fluorescence responses with stimulation at 0 (gray), 40 (blue) and 80 Hz (red).

4.5.2 Yellow Cameleon 2.3

Yellow Cameleon 2.3, an improved version of YC 2.0 with brighter fluorescence and pH stability showed a reasonably stable fluorescent ratio before the stimulus onset. During stimulation slight bleaching could be observed, whereas the control revealed bleaching of about 1.5 %. At 80 Hz stimulation the signal increased to a plateau (with slight bleach), while at 40 Hz steady state was not reached. The time constant for the rise τ_{rise} was faster than in YC 2.0, namely 720 ms for 40 Hz and 350 ms for 80 Hz. A maximum $\Delta R/R$ of 5.5 % and 9.4 %, respectively, was reached. This non-linear increase in $\Delta R/R$ provided a hint that the indicator was beginning to saturate. The time constants for the decay at both stimulation paradigms were rather slow with $\tau_{decay} =$ 530 ms and 3480 ms for 40 Hz stimulation, and 530 ms and 2370 ms for 80 Hz stimulation, respectively. The time course for decay could only be fit by a double-exponential function (Table 3). For the experiment plotted in Figure 25 81 boutons of five NMJs of three different animals were analyzed.
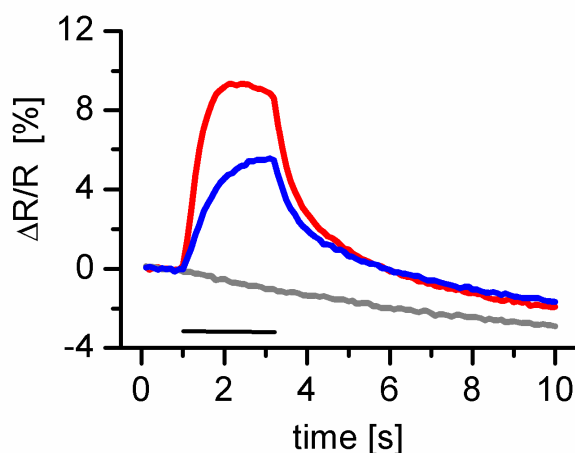

Figure 25: Fractional fluorescence change $\Delta R/R$ [%] of YC 2.3. Shown are the mean traces of fluorescence responses with stimulation at 0 (gray), 40 (blue) and 80 Hz (red).

4.5.3 Yellow Cameleon 3.3

Yellow Cameleon 3.3 is another improved version of Yellow Cameleon 2.0 with a lower affinity to calcium than YC 2.3 (Griesbeck et al., 2001). In the experiments at

the fly NMJ, however, it did not show superior performance. It showed a stable fluorescence ratio before stimulus onset and only - 1.5 % signal change during the control movie. This suggested that YC 3.3 signals were only moderately reduced by bleaching.
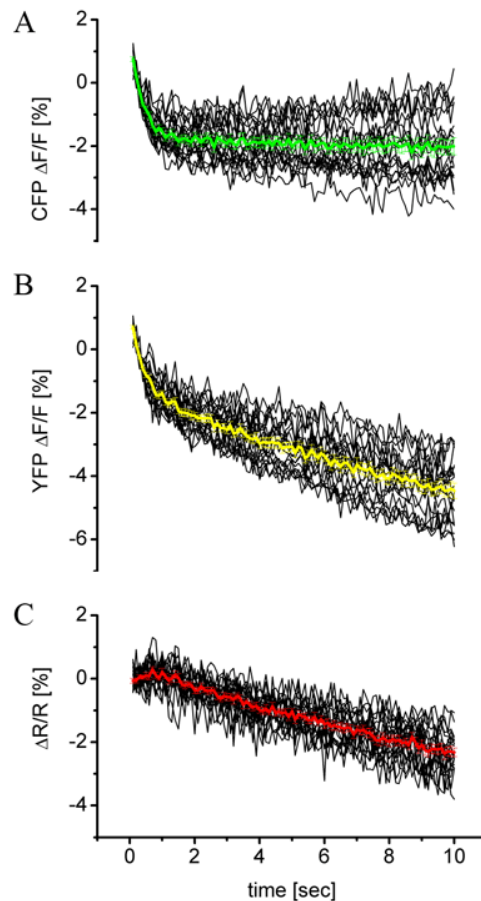
Figure 26: The relative fluorescence change ΔF/F of CFP (A) and Citrine (B) and the relative ratio change ΔR/R (C) calculated for 20 boutons of a YC 3.3-expressing larval NMJs at rest.

In Figure 26 the individual ΔF/F of CFP (A) and YFP (B) were plotted showing different bleaching of the two chromophores. CFP is more stable compared to Citrine (Figure 26 A and B). Consequently ΔR/R (C) shows a negative change over time that is, however, reduced to half by calculating the ratio.

At 40 Hz, a plateau was almost reached at the end of the stimulation, whereas stimulations at 80 Hz showed a roughly stable steady-state level (Figure 27). The rise at 40 Hz was relatively slow with τ_{rise} = 1070 ms (Table 3). The maximum amplitude reached 5.9 % and 9.6 %, respectively. After the stimulation period the signal decayed slowly with τ_{decay} = 620 ms and 3020 ms for 40 Hz and 510 ms and 2840 ms for 80 Hz.

The decay time was split into a fast and a slow component and could be fit by a double-exponential function.

Figure 27: Fractional fluorescence changes ΔR/R [%] of YC 3.3. Shown are the mean traces of fluorescence responses with stimulation at 0 (gray), 40 (blue) and 80 Hz (red).

4.5.4 TNL 15

TNL 15, the only indicator based on troponin C instead of calmodulin as the calcium sensor, showed a very stable fluorescence signal in the control (Figure 28, gray line) and before stimulus onset. 40 Hz stimulation gave the fastest rise of all indicators tested with τ_{rise} = 490 ms. At 80 Hz stimulation the signal reached a stable steady-state (Figure 28, red line). Increasing the stimulation from 40 to 80 Hz increased the maximum ΔR/R only moderately from 6.9 to 8.2%, indicating that the indicator is close to saturation. The time constant for decay was found to be τ_{decay} = 1290 ms (Table 3, fit by a single exponential function) for both stimulation paradigms. After stimulation the traces returned almost back to baseline without any bleach correction (Figure 28). In total 64 boutons of six NMJs of four animals were analyzed.
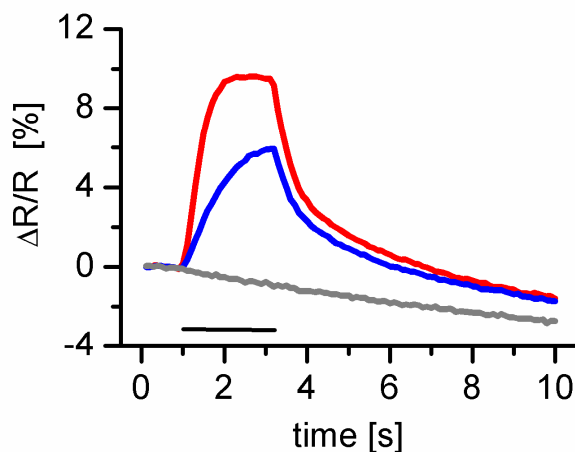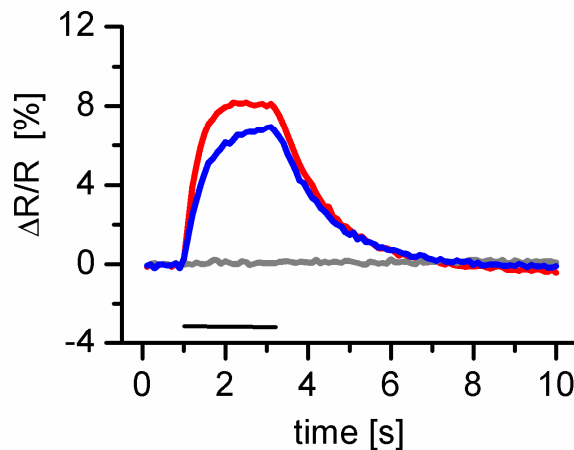
Figure 28: Fractional fluorescence changes ΔR/R [%] of TNL 15. Shown are the mean traces of fluorescence responses with stimulation at 0 (gray), 40 (blue) and 80 Hz (red).

4.6 Signals Over a Wide Range of Neural Activity

The fractional fluorescence changes in GCaMP 1.3 and YC 3.3 were compared in response to neural activity at different rates (5, 10, 20, 40, and 80 Hz) and the corresponding SNR was calculated. 50 boutons were analyzed per stimulus frequency in each genotype. The background was subtracted, and GCaMP 1.3 signals were additionally corrected for bleaching. GCaMP 1.3 amplitudes increased fairly linear over the entire stimulus range ($\Delta F/F$ = 0.7, 2.7, 12.7, 39.8 and 82.3 %), whereas YC 3.3 amplitudes increased linearly only in the lower stimulus range and sublinearly in the upper range ($\Delta R/R$ = 1.5, 5.5, 14.9, 26.7 and 31.0 %), indicating saturation of the probe. Because the response of YC 3.3 did not fully reach steady state during the stimulation period, the respective graph may slightly underestimate the true saturation characteristics of this probe. In simulations (data not shown) this effect was proven not to be relevant for the interpretation of the data. For both indicators, the SNR depended on the action potential frequency in a way that followed the increase in the fluorescence amplitudes, suggesting basically constant noise in the measurements. Thus, at high activity rates of 80 Hz, GCaMP 1.3 showed a much higher SNR compared with YC 3.3 (6.3 and 3.8, respectively). At 40 Hz both indicators showed similar SNR (3.3). However, in the lower activity range, YC 3.3 was slightly superior:

at 5, 10, and 20 Hz, we calculated for GCaMP 1.3 and YC 3.3 an SNR of 0.2, 0.9, 2.6 and 0.5, 1.4, 3.1, respectively.
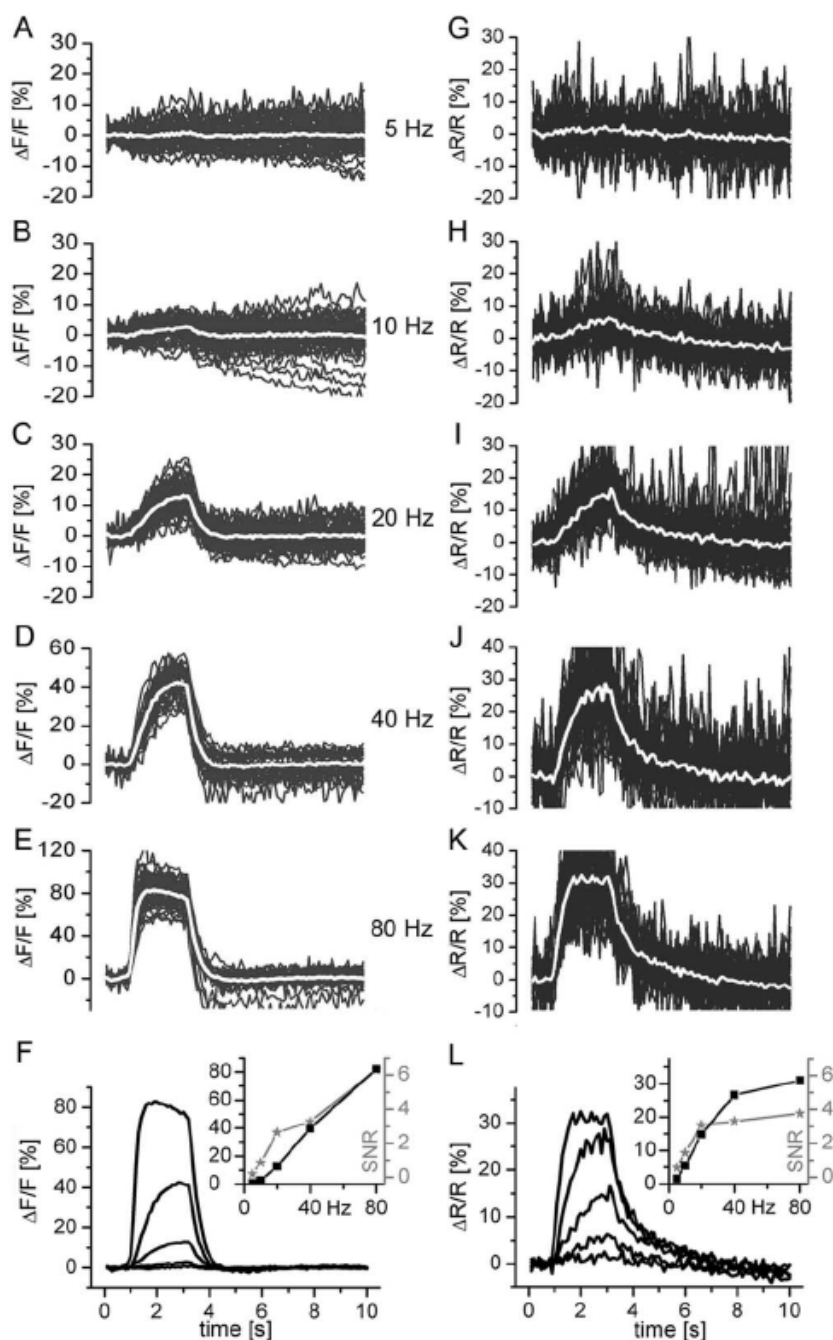
Figure 29: Linearity and SNR of fluorescence signals at different stimulation frequencies (A: 5, B: 10, C: 20, D: 40 and E: 80 Hz). Left: GCamP 1.3. Right: YC 3.3. Gray traces: signals from individual boutons (approx. 50 boutons at each stimulation frequency). White traces: corresponding average. Signals were corrected for the background fluorescence and GCaMP 1.3 signals were also corrected for bleaching. In F and L the mean fractional fluorescence changes are shown. In the inset, the peak amplitudes and SNR are given for individual stimuli. Figure from Reiff et al. (2005).

4.7 Kinetics and SNR Depend on the Expression Level

Two different YC 2.3 lines were compared. Line "5b" is a weakly (Figure 30, A) and "30l" (Figure 30, B) a strongly expressing line with a fourfold difference in expression level (Figure 30, D: YFP [a.u.]). Mean $\Delta R/R$ (white trace) and $\Delta R/R$ for every single bouton (gray traces) were plotted at stimulation of 40 Hz for each of the fly lines. For the weaker expressing indicator line, 71 boutons of six animals and for the higher expressing fly line, 94 boutons of seven animals were analyzed. Background fluorescence was subtracted as described in Materials and Methods. Comparison of A and B shows that the weakly expressing animals had a much lower SNR due to the low amount of indicator in the cell (see also D: gray squares). In Figure 30 C, $\Delta R/R$ of the two lines was plotted to compare the maximum amplitudes and the kinetics. The amplitudes were almost identical (16.94 ± 0.78 % for 5b and 16.68 ± 0.40 % for 30l). The kinetics, however, differed in such a way that the lower expressing line had a faster rise (τ_{rise} = 594 ± 58 ms) than the strong-expressing animals (τ_{rise} = 909 ± 48 ms). Figure 30 D gives a summary of the obtained results. As the actual concentration of the indicator expressed in the animal was unknown, only the relative level of Citrine expression could be determined after background subtraction (dashed square: YFP expression in a.u.). Maximum $\Delta R/R$ in both lines is almost the same (black squares) indicating that the expression level has no influence on the amplitudes. SNR differed from 2.58 to 4.30 for 5b and 30l, respectively (gray square). For calculation of SNR see Material and Methods.
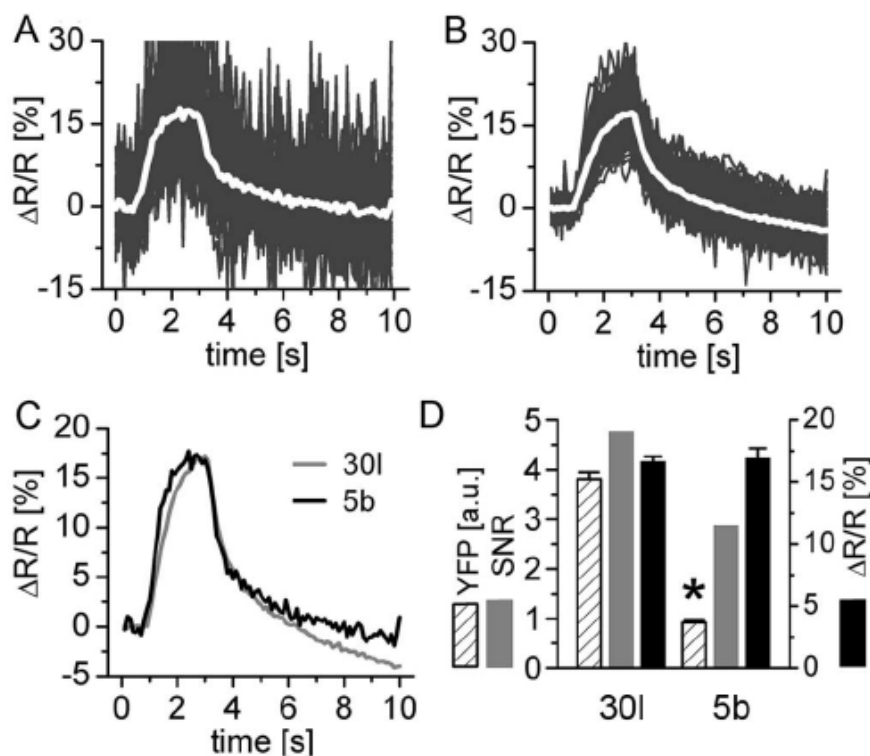
Figure 30: Kinetics and SNR of two UAS-YC 2.3 lines expressing different amounts of indicator (stimulations at 40 Hz). A: YC 2.3 5b (weakly expressing fly line), B: YC 2.3 30l (strongly expressing fly line). White lines: mean $\Delta R/R$ amplitudes. Gray traces: $\Delta R/R$ of individual boutons. C: comparison of mean $\Delta R/R$ of the two lines. D: quantification of the expression level (YFP intensity after background subtraction), SNR and mean $\Delta R/R$. Figure from Reiff et al. (2005).

4.8 Dynamic Properties of Genetically Encoded Indicators

Three different sensors were chosen to examine the dynamic properties of genetically encoded indicators of neural activity. Three successive action potential volleys were applied to investigate the signal dynamics of SpH, GCaMP 1.3 and YC 3.3 (80 Hz for 1 s, separated by 2 s). Background was not subtracted.

The traces in Figure 31 show that there was enough time for the GCaMP 1.3 fluorescence to reach its maximum level and undershoot (τ_{decay} = 480 ms, Table 3) during the interstimulus periods and to reliably report each AP volley. There was basically no reduction in the $\Delta F/F$ amplitudes of the individual peaks.

YC 3.3 in contrast, decayed much more slowly and therefore displayed a superposition of the following fluorescence change on the previous (Figure 31, B). However, it exhibited no increment of the following amplitudes due to saturation and bleaching effects.

A clear superposition of the fluorescent signal was found for SpH (Figure 31, C) which did not reach baseline by the end of the stimulus period.
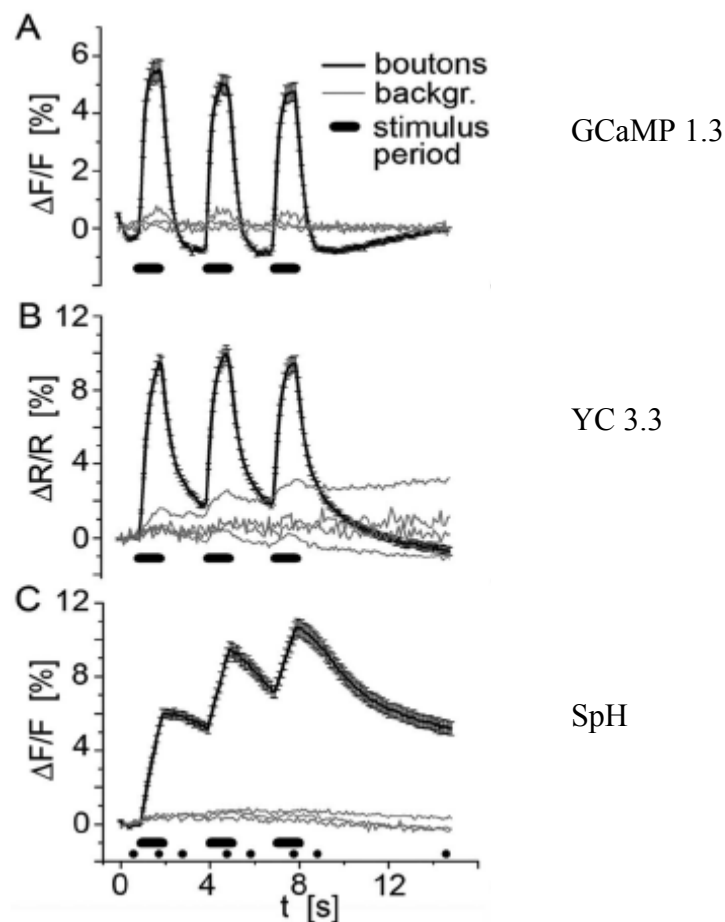
Figure 31: Fluorescence changes in response to three successive action potential volleys. Three consecutive AP volleys (80 Hz/1 s; horizontal black bars) were evoked, spaced by 2 s at rest and 7 s after the last stimulus. The fluorescence change is plotted as mean ΔF/F (A, C) or mean ΔR/R (B) (±SEM) for the following numbers of animals, NMJs, and boutons: A: 3, 3, and 36; B: 4, 4, and 61; and C: 3, 3, and 44, respectively. Images were taken at a rate of 10 Hz for 15 s. Figure from Reiff et al. (2005).

4.9 Reproducibility of Fluorescence Changes

For most investigations of neuronal calcium dynamics, it is important to reliably image the same anatomical structure in a series of experiments. The reproducibility of the fluorescence changes evoked by 50 Hz stimulation for 2.2 s was investigated by sequential imaging of NMJs in four trials. Between the trials, each NMJ was allowed to recover for 3 min. To reduce the excitation energy a neutral density filter (0.4) was

used. The calculated ratio change or fluorescence change is plotted versus time for the indicators YC 2.3 (two animals, two NMJs and 15 boutons), TNL 15 (three animals, three NMJs and 27 boutons), GCaMP 1.3 (three animals, three NMJs and 50 boutons) and IP (two animals, two NMJs and 23 boutons) (Figure 32 A-D).

YC 2.3 and TNL 15 exhibited completely reproducible responses. With GCaMP 1.3, the fluorescence change decreased by ~ 25%, from 8.1% $\Delta F/F$ in the first run to 6.1% $\Delta F/F$ in the fourth run. GCaMP 1.3 also changed in the time course before stimulus onset from $\tau = 0$ (first run) to $\tau = 2$ s (second, third and fourth run). The other circularly permuted indicator IP consistently showed an even larger change in the shape and time course of the fluorescence signal. The strong signal degradation during the individual runs and the lack of reliable onset and decay of the fluorescence signal are clear disadvantages of this indicator when applied to living animals. These results are summarized in Figure 32 E, in which the peak amplitudes of each run were normalized to the first run. The indicators based on two chromophores did not fluctuate at all, whereas both circularly permuted indicators deviated from the fluorescence change in the first run.

The raw fluorescence of individual boutons quantified before stimulus onset in each run was almost stable from run to run for the individual indicators (Figure 32 F). Thus, fluorescence at rest fully recovered during the 3 min resting period although bleaching was visible in the GCaMP 1.3 and IP traces.

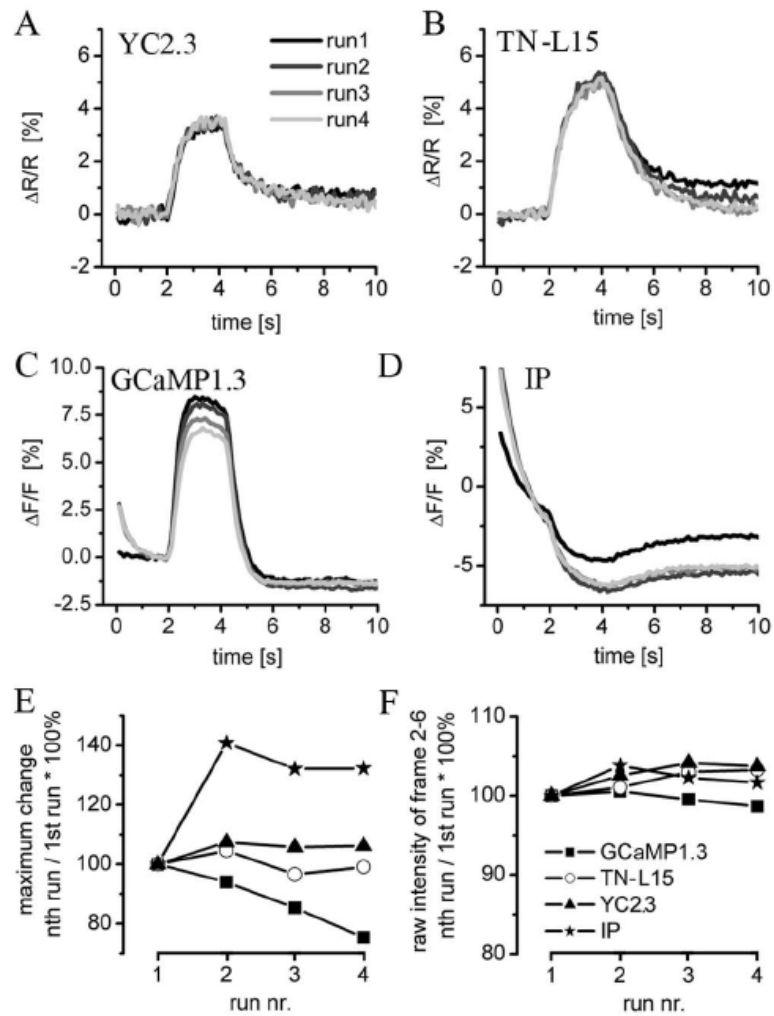**Figure 32: Reproducibility of the fluorescence changes at 50 Hz stimulation.** A: YC 2.3, B: TNL 15, C: GCaMP 1.3, D: Inverse Pericam. E: Maximum fluorescence change. The peak amplitudes of each run were normalized to the first. Five neighboring frames were averaged. F: Quantification of the raw fluorescence intensity before stimulus onset to measure bleaching from one run to the next. Figure from Reiff et al. (2005).

4.10 Indicators Tagged to the Active Zone

In all of the previous experiments indicators were expressed in the cytosol. Using the GAL4-UAS system genetically encoded calcium indicators can be directed to genetically determined populations of cells that might perform specific computational task. In addition to this property they may be targeted to subcellular compartments and defined parts of cells. This may be achieved by fusion to suitable proteins and localization sequences. A significant improvement in signal detection could be obtained if indicator localize near channels as calcium ions in principle would bind to the indicator before they dilute and disperse. As the calcium influx is highest close to calcium channels, even less sensitive indicators could detect a signal. Even small changes in local microdomains could be measured. Synapcam, for example, a Yellow Cameleon fused to the postsynaptic site by tagging to the transmembrane protein CD8 and the C-terminal PDZ interaction domain of the shaker K^+ channel (Zito et al., 1999), shows that lowest rates of activity such as single action potentials, can be detected in local microdomains (Guerrero et al., 2005).

Several indicators have been already localized to the nucleus, the endoplasmatic reticulum, mitochondria and the Golgi apparatus (Miyawaki et al., 1997; Griesbeck et al., 2001; Palmer et al., 2004). However, no functional labeling of calcium channels has been reported so far. Although membrane targeting experiments have been described before for ratiometric Pericam and Yellow Cameleons (Pinton et al., 2002; Isshiki et al., 2002), other unpublished observations and Heim and Griesbeck (2004) failed to obtain satisfactory results. As described in Heim and Griesbeck (2004) Cameleons lost their calcium sensitivity when targeted to the membrane, while indicators based on troponin C as the calcium binding site like TNL 15 still show calcium responses when expressed in HEK293 cells. Similar results were achieved by fusing the indicators to the presynaptic protein synaptobrevin and the C-terminal membrane targeting sequence of c-Ha-Ras.

To measure calcium levels close to the voltage-gated presynaptic Ca^{2+}-channels, the site of calcium influx and transmitter release (Borst and Sakmann, 1996), several indicators were targeted to the membrane and close to vesicle release sites, respectively. It is known that at these microdomains calcium concentrations are high (up to μM) and calcium changes are transient (Sinha et al., 1997; Llinas et al., 1992).

Distinguishing pre-and postsynaptic sites by targeting of fluorescent molecules gives also information about the anatomy and networking in highly complex structures as the brain. It narrows expression patterns and establishes a link to functional neuroanatomy.

As targeting sequences several membrane-associated proteins (4.10.1), some proteins involved in vesicle release (4.10.2) and a short sequence from an N-type calcium channel subunit (4.10.3) were chosen. In Figure 33 a schematic overview of all constructs that were cloned is shown.

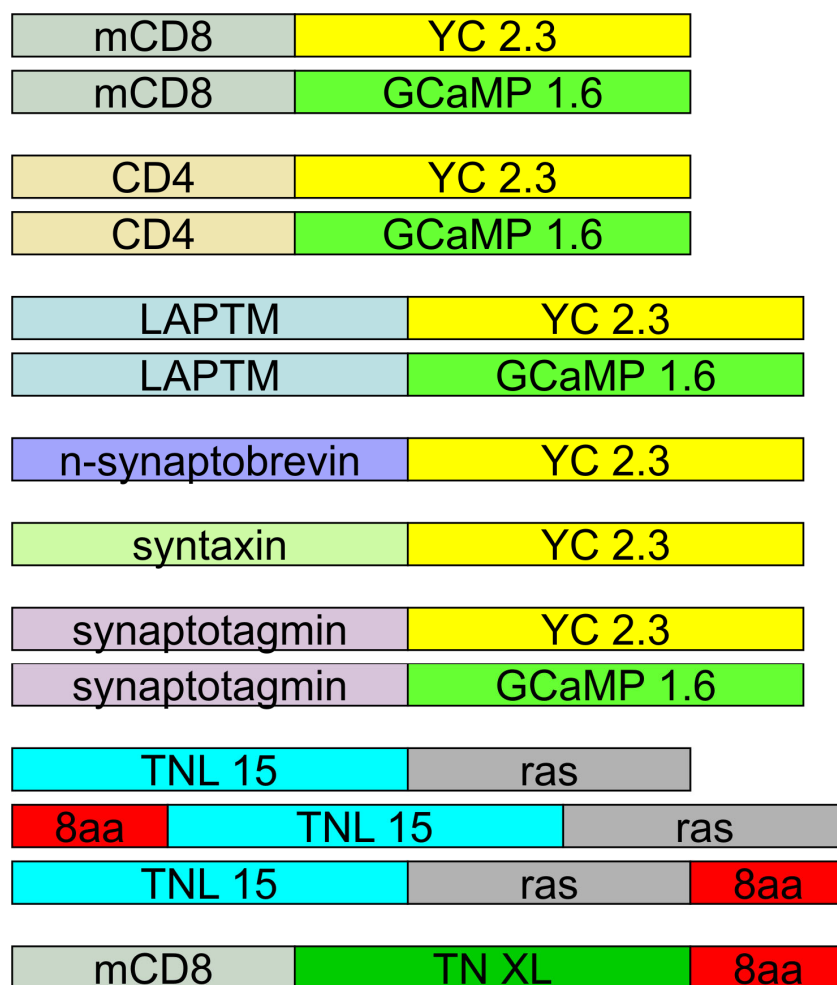**Figure 33: Schematic overview of the fusion molecules cloned.** Indicators are color-coded yellow for YC 2.3, green for GCaMP 1.6, dark green for TN XL and cyan for TNL 15. The fusion proteins are CD8, CD4, LAPTM, n-synaptobrevin, synatxin and synaptotagmin. An additional cloning strategy was to fuse the indicator to eight defined amino acids known to bind to PDZ-domains close to calcium channels (8aa, 4.10.3).

4.10.1 Targeting to Membrane-associated Proteins

Since calcium microdomains close to the membrane play important roles in vesicle release and signal transduction the plasma membrane was chosen as a target for fusing calcium indicators.

4.10.1.1 mCD8 and CD4

Mouse CD8 and human CD4 are membrane spanning proteins with one transmembrane domain (cDNAs kindly provided by L. Luo (Lee and Luo, 2001) and R. Kopan (Mumm et al., 2000), respectively). These proteins have already been used to target constructs to the lipid bilayer of cells. CD4 is a member of the immunoglobulin supergene family and may serve as the specific surface receptor for HIvirus (Maddon et al., 1985).
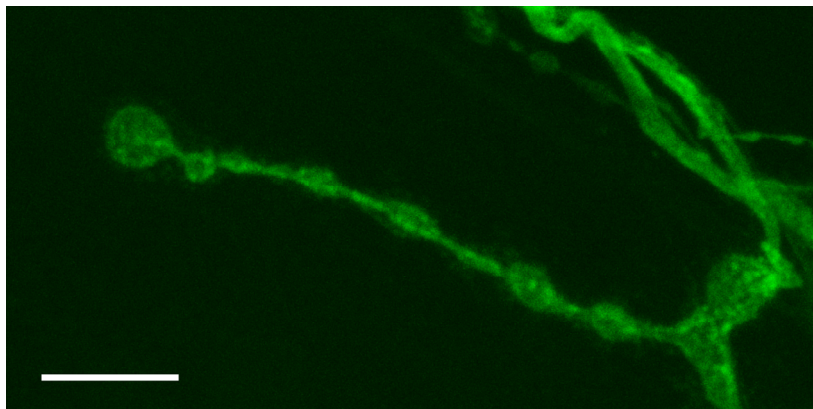
Figure 34: An NMJ expressing mCD8-GFP. Images were taken with a confocal laser scanning microscope (CLSM) and a z-projection (maximum intensity) was created. Scale bar: 10 μm.

Figure 34 shows an NMJ of a mCD8-GFP expressing animal. The staining was inhomogeneous along the boutons. The rather dotted pattern might result from the membrane targeting. Accumulations of fluorescent protein along the NMJ were clearly visible.

The NMJ is an excellent system to study for example synaptic transmission, vesicle release and glutamate receptor composition. But the goal is to solve the remaining questions about learning and memory, consciousness and the principles of vision and hearing.

The fly visual system, for example, shows reduced dimension and robustness of the experimental preparation. These favorable conditions have made it possible to identify individual neurons in the fly's visual information processing system. Three consecutive visual neuropils exist: the lamina, the medulla and the lobula complex, comprising the lobula and lobula plate. Within the lobula plate are about 60 tangential cells (LPTCs) which have large receptive fields and respond to motion in a way that is selective to direction of stimuli presented. Some cells respond to vertical motion, the Vertical System (VS) cells and others to horizontal motion, the Horizontal System (HS) and Centrifugal Horizontal (CH) cells. It is known that they pool the input of columnar elements, that represent the retinotopic pattern, and their receptive fields are often overlapping. In the blowfly it is thought that HS and VS cells are the major output elements of the lobula plate. Information is directed from these two cell types to descending neurons which themselves synapse onto motor neurons that control flight behavior (Borst and Haag, 2002).

Flies carrying the UAS-mCD8-GFP construct were crossed to DB331-GAL4. The driver line DB331-GAL4 allows the expression of Gal4 in all HS and VS cells. Fly brains were dissected and mounted as described in Materials and Methods. The preparations were imaged at a confocal laser scanning microscope (CLSM) and a z-projection (maximum intensity) was created (Figure 35). As GFP is fused to the membrane the protein can be detected in the whole cell. In the red box higher magnification of a primary and several secondary branches are shown. The lobula plate tangential cells exhibited the same dotted expression pattern as the NMJ. Accumulations of fluorescent protein could be detected along the dendritic trees, the axons and in the axon terminals.
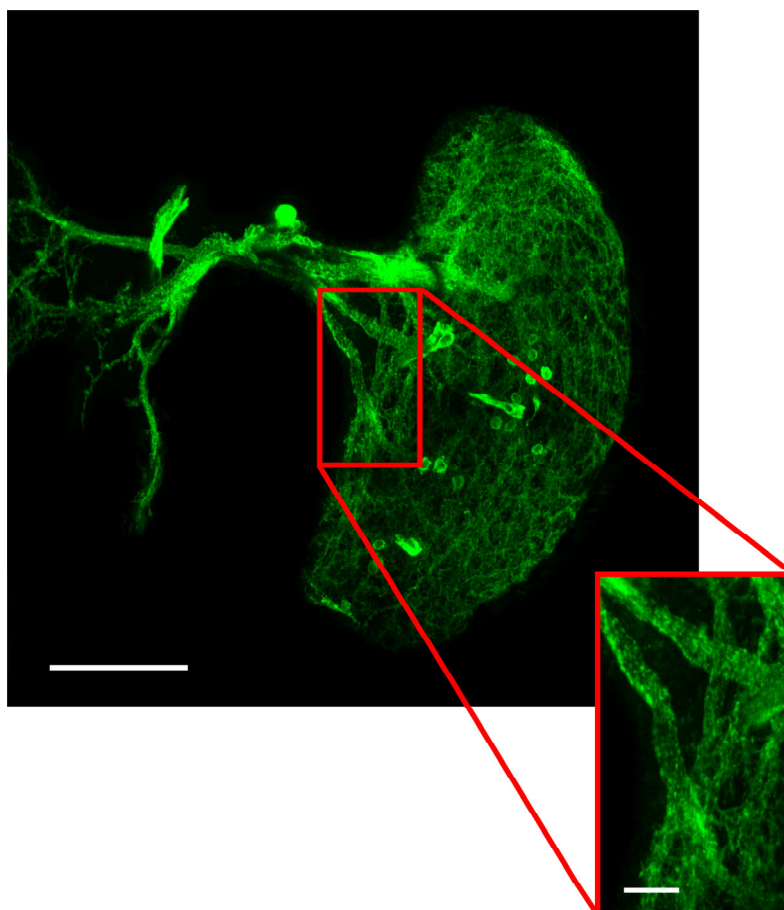
Figure 35: Dissected fly brain expressing mCD8-GFP in lobula plate tangential plate cells. Images were taken with a CLSM and a z-projection (maximum intensity) was created. Six VS and three HS cells can be distinguished. In the red box a higher magnification image of primary and secondary branches are shown. Scale bars: 50 µm and 10 µm (red box), respectively.

After analyzing the expression in mCD8-GFP flies, a fusion molecule with mCD8 at the N-terminus of GCaMP 1.6 was constructed. Transgenic flies were created (see Materials and Methods), crossed to the GAL4 driver elav[C155] and checked for expression and localization with epifluorescence microscopy. In all larvae carrying the transgene no detectable GFP fluorescence was visible. After incubating the dissected preparations with an anti-GFP antibody also no fluorescence could be detected.

The construct CD4-GCaMP 1.6 carrying the transmembrane domain human CD4 was engineered and transfected in Schneider cells S2 but did not show expression, even after several trials of transfection.

CD4-YC 2.3 expression and localization was tested in *Drosophila* Schneider S2 cells. The cells showed bright fluorescence. Localization to the membrane, however, could

not be seen. The protein seemed to be present in the entire cell and not only anchored to the membrane.

No experiments for expression and functionality were performed for mCD8-YC 2.3. At this point new indicators based on troponin C were available that seemed to perform better when tagged to targeting sequences.

4.10.1.2 LAPTM

Lysosomal-associated transmembrane protein (LAPTM) is a membrane spanning protein found in mammals, insects and nematodes. It functions to regulate the intracellular compartmentalization of amphipathic solutes and maybe the sensitivity of cells toward antibiotics, ionophores and organic cations (Hogue et al., 2002). It contains four membrane spanning domains and a 55 aminoacid C-terminal region that faces the cytoplasm. It was chosen for this study, because it is known that it is localized to lysosomes and late endosomes and therefore in vesicles that fuse with the membrane. The fusion contructs built with this transmembrane protein were LAPTM-GCaMP 1.6 and LAPTM-YC 2.3. They were expressed in Schneider cells, but only LAPTM-YC 2.3 showed expression, albeit in the entire cell with no detectable localization in vesicles or other sub compartments. When stimulated with 1 μM Ionomycin and 10 mM $CaCl_2$ the construct did not show any response. Transfection of self-made neuronal primary culture and a stable neuronal cell line were attempted. The primary culture, however, got molded after transfection. After trying many different strategies to transfect the stable cell line, it turned out that it can not be transfected with the common protocols available (see Materials and Methods).

4.10.1.3 Ras

Ras is a low-molecular-weight GDP/GTP-binding guanine triphosphatase (GTPase) with a role in malignant transformation. Ras goes through many posttranslational modifications, starting with a lipid modification called farnesylation that is catalyzed by farnesyltransferase (FTase). It depends on the enzymatic recognition of a specific C-terminal sequence CAAX where C is cystine, AA are aliphatic amino acids, and X is any amino acid, preferably methionine or serine. This process anchors Ras to the cell membrane, a required step for the cancer-causing activity of Ras. The C-terminal

membrane targeting sequence of Ha-Ras was used to direct calcium indicators to the membrane and to anchor them there (Aronheim et al., 1994).

TNL 15 was used for these tagging experiments. In contrast to other ratiometric indicators it is based on the calcium binding protein troponin C. It has already been reported that this indicator fused to Ras at the C-terminus showed clear and homogenous membrane labeling and performed well in HEK293 cells and hippocampal neurons when stimulated with KCl, or Ionomycin and high calcium (Heim and Griesbeck, 2004).

Different fly lines were generated with this fusion construct and analyzed at the NMJ. Line 75b showed expression in the whole NMJ with small accumulations in some boutons which were slightly swollen (Figure 36, top). By magnifying a single bouton, membrane staining could be detected (Figure 37, right). Another line (82e) showed swollen boutons bereft of any original shape. Accumulation at the membrane could be found but expression in the cytosol was detected as well. The NMJs of a third line (line 59n) exhibited a similar shape to line 75b, but gave strong accumulations of protein in the very distal boutons, an expression pattern that was not directed nor associated with the membrane (Figure 36, bottom).
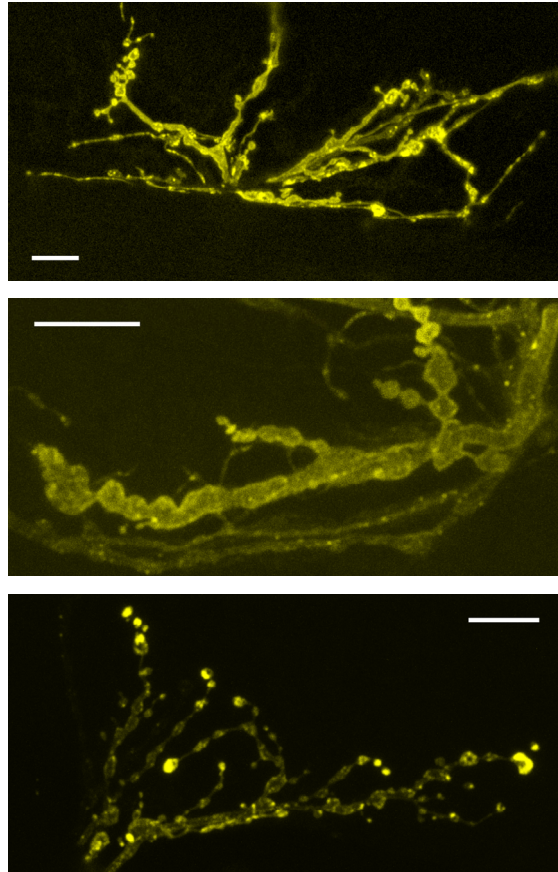
Figure 36: NMJ expressing TNL 15-ras. Images were taken with a CLSM and a z-projection (maximum intensity) was applied. Three different insertions were analyzed and gave diverse patterns. Top: line 75b showed slightly swollen boutons close to normal shape. Middle: the boutons in line 82e were swollen and lost their original shape. Bottom: line 59n showed accumulations at the very distal boutons (objective 63x, zoom: 2 x, 4.5 x and 3x respectively). Scale bar: 10 μm.
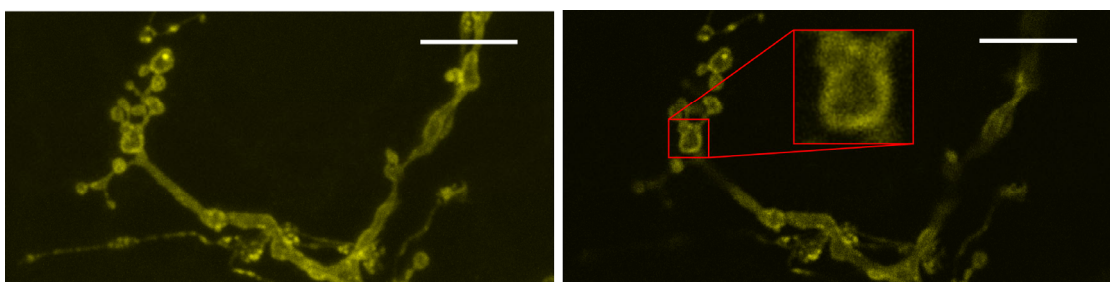
Figure 37: NMJ expressing TNL 15-ras (line 75b). Images were taken with a CLSM and a z-projection (maximum intensity) was applied in the left picture. In the right picture a single section of the whole scan is displayed and one bouton is highlighted in the red box. Note the specific labeling of the membrane. Scale bar: 10 μm.

Because the boutons of line 75b were close to normal shape measurements at the NMJ of a third instar larva were performed. Three different stimulation paradigms were applied (0, 40 and 80 Hz). The traces in Figure 38 demonstrate that the tagged

indicator shows fluorescence changes upon stimulation. The blue trace represents the mean of 40 Hz stimulation. The indicator showed fluorescence changes of almost 4 % with τ_{rise} = 0.6 s and τ_{decay} = 1.13 s. At 80 Hz stimulation the indicator gives a maximal response of $\Delta R/R$ = 6 % with τ_{rise} = 0.3 s and τ_{decay} = 1.31 s (red trace).
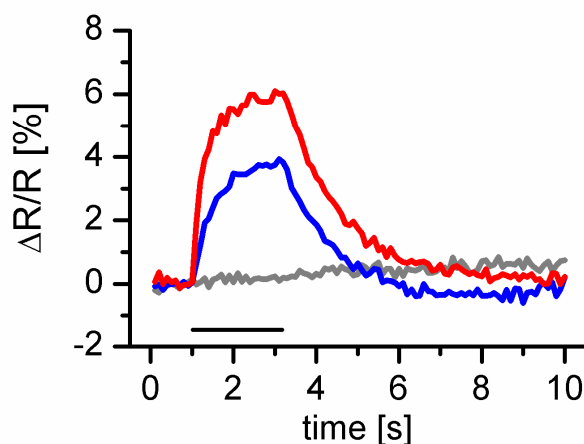
Figure 38: Fractional fluorescence changes $\Delta R/R$ [%] of TNL 15-ras. Shown are the mean traces of fluorescence responses with stimulation at 0 (gray), 40 (blue) and 80 Hz (red).
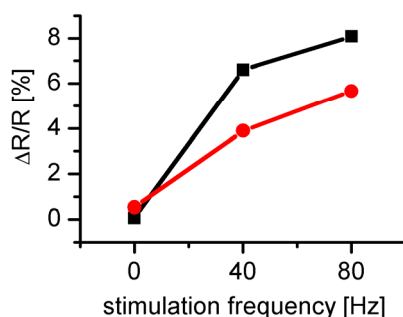
Figure 39: Comparison of mean $\Delta R/R$ between cytosolically expressed TNL 15 (black trace) and TNL 15-ras (red trace).

A comparison of $\Delta R/R$ between cytosolically expressed TNL 15 and the membrane standing TNL 15-ras is shown in Figure 39. For these measurements no background was subtracted. The cytosolically expressed indicator showed a higher maximum ratio

change while TNL 15-ras exhibited a more linear increase in the amplitudes (red trace).

Other approaches for targeting indicators to membrane associated compartments are described in the following chapters.

4.10.2 Targeting to Neurotransmitter Release Sites

To target indicators specifically to the neurotransmitter release sites, they were fused to synaptic vesicle or plasma membrane proteins close to release sites. These proteins are in part responsible for the synaptic vesicle cycle. They are very close to exocytosis sites and thus to calcium channels. Microdomains show calcium concentrations up to the micromolar range.

4.10.2.1 Neuronal Synaptobrevin

Neuronal Synaptobrevin (n-syb), also known as VAMP, is a vesicle-associated membrane protein. It is transported down the axons and localized to nerve terminals. It can be cleaved by botulinum toxin and tetanus toxin and is one protein of the SNARE complex which includes also SNAP-25 and Synatxin (Deitcher et al., 1998).

The indicator YC 2.3 was fused to n-syb. It is known that n-syb-GFP labels synaptic vesicle membranes at larval motor terminals and therefore n-syb seemed to be an ideal fusion partner for calcium indicators (Estes et al., 2000). The cDNA of n-syb (provided by David Deitcher, Ithaca, NY, USA) was fused to the N-terminus of YC 2.3 and the construct was injected into fly embryos. Transgenic flies were crossed to the GAL4 line elav[155]. Third instar larvae were dissected and motorneurons were examined with epifluorescence microscopy.

Figure 40: NMJ of a dissected larva expressing the transgene n-syb YC 2.3 in all neurons. For the left image an epifluorescence picture of the expressed construct was taken. In the middle an anti-synapsin antibody staining shows presynaptic sites at the NMJ. In the right panel the two staining are merged with perfect overlap.
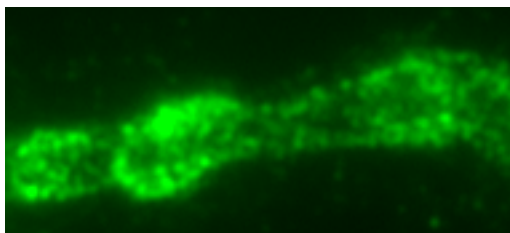
Figure 41: Magnification of the NMJ expressing n-syb YC 2.3 shown in Figure 40. Small spots are visible close to the membrane, suggesting targeting of the tagged GFP-based indicator to vesicle release sites.

YC 2.3 tagged to n-synaptobrevin localized to presynaptic terminals of the NMJ (Figure 40). No fluorescence could be detected in the axon. This suggests that the construct is at the vesicle release sites and not elsewhere in the cell (Figure 41). To verify the correct targeting I stained the presynaptic terminals with an anti-synapsin antibody that binds to the peripheral synaptic vesicle protein synapsin (Figure 40). A perfect overlap of the fusion construct and the anti-synapsin antibody staining demonstrated the tagging of n-syb YC 2.3 to presynaptic terminals. This indicator was tested at the NMJ. Nerves of dissected larvae were stimulated for 2.2 s, CFP and Citrine fluorescence was measured and ΔR/R calculated. No signal could be detected when stimulated with strong stimulations of 80 Hz (Figure 42).
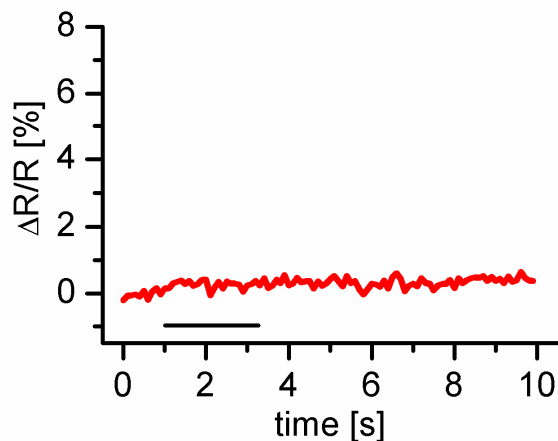
Figure 42: ∆R/R of an n-syb YC 2.3 expressing animal at 80 Hz stimulation. No signal change could be detected.

4.10.2.2 Syntaxin

Syntaxin (syx), a protein anchored to the plasma membrane and involved in vesicle release at the active zone plays multiple regulatory roles in neurotransmission (Wu et al., 1999). It is a t-SNARE and participates in the targeting and docking of vesicles (Wu and Bellen, 1997). However, Syntaxin is found along the entire axon, making it unlikely, that this protein is responsible for targeting the vesicles alone.

Syntaxin 1A, kindly provided by Hugo Bellen (Houston, Texas, USA), was fused to the N-terminus of YC 2.3. Transgenic flies were created and crossed to the GAL4 driver line elav[C155]. All lines analyzed showed no expression (Figure 43). The result was verified with an anti-GFP antibody staining: after the staining no emission could be detected, leading to the conclusion that no protein has been synthesized or the protein has not been targeted correctly. An anti-synapsin antibody staining was applied to highlight the NMJ. As seen in Figure 43 the NMJs were detectable by fluorescence emission of the fluorophore Alexa 594 linked to the antibody (Figure 43, middle). This approach was done for all transgenic lines created, but in none could the construct syx YC 2.3 be detected.
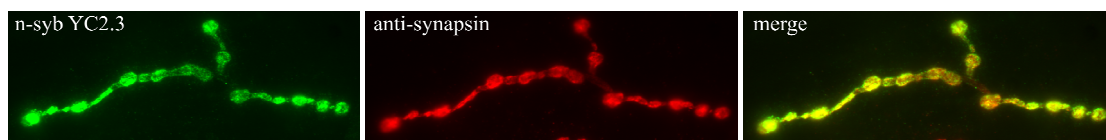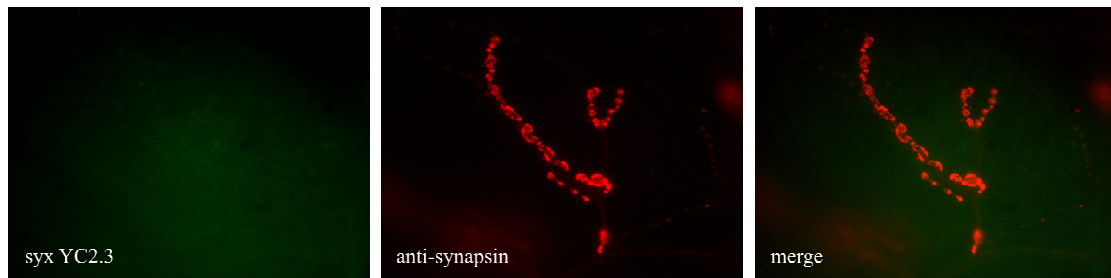
Figure 43: NMJ of a dissected larva carrying the transgene syx YC 2.3 in all neurons. For the left image an epifluorescence picture of the expressed construct was taken. No fluorescence could be detected. In the middle an anti-synapsin antibody staining shows presynaptic sites at the NMJ. In the right panel the two staining are merged.

4.10.2.3 Synaptotagmin

Synaptotagmin I (syt) is a vesicle-associated integral membrane protein that is mainly involved in transmitter release. It functions as the calcium sensor for synchronizing neurotransmitter release (Yoshihara and Littleton, 2002) and regulates fast excytosis at the synapse. It consists of two cytoplasmic domains (C2A and C2B) that bind in total five calcium ions (Chapman, 2002). Two fusion constructs were created, one with YC 2.3, the other with GCaMP 1.6, and transfected in Schneider cells. Both showed a bright fluorescence in the lumen of the cell.

4.10.3 Targeting to a Calcium Channel Subunit

N-type voltage gated calcium channels play important roles in synaptic function, but the mechanisms of how they are targeted in neurons are barely understood. A calcium channel consists of an α_1 pore-forming subunit associated with β and $\alpha_2\delta$ auxiliary subunits (Figure 44).
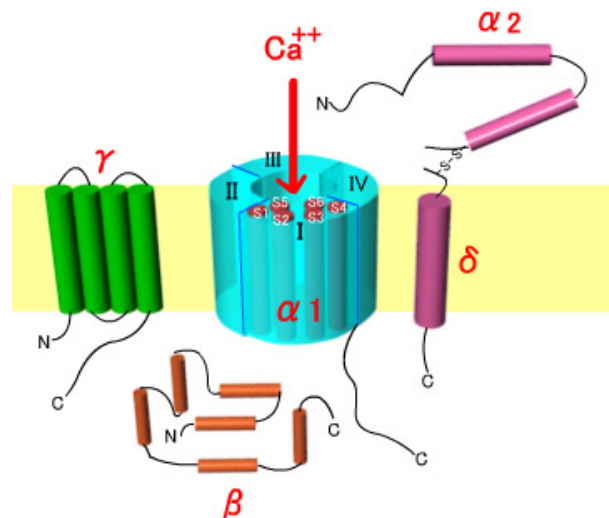
Figure 44: Schematic drawing of an N-type calcium channel. It consists of an α_1 pore-forming subunit associated with β and $\alpha_2\delta$ auxiliary subunits. Figure from http://pharma1.med.osaka-u.ac.jp/textbook/Receptors/ca-channel.html.

In their study, Maximov and Bezprozvanny (2002) analyzed the localization of N-type calcium channels in hippocampal neurons. They concluded that postsynaptic density-95/disc large/zona occludens-1 (PDZ1) binding motifs located within the α_{1B} subunit play a crucial role for synaptic targeting of the channels. This binding motif consists of only six amino acids, namely DQDHWC (Aspartic acid, Glutamine, Aspartic acid, Histidine, Tryptophan, Cysteine). Maximov et al. (1999) had already discovered in 1999 that Mint1-PDZ1 binds to the C-termini of the α_{1B} subunit (Figure 45, light green). Based on these findings they created constructs that contain an extracellular human CD4 receptor ectodomain, the human receptor CD4 transmembrane domain and a short fragment of the human α_{1B} cytosolic tail. Most of the C-terminus was removed and only a short region at the beginning of the C-terminus and the region containing the PDZ binding motif were left. To evaluate the importance of the PDZ1 domain binding motif for targeting, they generated a control construct that lacked the last six amino acids. And, in fact, the construct containing the six defined amino acids is clustered in axons and colocalized with synaptic sites, whereas the construct lacking these amino acids was diffusely distributed and did not colocalize with synaptic markers like Synapsin.

The idea described by Maximov and Bezprozvanny (2002) was used to target calcium indicators in close proximity to vesicle release sites and calcium channels. These six

amino acids that are known to bind to a PDZ domain of presynaptic Mint1 (X11L) were fused to the C-terminus of the indicators (Figure 45). Mint1 is part of a complex that also contains Veli and CASK and is necessary for synaptic vesicle docking.
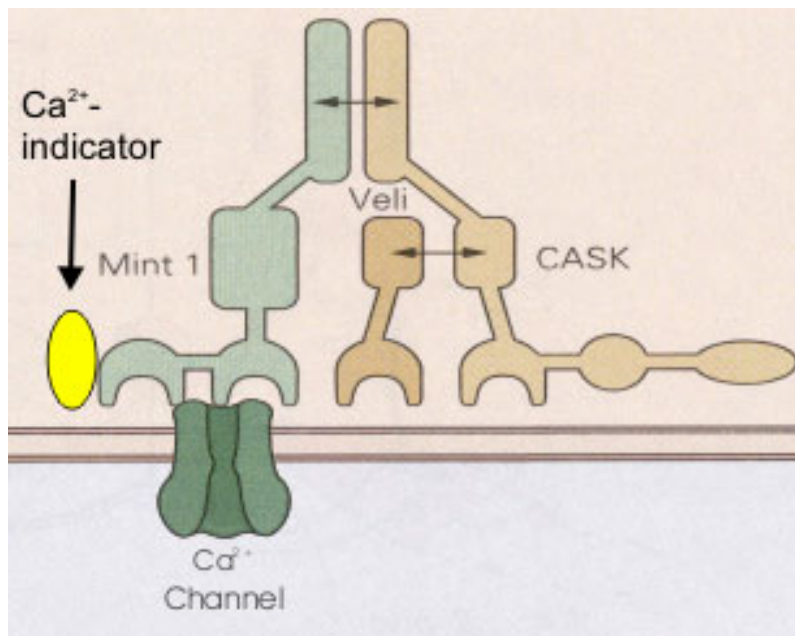
Figure 45: Schematic drawing of Ca²⁺ channel associated presynaptic proteins. Mint1, Veli and CASK. PDZ domains are shown by semicircles. The calcium channel binds to a PDZ domain of Mint1. The indicator includes six amino acids that are known to bind to the PDZ1 domain of Mint1 as well. Picture modified from Butz et al. (1998).

4.10.3.1 8aa TNL 15-ras

Another approach for targeting was to sandwich different troponin C-based indicators between two different localization sequences. These constructs always employed one membrane localization signal and an additional tag consisting of six aminoacids that form the C-terminus of N-type calcium channels. The additional base pairs were added by PCR to the N-terminus of the indicator. Between the targeting sequence and the indicator two linker amino acids (Glycin, Glycin) were inserted. Referring to the publication from Maximov and Bezprozvanny (2002) an additional transmembrane domain is necessary for correct synaptic targeting. As noted by Heim and Griesbeck (2004) ras targeting worked well when fused to the C-terminus of TNL 15. The ras domain was fused to the PDZ binding motif - TNL 15 and the construct was injected into flies. Two different transgenic fly stocks emerged. They were crossed to elav[C155] and analyzed for expression and localization at the NMJ.
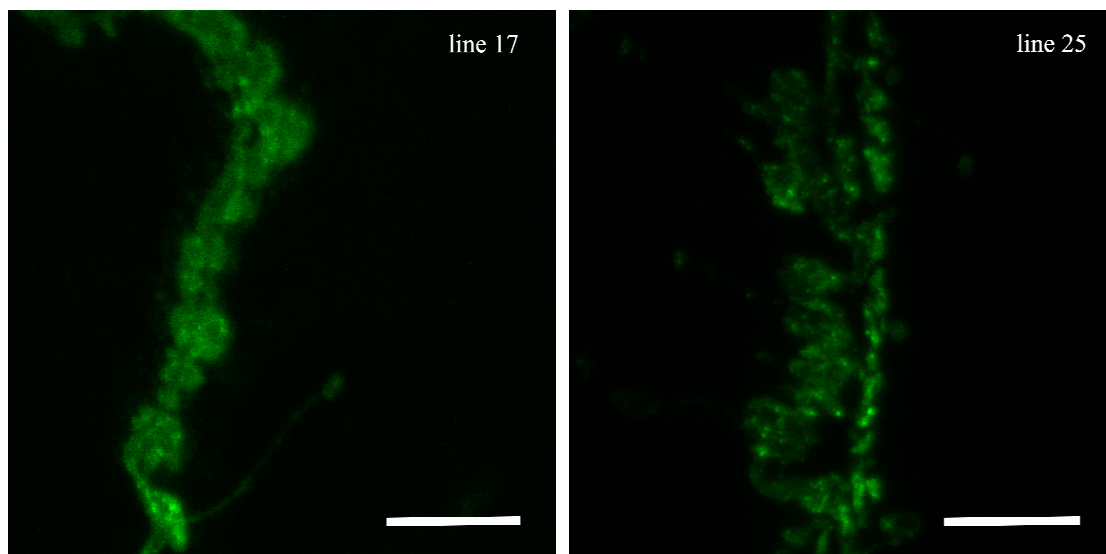
Figure 46: NMJ expressing 8aa TNL 15-ras. Images were taken with a CLSM and a z-projection (maximum intensity) was created. Two different insertions were analyzed and showed diverse patterns. Left: line 17 showed slightly blown up boutons close to normal shape. No targeting to presynaptic structures could be detected. Right: in line 25 the boutons lost their original shape. Scale bar: 10 µm.

Line 17 showed indicator expression at the whole NMJ with small accumulations in some parts of the boutons (Figure 46, left). The boutons were slightly swollen and the original shape was lost. A defined pattern due to localization close to calcium channels could not been detected. In comparison to the staining of cacophony-EGFP (cac-EGFP, Figure 47, Kawasaki et al., 2004), the indicator distribution looked different. The second line (25) showed a diffuse expression in the NMJ. It completely lost its original shape and small accumulations of indicator protein could be found.

The transgenic fly expressing the fusion construct cacophony-EGFP was used as a control for evaluating the correct localization of the constructs based on the fusion to calcium channels. The cacophony gene encodes a voltage-gated calcium channel α1 subunit in *Drosophila* homologous to vertebrate α1 subunits involved in transmitter release. The subunit consists of four repeating domains, each composed of six transmembrane domains. The subunit α1 alone is possibly able to form the calcium channel. However, additional subunits are needed to preserve the the function and regulation of the channel (Kawasaki et al., 2002). For Figure 47 a UAS-cac-EGFP fly was crossed to GAL4-elav[C155] and the expression and localization of this construct was analyzed at the NMJ. The very accurately precise pattern of expression showed

presumably the localization of EGFP to the calcium channel subunit α1. An anti-synapsin staining was applied to verify the targeting in presynaptic structures as well.
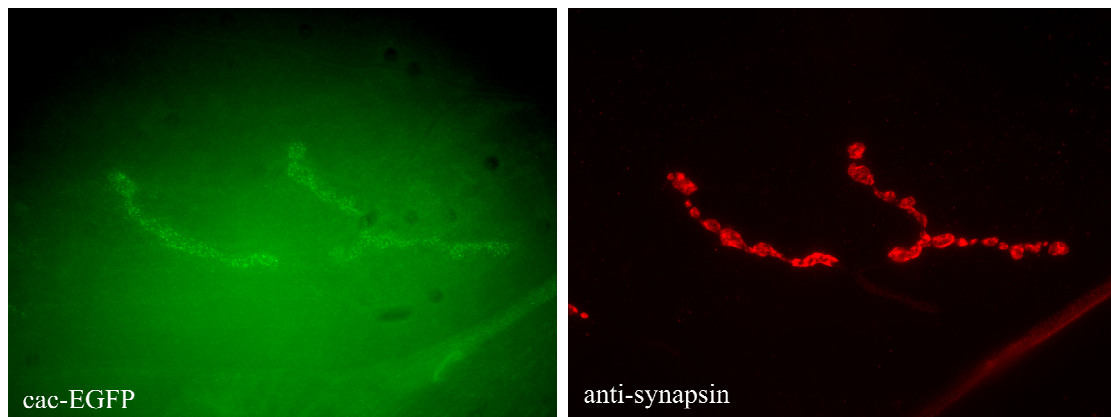
Figure 47: NMJ of a dissected larva carrying the transgene cac-EGFP in all neurons. For the left picture an epifluorescence picture of the expressed construct was taken with a 100x objective. A precise pattern of expression could be detected. The protein is localized to scattered fluorescent puncta. In the right picture an anti-synapsin antibody staining shows presynaptic sites in the NMJ.

4.10.3.2 TNL 15-ras 8aa

Another approach was to insert the transmembrane domain ras between the indicator and the eight amino acids required for binding to the PDZ domain of Mint1. Therefore the ras DNA was extended with the additional base pairs by PCR and linked to TNL 15 at the 3' end. The construct was inserted into pUAST and injected in fly embryos. The transgenic flies resulting from this were crossed to GAL4-elav[C155] and their NMJs were analyzed. As the expression in the boutons was too low, I enhanced the fluorescence signal by applying an anti-GFP antibody that recognized the two GFP variants of TNL 15 (Figure 48, left).
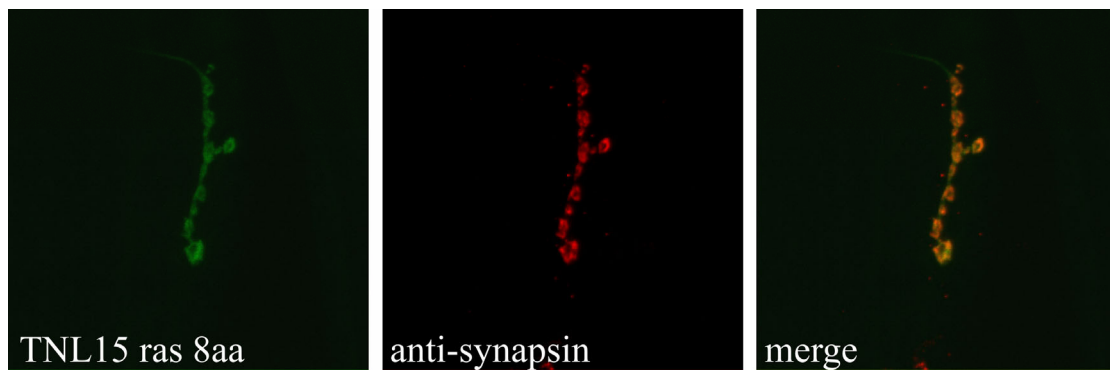
Figure 48: NMJ of a larva carrying the transgene TNL 15 ras 8aa in all neurons. For the left image an epifluorescence picture of an anti-GFP staining of the expressed construct was taken. In the middle an anti-synapsin antibody staining shows presynaptic sites in the NMJ. In the right panel the two staining are merged.

The indicator seemed to be localized in the membrane of the NMJ when analyzed with CLSM. In Figure 49 a NMJ of an animal expressing TNL 15-ras 8aa in all neurons is shown. In the more proximal boutons the indicator is mostly restricted to the membrane with little protein in the lumen of the cell. The distal boutons often showed accumulations of protein leading to mislocalization.
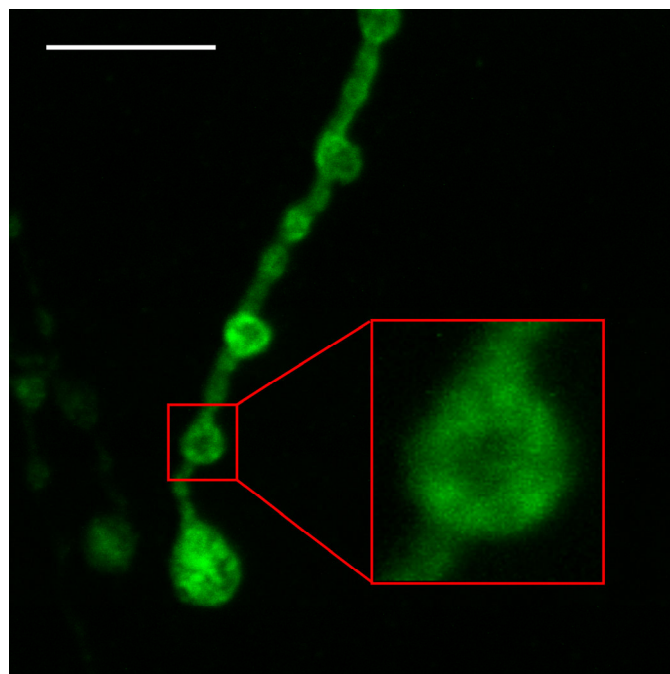
Figure 49: NMJ of a larva carrying the transgene TNL 15-ras 8aa in all neurons. The signal was enhanced by applying an anti-GFP antibody to the preparation. One bouton is magnified in the red square and shows localization at the membrane. Scale bar: 10 μm.

Experiments were performed at the NMJ by stimulating the cut nerve of a dissected larva with 20 Hz, 40 Hz and 80 Hz, respectively (see Materials and Methods). Figure 50 shows the ratio changes of the indicator with the different stimulation paradigms. For this analysis the background was subtracted for every bouton. Prominent was the poor SNR in all measurements, which may be attributed to the low expression level in single boutons. Already with 20 Hz stimulation (green trace) a reasonable signal was exhibited by the indicator with a maximum amplitude of 12.6 % and $\tau_{rise} = 1.1$ s and $\tau_{decay} = 1.1$ s. At 40 Hz the signal reached a maximum amplitude of 33 % with $\tau_{rise} = 0.67$ s and $\tau_{decay} = 1.2$ s (blue trace). Increasing the stimulations from 40 Hz to 80 Hz increased the mean maximum $\Delta R/R$ to 42 % (red trace). τ_{rise} was small ($\tau_{rise} = 0.38$ s) and the τ_{decay} almost the same as for 40 Hz stimulation ($\tau_{decay} = 1.25$ s).
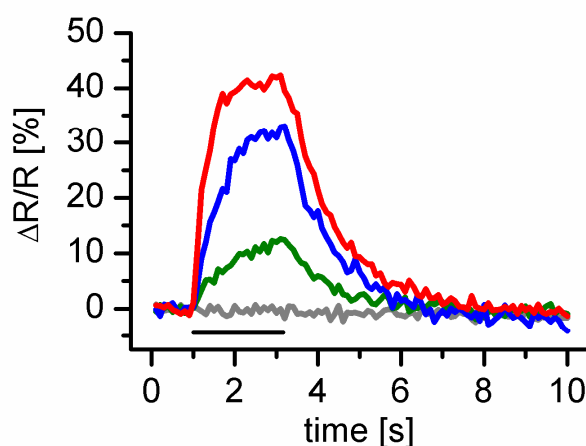
Figure 50: Fractional fluorescence changes $\Delta R/R$ [%] of TNL 15-ras 8aa. Shown are the mean traces of fluorescence responses with stimulation at 0 (gray), 20 (green), 40 (blue) and 80 Hz (red). Background is subtracted for every bouton.

To compare this indicator with the cytosolically expressed TNL 15 and the membrane tagged TNL 15-ras, data was analyzed without subtraction of the background. TNL 15-ras 8aa showed no bleaching during stimulation. Its fluorescence was stable before stimulus onset and rose quickly during stimulation. At 40 Hz the indicator reached a maximum amplitude of 4.6 % with a $\tau_{rise} = 740$ ms (TNL 15 has a $\tau_{rise} = 490$ ms at 40 Hz, see 4.5.4). It almost reached a steady-state-level. The time constant for decay was similar to that of cytosolically expressed TNL 15, namely $\tau_{decay} = 1.25$ s. At 80 Hz

stimulation the maximum ΔR/R increased only to 6.3 %, indicating that the indicator is close to saturation. The time course could be fitted by a single exponential function with τ_{rise} = 320 ms and τ_{decay} = 1.38 s.
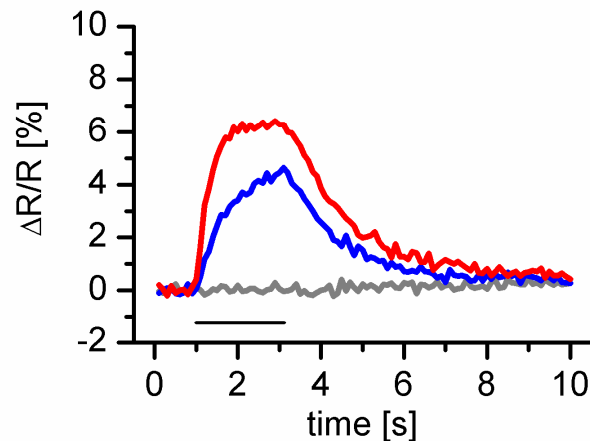
Figure 51: Fractional fluorescence changes ΔR/R [%] of TNL 15-ras 8aa. Shown are the mean traces of fluorescence responses with stimulation at 0 (gray), 40 (blue) and 80 Hz (red). No background fluorescence was subtracted.

Comparison of mean ΔR/R of TNL 15, TNL 15-ras and TNL 15-ras 8aa revealed that cytosolic TNL 15 had the highest response amplitudes, while TNL 15 ras and TNL 15-ras 8aa showed almost the same performance in experiments at the NMJ.
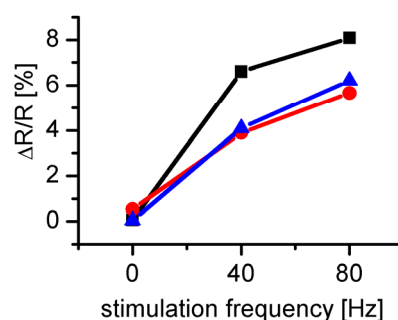
Figure 52: Comparison of mean ΔR/R between cytosolically expressed TNL 15 (black trace), TNL 15-ras (red trace) and TNL 15-ras 8aa (blue trace). TNL 15 exhibited the highest maximal ΔR/R, while TNL 15-ras 8aa performed similarly to TNL 15-ras.

4.10.3.3 mCD8 TN XL 8aa

Another construct that was cloned was mCD8 TN XL 8aa. It consists of the transmembrane domain mCD8 at the N-terminus of TN XL (4.10.1.1) and the six aminoacids known to bind to the PDZ domain of Mint (4.10.3) with a short glycine-linker at the C-terminus. The transgenic flies were crossed to the pan neuronal driver line elav^{C155} and their motorneurons were analyzed at the neuromuscular junction.
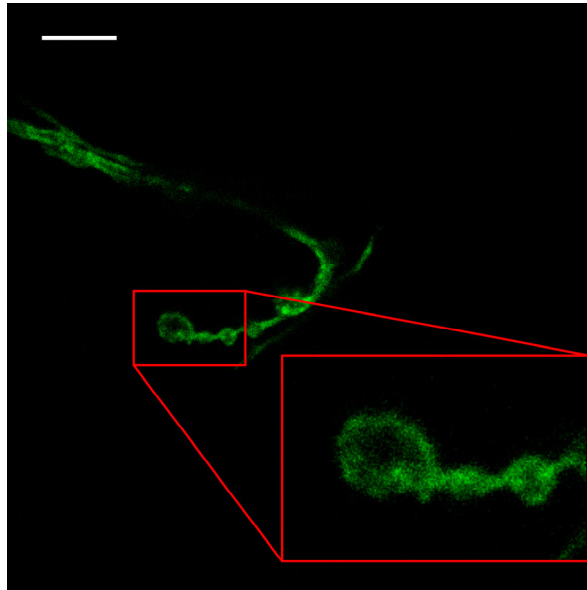
Figure 53: NMJ of a larva carrying the transgene mCD8 TN XL 8aa in all neurons (z-projection). In the red square the distal boutons are magnified. They show localization of the construct in the membrane. Scale bar: 5 µm.
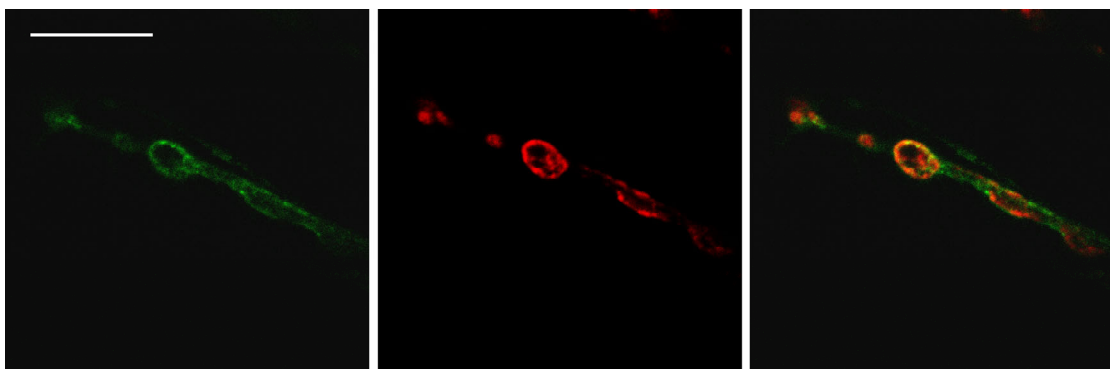
Figure 54: NMJ of a larva carrying the transgene mCD8 TN XL 8aa in all neurons (z-projection). The left picture shows the z-projection (maximum projection) of a confocal stack. Fluorescence in the presynaptic membrane could be detected. In the middle an anti-synapsin antibody staining shows presynaptic sites in the NMJ. In the right panel the two staining are merged. Scale bar: 10 µm.

Figure 53 and Figure 54 show confocal scans of NMJs from larvae expressing mCD8 TN XL 8aa in all neurons. The construct is localized at the membrane and no fluorescence could be detected in the lumen of the boutons. Presynaptic sites in the boutons were highlighted with an anti-synapsin antibody in Figure 54 (middle picture) to emphasize the targeting. The functionality of this indicator was tested with experiments at the NMJ.
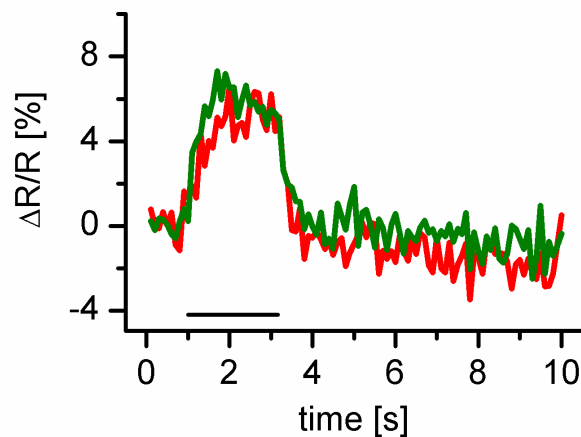
Figure 55: Fractional fluorescence changes ΔR/R [%] of mCD8 TN XL 8aa with 1.5 mM extracellular Ca^{2+}. Shown are the mean traces of fluorescence responses with stimulation at 80 (red) and 160 Hz (green).

Figure 55 shows the fluorescence changes in the boutons of the neuromuscular junction at stimulations of 80 Hz and 160 Hz with 1.5 mM Ca^{2+} in the extracellular bath. A maximum ΔR/R of 6.5 % was reached during 80 Hz stimulation. At 160 Hz the same maximum amplitude was achieved. The tagged indicator reached a steady state level in both stimulation paradigms. The expression in the NMJ is relatively low compared to cytosolically expressed indicators, therefore the SNR is low.

Increasing the extracellular calcium concentration in the bath to 10 mM revealed a higher maximum amplitude (~ 10 %) (Figure 56). At 160 Hz stimulation 12 % was achieved and the signal was close to saturation. Notable is that at 160 Hz the response was fast in its onset and fast in its decay.
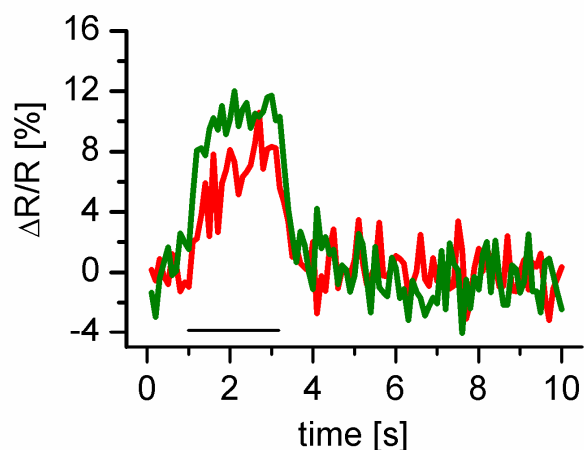
Figure 56: Fractional fluorescence changes ΔR/R [%] of mCD8 TN XL 8aa with 10 mM extracellular Ca^{2+}. Shown are the mean traces of fluorescence responses with stimulation at 80 (red) and 160 Hz (green).

Subsequently, this construct was expressed in the fly visual system by crossing the transgenic fly to either the GAL4-lines DB331 or 3A. Figure 57 is an image of a confocal stack that was taken of the lobula plate (crossing to DB331). The VS cells and the HS cells exhibited a dotted pattern on the dendrites. A magnification of the primary and secondary branches of one HS cell is highlighted in the red square. The protein appears scattered fluorescent puncta. In Figure 58 the axon terminals of VS cells are highlighted. As in the dendrites the protein localized to scattered puncta.
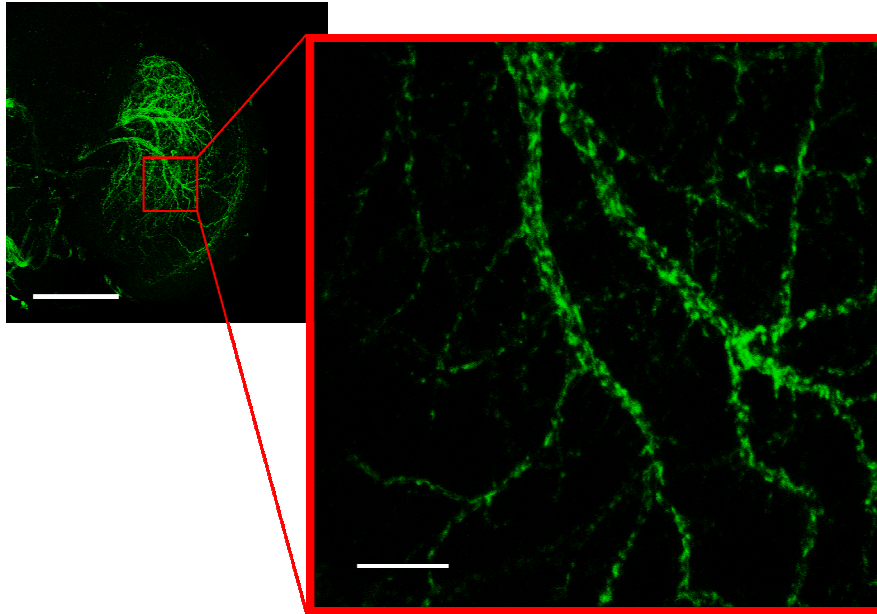
Figure 57: DB331 crossed to mCD8 TN XL 8aa. Maximum intensity projection of a confocal stack is presented. Red square: magnification of the selected area in the dendritic tree (red box). Scale bars: 100 µm in the original picture, 10 µm in the magnification.
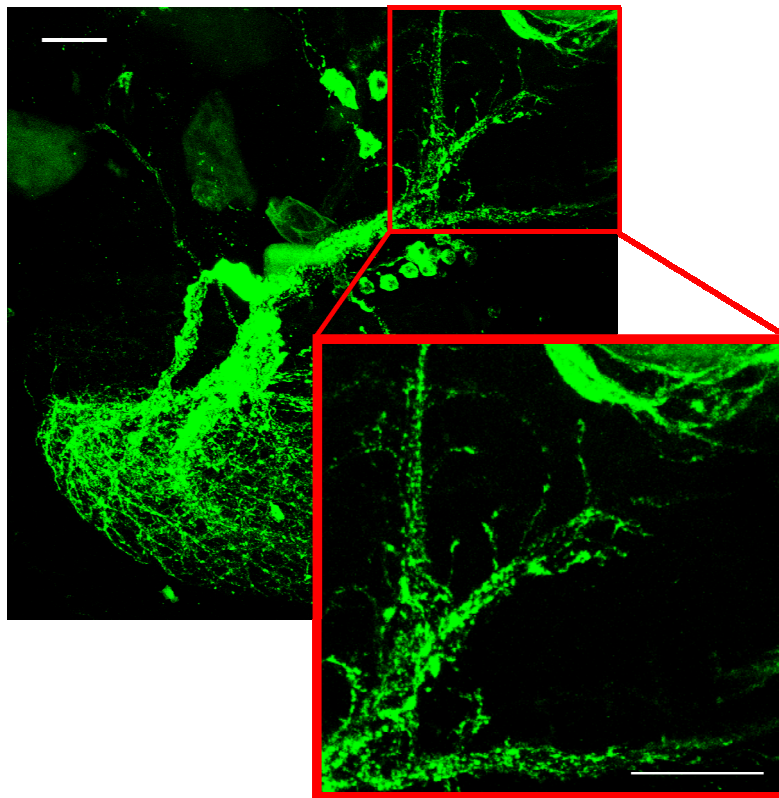
Figure 58: Z-projection (maximum intensity) of a confocal stack. A fly carrying the construct mCD8 TN XL 8aa was crossed to the GAL4 line DB331. Red square: The axon terminal of VS cells shows a distinct pattern of fluorescent protein. Scale bars: 20 µm.

Crossing of the transgenic fly to driver-line 3A exhibited the same expression pattern, but with a lower level of protein (Figure 59). Expression could be detected in all dendrites and the axon terminals leading to the ideas that calcium channels are distributed all along the cell or that the presynaptic input from other, to date, unknown cells is revealed by the staining. So far, however, no functional signals have been measured in theses cells with visual stimulation.
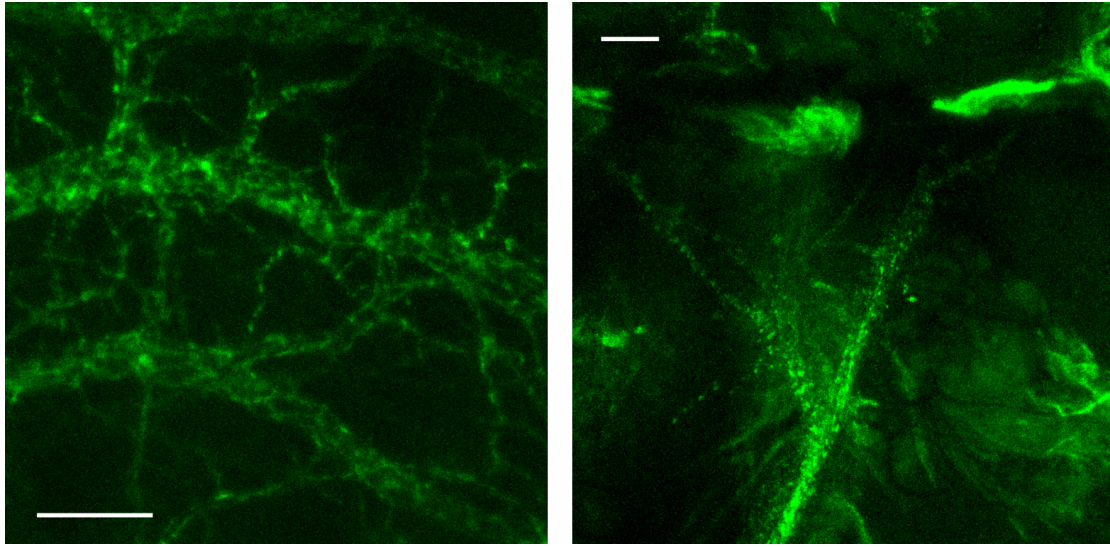
Figure 59: Maximum intensity projection of a confocal stack of a fly carrying mCD8 TN XL 8aa and the GAL4 driver 3A that allows GAL4 expression in all VS and HS cells. Left: Primary and secondary branches of the dendritic tree show a dotted pattern of fluorescence. Right: the axon terminal exhibit speckled distribution of the calcium indicator. Scale bars: 10 µm.

In Table 4 all targeted indicators described above are summarized. The fusion constructs were tested for their expression levels and localization in the fly or in cell culture (Schneider Cells). Targeting and functional properties are presented in the right column.

Fusion construct	Test System	Expression level	Properties
mCD8 GCaMP 1.6	fly NMJ	none	
CD4 YC 2.3	Schneider Cells	high	no targeting
CD4 GCaMP 1.6	Schneider Cells	none	
LAPTM YC 2.3	Schneider Cells	high	no targeting, no response upon ionomycin stimulation
LAPTM GCaMP 1.6	Schneider Cells	none	
n-syb YC 2.3	fly NMJ	high	targeting at presynaptic terminals, no signal changes upon stimulation
syx YC 2.3	fly NMJ	none	
syt YC 2.3	Schneider Cells	high	no targeting
syt GCaMP 1.6	Schneider Cells	high	no targeting
TNL 15-ras	fly NMJ	high	membrane staining, boutons swollen
8aa TNL 15-ras	fly NMJ	moderate	boutons swollen, lost original shape
TNL 15-ras 8aa	fly NMJ	low	membrane staining, accumulation in distal boutons
mCD8 TN XL 8aa	fly NMJ and LPTCs	high	membrane staining in NMJ, signal changes upon stimulation, scattered fluorescent puncta in LPTCs

Table 4: Overview of fusion constructs generated in this study. Test systems, expression levels and functional properties are summarized.

5 Discussion

In this work I characterized different genetically encoded calcium indicators and one indicator of synaptic vesicle release *in vivo* at the NMJ of *Drosophila melanogaster*. I also engineered several indicators targeted to the membrane and to presynaptic sites of neurons. The localization and the functional properties of some were tested *in vitro* and *in vivo*.

5.1 Genetically Encoded Indicators of Neural Activity In Vivo

A total of eleven indicators were tested at the NMJ of *Drosophila melanogaster*. Eight of them were identified to be reliable indicators of neural activity. The NMJ offered an ideal model system to perform well controlled and reproducible experiments. This system allowed comparison of the different calcium indicators based on one or two chromophores and SpH.

Fluorescence signals differed for the individual indicators. Fluorescence changes were related to neural activity. The corresponding changes, however, were smaller than what has been observed before with indicators *in vitro*. Furthermore, a shift in K_d and more severe photobleaching as compared to the *in vitro* situation often occurred. Kinetics and SNR depended on the expression level of the indicators.

In recent years new indicators have been generated: GCaMP 1.6 (Ohkura et al., 2005), TNL 15 (Heim and Griesbeck, 2004), TN XL (Mank et al., 2006) and YC 3.60 (Nagai et al., 2004). GCaMP 1.6 exhibited higher fluorescence at rest compared to GCaMP 1.3 and exhibited larger fluorescence changes with faster signal kinetics. Of the indictors analyzed in this study TNL 15 gave the fastest rise at lower rates of activity (stimulations at 40 Hz). Compared to the indicators TN XL and YC 3.60, however, TNL 15 had significantly slower kinetics.

5.1.1 Nonfunctional and Unreliable Indicators *In Vivo*

FP did not show any fluorescence *in vivo*. *In vitro*, similar results were described by Hasan et al. (2004), although Nagai et al. (2001) reported highly dynamic signals. Camgaroo-1 and Camgaroo-2 exhibited no or only very small fluorescence changes. Camgaroo-1 was difficult to measure because of very low fluorescence at rest. Hasan et al. (2004) expressed Camgaroo-2 under a tetracycline-inducible (tet) promoter and achieved ΔF/F of about 4 %. In *Drosophila* mushroom bodies Camgaroo-1 and Camgaroo-2 showed even higher signals (Yu et al., 2003). In my experiments at the NMJ, however, Camgaroo-1 showed a fluorescence change of about 0.5 % at 80 Hz stimulation, but the SNR was too low to allow a reasonable statement about fluorescence changes. Camgaroo-2 tended to drop with onset of stimulation. With a calcium concentration of 10 mM in the extracellular bath the signal degraded strongly (Figure 19). Yu et al. (2003) reported this drawback as well. One possible explanation might be the illumination protocol. In order to focus on the structure of interest, the specimen had to be excited before starting the experiment. This might cause photoconversion of the indicator to an almost completely calcium-insensitive form (Filippin et al., 2003).

5.1.2 Reliable Indicators of Neural Activity *In Vivo*

Reliable optical recordings have already been reported for different indicators. SpH, Inverse Pericam, GCaMP 1.3 and the ratiometric indicator YC 2.0 showed significant signals when analyzed in flies and mice (Ng et al., 2002; Reiff et al., 2002; Wang et al., 2003; Bozza et al., 2004; Hasan et al., 2004; Wang et al., 2004). In the study of Ng et al. (2002), for example, SpH was targeted to each of the three classes of neurons that form synapses in the antennal lobe of *Drosophila* and population responses to natural odors were visualized. SpH reported odor responses reliably. At a certain odorant concentration the point of inflection of the SpH transient trailed the onset of the odor pulse within 133 – 665 ms and the peak, with an amplitude of 5 % – 20 % ΔF/F, within 1.2 – 4 s. This time course is consistent with the estimated kinetics of odor delivery. The declining phase of the fluorescence transient, which reflects the synaptic processes of membrane retrieval and vesicle acidification followed single-exponential kinetics. Bozza et al. (2004) expressed SpH in olfactory sensory neurons of mice. They reported photobleaching of the indicator. A decrease in the average

resting fluorescence of ~ 7 % was observed. Resting fluorescence levels, however, recovered spontaneously and rapidly from photoconversion. The rise time of the glomerular SpH signal was slow and SpH fluorescence increased during prolonged odorant presentations. Recovery of the signal was also slow. The fractional change in odorant-evoked SpH fluorescence averaged 4.0 % for 2 s presentations of low odorant concentrations. Longer stimuli or higher concentrations evoked signals as large as 15 % $\Delta F/F$. They also reported that SpH responses were consistent over time. Repeated stimulus presentations resulted in responses with similar amplitudes.

The time course of SpH signals depends on the accumulation and retrieval of membrane on the presynaptic cell surface (Nicholson-Tomishima and Ryan, 2004). Small changes in the presynaptic release frequency will be filtered and produce only small fluorescence changes (Ng et al., 2002). Such filtering properties may explain recent differences in results from electrophysiological recordings (Wilson et al., 2004) and optical imaging studies in the *Drosophila* olfactory system (Ng et al., 2002; Yu et al., 2004) in which SpH may have underreported the electrical response to low odorant concentrations.

SpH responses were different from the calcium indicators as the signal changes relate to synaptic vesicle cycling. Its fluorescent change during stimulation reflects vesicle fusion and endocytosis occurring at the same time. Steady state was not reached during stimulation, leading to the conclusion that not all vesicles of the active zone were fused with the membrane. The fluorescent signal did not go back to baseline during consecutive stimulation. This is probably due to a higher rate of vesicle fusion during stimulation compared to the rate of vesicle recycling. The time course depended on the amount of vesicles fused with the presynaptic membrane. The signal rise slowed down from one AP volley to the next and the signal decay became faster (Figure 31).

Wang et al. (2003) developed an imaging system to monitor activity in specific neurons throughout the fly brain with high sensitivity and excellent spatial resolution. They coupled two-photon microscopy with the specific expression of the calcium-sensitive fluorescent protein GCaMP 1.3 to obtain images of activity in both the glomeruli and cell bodies of the projection neurons in the antennal lobe. They observed fluorescent intensity changes as large as 120 % in specific glomeruli when odor was applied at high concentration to the antennae. Furthermore, the high SNR

permitted analysis over a broad range of odor concentrations that are likely to approximate those encountered in nature.

Improved versions such as GCamP 1.6 with an additional sequence of 64 amino acids at the N-terminus and two amino acid changes within the wildtype GFP, YC 2.3 and YC 3.3 with Citrine instead of YFP and TNL 15, one ratiometric indicator based on troponin C also reliably reported neuronal activity *in vivo*.

GCaMP 1.6 exhibited higher fluorescence at rest and a smaller τ_{rise} and τ_{decay} compared to GCaMP 1.3. Unfortunately both GCAMP 1.6 and the other two circularly permuted indicators GCaMP 1.3 and Inverse Pericam showed limited photostability, causing lower repeatability (Figure 32 C, D) and limited signal detection (Figure 17). However, GCaMP 1.3 showed an almost linear relationship to neural activity and a high SNR at high activity levels. Saturation of GCaMP 1.3 might be expected since calcium concentrations of hundreds of nanomoles into the micromolar range can be expected in the *Drosophila* boutons under these conditions (Macleod et al., 2004), and K_d values of 235 nM have been reported for GCaMP 1.3 (Nakai et al., 2001) when measured *in vitro*.

IP bleached quickly before onset of stimulation. We found a decay of 20 % ΔF/F within the first second after onset of illumination, which corrupted signal detection substantially. Because the initial period before stimulation displays identical behavior, it might be adequate to subtract the control movies from the stimulus movies (Figure 17). The maximum ΔF/F amplitude increased only slightly relative to 40 Hz while the initial rate of rise was faster for 80 Hz stimulation, indicating that the evoked presynaptic calcium increase was sufficient to partially saturate IP. Clear saturation is suggested by the reported *in vitro* K_d of 200 nM (Nagai et al., 2001). The measured moderate saturation is in better accordance with the reported K_d of 900 nM in brain slices (Pologruto et al., 2004). Hasan et al. (2004) expressed IP under a tet promoter and looked for odor-evoked fluorescence changes. They achieved ΔF/F of about − 8 %. Signals were significant even for low odor concentrations and increased with concentration.

YC 2.3, YC 3.3 and TNL 15 showed improved photostability relative to earlier indicators due to amino acid exchanges within YFP which makes the fluorophore brighter and more pH stable. In accordance with this, accurate reproducibility of the

signals was measured in YC 2.3 and TNL 15 (Figure 32 A, B). TNL 15 has the fastest time constant for rise of all indicators tested. The pk_a is ~ 5.7, suggesting that mild pH changes might not interfere with the function of this indicator. In contrast, single chromophore indicators possess a pK_a that is within the physiological range, and their fluorescence change is caused by a change in the protonation of the chromophore during calcium binding (Baird et al., 1999; Griesbeck et al., 2001; Nagai et al., 2001; Nakai et al., 2001).

Reiff et al. (2002) used the indicator YC 2.0 to analyze the mechanisms underlying evoked vesicle release. They detected a rapid onset of $\Delta R/R$ changes that reached up to 40 % on a single bouton level when stimulated at 40 Hz for 3.5 s. In our study, however, this indicator showed only maximum fluorescence changes of ~ 8 % at 40 Hz stimulation. Nevertheless, the YC 2.0 signals agree with the characterization of the other YC variants analyzed with only minor differences. The kinetic were slightly slower and the maximum signal changes were larger compared with the YC .3 variants.

5.1.3   Relationship to Neural Activity

None of the indicators match the requirements of optimal sensors of neural activity. Optimal sensors would provide an easily detectable baseline fluorescence, a high SNR at minimum stimulation and indicator concentration, a large fluorescence change, and a linear relationship to activity or calcium (Yasuda et al., 2004).

Nevertheless, reliable optical recordings could be achieved that report neuronal activity *in vivo*. At the crayfish NMJ a low endogenous calcium buffer capacity and a fast calcium efflux after stimulation was described by Tank et al. (1995). In this model calcium quickly reaches a plateau when influx and efflux of calcium are in balance. Thus, τ_{rise}, amplitude of fluorescence change and τ_{decay} can depend on the expression level of the indicator, the dissociation constant and the intrinsic properties of the cell. In our study we showed that the kinetics of YC 2.3 in an animal with strong expression of indicator were slowed down, whereas the amplitude did not change with increasing expression level, concluding that even a high amount of indicator molecules has no effect on endogenous buffers. The SNR instead increased with expression level. Tank et al. (1995) reported that $[Ca^{2+}]$ decay kinetics could be profoundly slowed when the synthetic dye fura-2, an exogenous calcium buffer, was

added to the cytoplasm of the presynaptic terminal of a crayfish NMJ. They observed that increasing exogenous buffer concentration slowed the buildup and decay kinetics but not the level reached during the plateau phase.

Using low concentrations of the synthetic dye Oregon-Green-BAPTA with a K_d of ~ 500 nM, (Macleod et al., 2002; 2004) showed that the decay in calcium after a single AP as well as after long stimulus trains was around 60 ms in type Ib boutons of muscle 6/7 in *Drosophila* NMJs. 60 ms is likely to correspond to the calcium extrusion rate. This value could not be achieved as the fastest time constant for decay was 350 ms reported by GCaMP 1.6. Single action potentials could not be resolved and even responses to low frequency AP trains were generally hard to detect. Similar findings have been published in transfected cortical slices (Pologruto et al., 2004). Interestingly, in my experiments, YC 3.3 showed a better SNR at low activity rates compared to GCaMP 1.3. However, as the general SNR was rather low, I chose robust stimuli to characterize the indicators. The 80 Hz stimuli appeared to saturate the high K_d double chromophore indicators, whereas the low K_d GCaMP 1.3 showed a linear relationship to neural activity over the entire stimulus range (Figure 29).

Thus, double chromophore indicators tested have a limited dynamic range *in vivo*, whereas GCaMP 1.3 most likely has a substantial increase in its K_d compared to *in vitro* data. This increase has already been reported for some synthetic dyes (Bassani et al., 1995; Baylor and Hollingworth, 2000) and for Camgaroo-2 and GCaMP 1.3 which exhibited a 1.5-fold and 8-fold increase, respectively, in their K_d compared with *in vitro* (Pologruto et al., 2004). However, in the same study, a nonlinear relationship of the GCaMP 1.3 fluorescence to neural activity has been shown. My data differs from these results because of the linear behavior of both amplitudes and SNR for GCaMP 1.3 and YC 3.3 which saturated at 80 Hz.

Haag and Borst studied the influence of the affinity of synthetic dyes on the time course of the fluorescence signal (Haag and Borst, 2000). Three different synthetic dyes with different K_d values were used to measure calcium dynamics in CH and HS cells of the fly visual system: fura-2 (K_d = 145 nM), Calcium Green-1 (K_d = 190 nM) and Calcium Green-5N (K_d = 14 µM). After applying depolarizing current pulses fluorescent changes were measured in the synaptic terminals. Calcium Green-5N and Calcium Green-1 resulted in similar time courses leading to the conclusion that the time constants of the dyes represented the voltage-activated calcium release properties

of the cell. Using fura-2 the signals were slowed down significantly, probably due to the fact that higher concentrations of dye were applied.

5.2 Targeting Indicators

Genetically encoded indicators in principle offer the great advantage that they can be targeted to sites of interest by fusing them to suitable signal sequences. Several functional targetings of genetically encoded indicators have been reported previously (Miyawaki et al., 1997; Griesbeck et al., 2001; Palmer et al., 2004).

Miyawaki et al. (1997) designed for the first time genetically encoded fluorescent indicators for imaging Ca^{2+} and expressed them in the cytosol. They were also able to target them to the nucleus and endoplasmic reticulum of HeLa cells by transfecting the cells with cDNAs encoding chimaeras bearing appropriate localization signals. Addition of a nuclear localization signal to YC 2.0 yielded 'cameleon-2nu'. Its fluorescence was tightly localized to nuclei. Two other low-affinity indicators, yellow cameleon.3er and 4er, were engineered to reside in the lumen of the endoplasmic reticulum (ER) by an additional signal sequence at the N terminus and a KDEL signal for ER retention at the C terminus. Reticular patterns of fluorescence were seen in HeLa cells expressing these proteins. Combined results from the two indicators separately showed $[Ca^{2+}]er$ ranging from 60 to 400 mM before and 1 to 50 mM after application of a maximal dose of agonists (histamine).

Griesbeck et al. (2001) targeted Camgaroo-2 to mitochondria using the targeting sequence of subunit VIII of cytochrome c oxidase. Transfected cells showed a pattern typical of mitochondria. It was functional in mitochondria because a response to histamine was detected and ionomycin produced a significant fluorescence increase, although lower in dynamic range than in the cytosol. They also claimed that YC 3.3 was well expressed in the ER.

Palmer et al. (2004) created a genetically encoded Ca^{2+} indicator by redesigning the binding interface of calmodulin and a calmodulin-binding peptide. The sensor has improved reaction kinetics and a K_d ideal for imaging Ca^{2+} in the ER and is no longer perturbed by wt calmodulin. Addition of the calreticulin signal sequence and a KDEL ER-retention tag led to effective and specific localization of the indicator to the ER in HeLa cells. They could directly observe oscillations in $[Ca^{2+}]er$ with this construct.

109

To date only one functional targeting has been reported in a semi-intact preparation *in vivo*. Guerrero et al. (2005) targeted a YC 3.1 to the postsynaptic terminals by fusing it to the transmembrane domain of CD8 at the N-terminus and a PDZ interaction domain of the Shaker K$^+$ channel at the C terminus (Synapcam). Synapcam was created to address how transmission strength is distributed among the boutons of the NMJ. It reports Ca^{2+} influx through glutamate receptors in response to action potentials and can spatially segregate signals from individual boutons from neighboring boutons.

Different targeting strategies to transmembrane domains or synaptic vesicle proteins have been applied to target GFP to distinct parts of the cell (Lee and Luo, 1999; Estes et al., 2000). Lee and Luo (1999) used the mCD8-GFP fusion construct to study gene function in neuronal mophogenesis. Using the MARCM system, they were able to visualize axonal projections and dendritic elaboration in large neuroblast clones and single neuron clones with this membrane-targeted GFP marker. Estes et al. (2000) generated a neuronal synaptobrevin-GFP chimera (n-syb GFP). In third instar wandering larvae of flies they observed that the fusion construct was transported down axons and specifically localized to nerve terminals.

Targeting of calcium indicators close to the plasma-membrane or assumed sites of calcium influx, however, has not been reported *in vivo* except for the study of Guerrero et al. (2005) mentioned above. Up to my study it was not clear if calcium indicators were suitable for targeting experiments with regards to localization and retaining functional properties.

5.2.1   Targeting to Membrane-associated Proteins

YC 2.3 and GCaMP 1.6 were fused to protein trafficking sequences that are known to direct and insert proteins to the plasma membrane of a cell. The signal peptide and the transmembrane domain of mouse CD8 (Liaw et al., 1986), human CD4 (Mumm et al., 2000), c-Ha-Ras (Aronheim et al., 1994) or LAPTM, a lysosomal-associated transmembrane protein (Hogue et al., 2002), were chosen to target indicators to the membrane.

The expression pattern of a reference fly line containing UAS mCD8-GFP (Lee and Luo, 1999) was analyzed at the NMJ and in cells of the fly visual system (VS and HS cells). The dotted pattern was distributed along the entirety of each cell. This might

result from the membrane targeting (Figure 34 and Figure 35). Accumulations of fluorescent protein along the NMJ were clearly visible (Figure 34). One explanation could be the occurrence of "hotspots", parts of the cell membrane where proteins were likely to insert. Other groups used the same fly line for their studies and reported a similar expression pattern in lobula plate tangential cells (Scott et al., 2002; Lee and Luo, 2001).

Several transgenic fly lines were created containing the mCD8 protein at the N-terminus of GCaMP 1.6. In none of the flies could detectable GFP fluorescence be observed even after staining with an anti-GFP antibody linked to Alexa 488. A possible reason could be that the transgenic flies failed to express the indicator, a phenomenon that I saw in other fly lines as well (4.10.2.2, Figure 43).

CD4-YC 2.3 expression and localization were tested in *Drosophila* Schneider cells. This construct led to bright fluorescence in the whole cell, however successful targeting to the membrane could not be detected. Schneider cells were transfected with the fusion construct CD4-GCaMP 1.6 as well. Compared to the YC 2.3 construct, however, no fluorescence could be observed.

GCaMP 1.6 and YC 2.3 were also fused with LAPTM at the N-terminus. This membrane spanning protein is known to localize to lysosomes and late endosomes (Hogue et al., 2002). When Schneider cells were transfected with LAPTM-YC 2.3 or LAPTM-GCaMP 1.6 only expression of the first could be detected. However this construct did not lead to a directed localization to the membrane.

A third approach to target indicators to membranes was fusion to the C-terminal membrane targeting sequence of c-Ha-Ras (Aronheim et al., 1994). TNL 15 was used in these experiments to study calcium dynamics at the cell membrane. A study by Heim and Griesbeck (2004) reported that stimulation of TNL 15 D107A-ras with glutamate or high potassium concentrations gave reproducible average ratio changes of about 19 %. However, the same ratio change value was also measured with the cytosolically expressed form of the indicator molecule. Reasons for this might be that the K_d for TNL 15-ras of 29 µM was only determined through *in vitro* measurements. It assumed very likely a different value in the cytosol of a cell. This effect could be even stronger close to the plasma membrane where protein movement and ion diffusion rates are often hindered sterically and kinetically. This is consistent with a study by Pologruto et al. (2004) where they investigated the function of a variety of

GFP-based calcium indicators in cultured hippocampal brain slices and found variations between *in vitro* and *in vivo* K_d values.

The various fly lines created with TNL 15-ras were analyzed at the NMJ in an *in vivo* situation. The protein fusions to this membrane targeting sequence led to membrane targeting in some lines; the shape of the NMJ, however, was in most lines completely disrupted. The boutons were swollen and beyond any original shape. Accumulations of fluorescent protein could be found preferentially in the distal boutons (Figure 36). Interference with endogenous proteins, especially with proteins that are involved in assembly of the NMJ, could be one reason why the shape of the boutons was disrupted. Experiments at the NMJ of one line (line 75b) showed that the indicator still exhibited fluorescence changes up to 4 % at 40 Hz and 6 % at 80 Hz stimulation. The cytosolically expressed indicator exhibited a higher maximal ratio change at 40 and 80 Hz. The time constants were similar for both constructs. As this construct did not seem to be targeted only at the membrane, no conclusions could be made about kinetics.

5.2.2   Targeting to Neurotransmitter Release Sites

Indicators were directly fused to proteins involved in triggered synaptic vesicle release. The idea is to bring them in close proximity to exocytosis sites and presynaptic calcium channels. Three targeting molecules were chosen: neuronal-synaptobrevin (n-syb) (Broadie et al., 1995), syntaxin (syx) (Wu et al., 1999) and synaptotagmin (syt) (Adolfsen and Littleton, 2001). YC 2.3 fused to the C-terminus of n-synaptobrevin led to successful presynaptic targeting at the NMJ. No fluorescence was visible in the axons. Optical imaging with stimulations at 80 Hz, however, revealed no detectable fluorescence change. Heim and Griesbeck (2004) stimulated HEK293 cells expressing the fusion construct YC 2.3-synaptobrevin with carbachol. They claimed that this construct had totally lost responsiveness upon stimulation, although a small increase in ratio could be detected by using ionomycin with 10 mM $CaCl_2$ suggesting that the indicator had lost significant features of its calcium binding properties on the pathway to membrane insertion. TNL 15-synaptobrevin in contrast retained calcium sensitivity in response to stimulation, although a decreased dynamic range could be seen with this construct.

No expression could be detected in flies expressing the fusion construct Syntaxin-YC 2.3. Even after amplifying fluorescence with an anti-GFP antibody, no fluorescence was visible indicating that the flies failed to express this indicator. Similar results were obtained with the fusion construct mCD8-GCaMP 1.6 as mentioned above. Synaptotagmin I (Yoshihara and Littleton, 2002), the third protein involved in transmitter release was fused to YC 2.3 or GCaMP 1.6 and expressed in Schneider cells. Bright fluorescence in the lumen of the cell was observed. Syt I can only be found in presynaptic vesicles (Adolfsen and Littleton, 2001). Syt was not present in the vesicles of Schneider cells and the construct could not been targeted.

5.2.3 Targeting Close to Calcium Channels

Another approach of targeting different troponin C-based indicators was the fusion to two different localization sequences. These constructs always employed one membrane localization signal and an additional tag consisting of six amino acids that form the C-terminus of N-type calcium channels. This tag was shown to bind to a PDZ- domain of presynaptic Mint1 (X11L) involved in synaptic vesicle docking (Maximov and Bezprozvanny, 2002). The construct contains the six amino acids at the N-terminus and the membrane targeting sequence of ras at the C-terminus (Aronheim et al., 1994). The study of Heim and Griesbeck (2004) reported a ring-shaped labeling of the plasma membrane in HEK 293 cells after expressing the indicator fused to ras (5.2.1). At the NMJ, however, the two localization sequences caused a disrupted shape. This result was similar to the results achieved by fusion to ras alone. Boutons were swollen. The interference of ras with endogenous proteins seemed to have taken a stake in forming the synapse. The additional fusion to the six amino acids had no rescue effect.

To mask the negative effects of ras, while maintaining membrane targeting, ras was inserted between the indicator and the six amino acids. NMJs exhibited a normal shape and membrane targeting could be observed in the more proximal boutons. Experiments at the NMJ revealed that TNL 15-ras 8aa performed similarly to TNL 15-ras alone, but still exhibited lower maximum fluorescence changes than the cytosolically expressed TNL 15. These results did not correspond to the high calcium concentrations that are expected in microdomains at the submembrane. Such submembrane calcium microdomains could reach concentrations of up to 100 µM and

even during resting conditions submembrane calcium levels appeared to be elevated in a rat smooth muscle-derived cell line (Marsault et al., 1997). Heim and Griesbeck (2004), however, reported no elevated calcium concentrations at the plasma membrane compared to cytosolic transients when co-transfecting hippocampal neurons with membrane-targeted TNL 15-ras and nucleus-targeted YC 2.3 on the time scale of their experiments, suggesting that no permanent gradient in calcium concentration from the membrane towards the cytosol is maintained. Measurements with improved spatial and temporal resolution would be necessary to obtain more detailed information about a possible gradient in calcium concentration. Producing faster indicators could also help further addressing this question.

As already mentioned above TN XL exhibits much faster kinetics than the indicators described before (5.1). Time constants of τ_{rise} = 430 ms and τ_{decay} = 240 ms have been measured for this indicator (Mank et al., 2006).

This indicator was chosen for further tagging experiments as it was the fastest genetically encoded indicator available at the time. It was flanked by the transmembrane domain mCD8 at the N-terminus and the six amino acids known to bind to the PDZ domain of Mint1 at the C-terminus. The idea resulted from a study of Maximov and Bezprozvanny (2002) (4.10.3).

The protein fusion to mCD8 and the six amino acids resulted in membrane targeting in the boutons of the NMJ. No expression in the cytosol of the boutons could be observed. In experiments at the NMJ mCD8 TN XL 8aa showed a maximum fluorescence change of about 6.5 % for 80 and 160 Hz. The expression level, however, was low. As determined from the indicator YC 2.3, the kinetics slowed down, the SNR, however, increased with the expression level, illustrating an important compromise between signal kinetics and SNR (4.7). Expression could be enhanced by increasing the number of insertions. The maximum $\Delta R/R$ increased only slightly (from 10 % at 80 Hz to 12 % at 160 Hz) with increased extracellular calcium concentration from 1.5 to 10 mM indicating that the evoked presynaptic calcium increase was sufficient to partially saturate the indicator.

Expression of this fusion construct in lobula plate tangential cell of *Drosophila* revealed a punctate pattern on the dendrites, the axon and the axon terminal. This dotted pattern indicates that the protein is localized at distinct sites within the cell.

Clustering of calcium channels at the presynaptic terminal, in the axonal shaft and in the dendrites has been reported in lobula plate tangential cells (Haag and Borst, 2000). It is not proven, however, if these channels are similar to vertebrate N-type calcium channels. These kinds of channels could be present in the entire cell although this has not been reported so far. Also input neurons from the medulla branch on the dendrites of LPTCs and therefore could be responsible for the consistent staining. The most likely reason for this staining is that the indicator could be targeted to different calcium indicators that are distributed all over the cell.

5.3 Outlook

Single action potentials could not be resolved in our experiments, and even responses to low frequency AP trains were generally hard to detect. Similar findings have been published recently in transfected cortical slices (Pologruto et al., 2004). Therefore further improvements in the design of indicators are required (Griesbeck, 2004). At present, the indicators reliably report higher-frequency bursts, which have been observed in many systems. To represent single spikes faster indicators are needed. New indicators would report calcium with better SNR and thus better resolve the underlying electrical events that happen on the timescale of milliseconds and are believed to be a prerequisite of information processing in neural circuits (Borst and Theunissen, 1999; Ikegaya et al., 2004; Miesenbock, 2004). Ratiometric indicators with increased maximum fluorescence change (Nagai et al., 2004; Mank et al., 2006) demonstrate that the field is heading toward such probes.

Summarizing the experiments in which indicators were targeted to subcellular sites it can be said that in all cases tested so far, the indicators based on troponin C retained their activity. However, the anatomy of the expressing structure is often destroyed. Calmodulin-based probes could be targeted to specific compartments in the cell; however they lost their functional properties. Little is known about why the calcium sensitivity of calmodulin based indicators is restricted in many targetings. Possible reasons could be post-translational modifications such as phosphorylation on the pathway to membrane insertion or interactions with calmodulin-binding proteins, or

simply endogenous calmodulin binding which may be present at high concentrations close to the membrane.

The targeted mCD8 TN XL 8aa seemed to be a promising tool to investigate neural circuits as the fly visual system. It remains to be determined whether the anatomical and functional properties observed in the NMJ can be transferred to complex environments such as the brain. Another ratiometric indicator (YC 3.60) that was published recently consists of a similar molecular assembly as the TN XL. Instead of troponin C as calcium binding site it contains calmodulin (Nagai et al., 2004). This indicator has a K_d of 250 nM and shows a dynamic range of 560 % *in vitro*. To demonstrate the benefits of YC 3.60, (Nagai et al., 2004) targeted it to the plasma membrane by fusing the membrane anchor sequence of Ki-Ras to the C terminus of the indicator and created transgenic mice. Reproducible signals could be observed. However, the same problem mentioned above occurred in using calmodulin-based genetic sensors. Only a reduced dynamic range could be observed when this construct was expressed in the central nervous system of transgenic animals. Our group created transgenic flies with this construct and tested it at the NMJ. Using YC 3.60, signals could be already detected at stimulations of 5 and 10 Hz. The time constants for rise, however, were much slower than measured for TN XL (YC 3.60: τ_{rise} at 40 Hz = 1.55 s, τ_{rise} at 80 Hz = 1.21 s; TN XL: τ_{rise} at 40 Hz = 0.25 s, τ_{rise} at 80 Hz = 0.3 s) (Joesch, diploma thesis, 2005). YC 3.60 amplitudes increased fairly linearly over the entire stimulus range. These properties make this indicator suitable for further tagging experiments to presynaptic sites in neurons. Additional two photon measurements showed that YC 3.60 yielded the highest fluorescence changes and SNR for small stimulus paradigms ($\Delta R/R$: 30 %, 50 % and SNR 3, 6 for 10 and 20 Hz, respectively; data is subtracted for background fluorescence, Hendel et al., unpublished data). For detection of small Ca^{2+} changes evoked by only few action potentials this is probably the most promising indicator currently available.

Since up to date only a few functional fusion constructs with indicators have been published, it might be a challenge to further engineer and characterize more targetings. It seems more promising to fuse the indicators to signal sequences that are not anchored or inserted into membranes but rather bind specific proteins, domains or motifs such as the PDZ domains of synaptic proteins. Thereby unwanted interactions with endogenous proteins could be avoided.

116

Genetically encoded indicators offer a huge potential to decypher the dynamics of biochemical and physiological signals that are used to process information, either within individual neurons or within neural networks. Compared to electrophysiology they feature the advantage of being non-invasively directed to entire circuits or populations of cells that could not be accessed otherwise. Furthermore, successful targeting of these indicators to pre- and postsynapses will help us to understand how neurons receive, compute and transfer information to adjacent cells upon stimulation.

6 References

1. **Adams MD et al. (2000**) The genome sequence of *Drosophila melanogaster*. *Sci* 287: 2185-2195.

2. **Adolfsen B, Littleton JT (2001**) Genetic and molecular analysis of the synaptotagmin family. *Cell Mol Life Sci* 58: 393-402.

3. **Amsterdam A, Lin S, Hopkins N (1995**) The Aequorea victoria green fluorescent protein can be used as a reporter in live zebrafish embryos. *Dev Biol* 171: 123-129.

4. **Aronheim A, Engelberg D, Li N, al Alawi N, Schlessinger J, Karin M (1994**) Membrane targeting of the nucleotide exchange factor Sos is sufficient for activating the Ras signaling pathway. *Cell* 78: 949-961.

5. **Ataka K, Pieribone VA (2002**) A genetically targetable fluorescent probe of channel gating with rapid kinetics. *Biophys J* 82: 509-516.

6. **Baird GS, Zacharias DA, Tsien RY (1999**) Circular permutation and receptor insertion within green fluorescent proteins. *Proc Natl Acad Sci U S A* 96: 11241-11246.

7. **Barclay JW, Atwood HL, Robertson RM (2002**) Impairment of central pattern generation in *Drosophila* cysteine string protein mutants. *J Comp Physiol A Neuroethol Sens Neural Behav Physiol* 188: 71-78.

8. **Bassani JW, Bassani RA, Bers DM (1995**) Calibration of indo-1 and resting intracellular [Ca]i in intact rabbit cardiac myocytes. *Biophys J* 68: 1453-1460.

9. **Baylor SM, Hollingworth S (2000**) Measurement and interpretation of cytoplasmic [Ca^{2+}] signals from calcium-indicator dyes. *News Physiol Sci* 15: 19-26.

10. **Borst A, Egelhaaf M (1992**) *In vivo* imaging of calcium accumulation in fly interneurons as elicited by visual motion stimulation. *Proc Natl Acad Sci U S A* 89: 4139-4143.

11. **Borst A, Theunissen FE (1999**) Information theory and neural coding. *Nat Neurosci* 2: 947-957.

12. **Borst JGG, Sakmann B (1996**) Calcium influx and transmitter release in a fast CNS synapse. *Nature* 383: 431-434.

13. **Bozza T, McGann JP, Mombaerts P, Wachowiak M (2004**) *In vivo* imaging of neuronal activity by targeted expression of a genetically encoded probe in the mouse. *Neuron* 42: 9-21.

14. **Brand AH, Perrimon N (1993**) Targeted gene expression as a means of altering cell fates and generating dominant phenotypes. *Development* 118: 401-415.

15. **Broadie K, Prokop A, Bellen HJ, O'Kane CJ, Schulze KL, Sweeney ST (1995**) Syntaxin and synaptobrevin function downstream of vesicle docking in *Drosophila. Neuron* 15: 663-673.

16. **Butz S, Okamoto M, Sudhof TC (1998**) A tripartite protein complex with the potential to couple synaptic vesicle exocytosis to cell adhesion in brain. *Cell* 94: 773-782.

17. **Chalfie M, Tu Y, Euskirchen G, Ward WW, Prasher DC (1994**) Green fluorescent protein as a marker for gene expression. *Sci* 263: 802-805.

18. **Chapman ER (2002**) Synaptotagmin: a Ca^{2+} sensor that triggers exocytosis? *Nat Rev Mol Cell Biol* 3: 498-508.

19. **Cohen LB, Salzberg BM, Grinvald A (1978**) Optical methods for monitoring neuron activity. *Annu Rev Neurosci* 1: 171-182.

20. **Davis GW, DiAntonio A, Petersen SA, Goodman CS (1998**) Postsynaptic PKA controls quantal size and reveals a retrograde signal that regulates presynaptic transmitter release in *Drosophila. Neuron* 20: 305-315.

21. **Deitcher DL, Ueda A, Stewart BA, Burgess RW, Kidokoro Y, Schwarz TL (1998**) Distinct requirements for evoked and spontaneous release of neurotransmitter are revealed by mutations in the *Drosophila* gene neuronal-synaptobrevin. *J Neurosci* 18: 2028-2039.

22. **DiAntonio A, Petersen SA, Heckmann M, Goodman CS (1999**) Glutamate receptor expression regulates quantal size and quantal content at the *Drosophila* neuromuscular junction. *J Neurosci* 19: 3023-3032.

23. **Erickson MG, Alseikhan BA, Peterson BZ, Yue DT (2001**) Preassociation of calmodulin with voltage-gated Ca^{2+} channels revealed by FRET in single living cells. *Neuron* 31: 973-985.

24. **Estes PS, Ho GL, Narayanan R, Ramaswami M (2000**) Synaptic localization and restricted diffusion of a *Drosophila* neuronal synaptobrevin--green fluorescent protein chimera *in vivo*. *J Neurogenet* 13: 233-255.

25. **Fiala A, Spall T, Diegelmann S, Eisermann B, Sachse S, Devaud JM, Buchner E, Galizia CG (2002**) Genetically expressed cameleon in *Drosophila melanogaster* is used to visualize olfactory information in projection neurons. *Curr Biol* 12: 1877-1884.

26. **Filippin L, Magalhaes PJ, Di Benedetto G, Colella M, Pozzan T (2003**) Stable interactions between mitochondria and endoplasmic reticulum allow rapid accumulation of calcium in a subpopulation of mitochondria. *J Biol Chem* 278: 39224-39234.

27. **Giniger E, Varnum SM, Ptashne M (1985**) Specific DNA binding of GAL4, a positive regulatory protein of yeast. *Cell* 40: 767-774.

28. **Griesbeck O, Baird GS, Campbell RE, Zacharias DA, Tsien RY (2001**) Reducing the environmental sensitivity of yellow fluorescent protein. Mechanism and applications. *J Biol Chem* 276: 29188-29194.

29. **Griesbeck O (2004**) Fluorescent proteins as sensors for cellular functions. *Curr Opin Neurobiol* 14: 636-641.

30. **Grynkiewicz G, Poenie M, Tsien RY (1985**) A new generation of Ca^{2+} indicators with greatly improved fluorescence properties. *J Biol Chem* 260: 3440-3450.

31. **Guerrero G, Isacoff EY (2001**) Genetically encoded optical sensors of neuronal activity and cellular function. *Curr Opin Neurobiol* 11: 601-607.

32. **Guerrero G, Rieff DF, Agarwal G, Ball RW, Borst A, Goodman CS, Isacoff EY (2005**) Heterogeneity in synaptic transmission along a *Drosophila* larval motor axon. *Nat Neurosci* 8: 1188-1196.

33. **Guerrero G, Siegel MS, Roska B, Loots E, Isacoff EY (2002**) Tuning FlaSh: redesign of the dynamics, voltage range, and color of the genetically encoded optical sensor of membrane potential. *Biophys J* 83: 3607-3618.

34. **Haag J, Borst A (2000**) Spatial distribution and characteristics of voltage-gated calcium signals within visual interneurons. *J Neurophysiol* 83: 1039-1051.

35. **Hasan MT, Friedrich RW, Euler T, Larkum ME, Giese G, Both M, Duebel J, Waters J, Bujard H, Griesbeck O, Tsien RY, Nagai T, Miyawaki A, Denk W (2004**) Functional fluorescent Ca^{2+} indicator proteins in transgenic mice under TET control. *PloS Biol* 2: 763-775.

36. **Heim N, Griesbeck O (2004**) Genetically encoded indicators of cellular calcium dynamics based on troponin C and green fluorescent protein. *J Biol Chem* 279: 14280-14286.

37. **Heim R, Tsien RY (1996**) Engineering green fluorescent protein for improved brightness, longer wavelengths and fluorescence resonance energy transfer. *Curr Biol* 6: 178-182.

38. **Helmchen F (2000)** Calibration of fluorescent calcium indicators. In: Imaging Neurons: A Laboratory Manual (Yuste R, Lanni F, Konnerth A, eds), pp 32.1-32.9. Cold Spring Harbor: CSHL Press.

39. **Higashijima Si, Masino MA, Mandel G, Fetcho JR (2003**) Imaging neuronal activity during zebrafish behavior with a genetically encoded calcium indicator. *J Neurophysiol* 90: 3986-3997.

40. **Hoang B, Chiba A (2001**) Single-cell analysis of *Drosophila* larval neuromuscular synapses. *Developmental Biology* 229: 55-70.

41. **Hogue DL, Nash C, Ling V, Hobman TC (2002**) Lysosome-associated protein transmembrane 4 alpha (LAPTM4 alpha) requires two tandemly arranged tyrosine-based signals for sorting to lysosomes. *Biochem J* 365: 721-730.

42. **Ikegaya Y, Aaron G, Cossart R, Aronov D, Lampl I, Ferster D, Yuste R (2004**) Synfire chains and cortical songs: temporal modules of cortical activity. *Sci* 304: 559-564.

43. **Isshiki M, Ying Ys, Fujita T, Anderson RGW (2002**) A molecular sensor detects signal transduction from caveolae in living cells. *J Biol Chem* 277: 43389-43398.

44. **Ji G, Feldman ME, Deng KY, Greene KS, Wilson J, Lee JC, Johnston RC, Rishniw M, Tallini Y, Zhang J, Wier WG, Blaustein MP, Xin HB, Nakai J, Kotlikoff MI (2004**) Ca^{2+}-sensing transgenic mice: postsynaptic signaling in smooth muscle. *J Biol Chem* 279: 21461-21468.

45. **Jurado LA, Chockalingam PS, Jarrett HW (1999**) Apocalmodulin. *Physiol Rev* 79: 661-682.

46. **Kawasaki F, Collins SC, Ordway RW (2002**) Synaptic calcium-channel function in *Drosophila*: analysis and transformation rescue of temperature-sensitive paralytic and lethal mutations of cacophony. *J Neurosci* 22: 5856-5864.

47. **Kawasaki F, Zou B, Xu X, Ordway RW (2004**) Active zone localization of presynaptic calcium channels encoded by the cacophony locus of *Drosophila*. *J Neurosci* 24: 282-285.

48. **Kerr R, Lev-Ram V, Baird G, Vincent P, Tsien RY, Schafer WR (2000**) Optical imaging of calcium transients in neurons and pharyngeal muscle of C. elegans. *Neuron* 26: 583-594.

49. **Keshishian H, Broadie K, Chiba A, Bate M (1996**) The *Drosophila* neuromuscular junction: a model system for studying synaptic development and function. *Annual Review of Neuroscience* 19: 545-575.

50. **Kimura KD, Miyawaki A, Matsumoto K, Mori I (2004**) The C. elegans thermosensory neuron AFD responds to warming. *Curr Biol* 14: 1291-1295.

51. **Laughon A, Gesteland RF (1982**) Isolation and preliminary characterization of the GAL4 gene, a positive regulator of transcription in yeast. *PNAS* 79: 6827-6831.

52. **Lee D, O'Dowd DK (1999**) Fast excitatory synaptic transmission mediated by nicotinic acetylcholine receptors in *Drosophila* neurons. *J Neurosci* 19: 5311-5321.

53. **Lee T, Luo L (1999**) Mosaic analysis with a repressible cell marker for studies of gene function in neuronal morphogenesis. *Neuron* 22: 451-461.

54. **Lee T, Luo L (2001**) Mosaic analysis with a repressible cell marker (MARCM) for *Drosophila* neural development. *Trends Neurosci* 24: 251-254.

55. **Liaw CW, Zamoyska R, Parnes JR (1986**) Structure, sequence, and polymorphism of the Lyt-2 T cell differentiation antigen gene. *J Immunol* 137: 1037-1043.

56. **Lin DM, Goodman CS (1994**) Ectopic and increased expression of Fasciclin II alters motoneuron growth cone guidance. *Neuron* 13: 507-523.

57. **Lippincott-Schwartz J, Patterson GH (2003**) Development and use of fluorescent protein markers in living cells. *Sci* 300: 87-91.

58. **Liu L, Yermolaieva O, Johnson WA, Abboud FM, Welsh MJ (2003**) Identification and function of thermosensory neurons in *Drosophila* larvae. *Nat Neurosci* 6: 267-273.

59. **Llinas R, Sugimori M, Silver RB (1992**) Presynaptic calcium concentration microdomains and transmitter release. *J Physiol Paris* 86: 135-138.

60. **Macleod GT, Hegstrom-Wojtowicz M, Charlton MP, Atwood HL (2002**) Fast calcium signals in *Drosophila* motor neuron terminals. *J Neurophysiol* 88: 2659-2663.

61. **Macleod GT, Marin L, Charlton MP, Atwood HL (2004**) Synaptic Vesicles: Test for a Role in Presynaptic Calcium Regulation. *J Neurosci* 24: 2496-2505.

62. **Maddon PJ, Littman DR, Godfrey M, Maddon DE, Chess L, Axel R (1985**) The isolation and nucleotide sequence of a cDNA encoding the T cell surface protein T4: a new member of the immunoglobulin gene family. *Cell* 42: 93-104.

63. **Mank M, Reiff DF, Heim N, Friedrich MW, Borst A, Griesbeck O (2006**) A FRET-based calcium biosensor with fast signal kinetics and high fluorescence change. *Biophys J* 90: 1790-1796.

64. **Marsault R, Murgia M, Pozzan T, Rizzuto R (1997**) Domains of high Ca^{2+} beneath the plasma membrane of living A7r5 cells. *EMBO J* 16: 1575-1581.

65. **Matz MV, Fradkov AF, Labas YA, Savitsky AP, Zaraisky AG, Markelov ML, Lukyanov SA (1999**) Fluorescent proteins from nonbioluminescent Anthozoa species. *Nat Biotechnol* 17: 969-973.

66. **Maximov A, Bezprozvanny I (2002**) Synaptic targeting of N-type calcium channels in hippocampal neurons. *J Neurosci* 22: 6939-6952.

67. **Maximov A, Sudhof TC, Bezprozvanny I (1999**) Association of neuronal calcium channels with modular adaptor proteins. *J Biol Chem* 274: 24453-24456.

68. **Miesenbock G (2004**) Genetic methods for illuminating the function of neural circuits. *Curr Opin Neurobiol* 14: 395-402.

69. **Miesenbock G, De Angelis DA, Rothman JE (1998**) Visualizing secretion and synaptic transmission with pH-sensitive green fluorescent proteins. *Nature* 394: 192-195.

70. **Miyawaki A, Llopis J, Heim R, McCaffery JM, Adams JA, Ikura M, Tsien RY (1997**) Fluorescent indicators for Ca^{2+} based on green fluorescent proteins and calmodulin. *Nature* 388: 882-887.

71. **Miyawaki A (2003a**) Fluorescence imaging of physiological activity in complex systems using GFP-based probes. *Current Opinion in Neurobiology* 13: 591-596.

72. **Miyawaki A (2003b**) Visualization of the spatial and temporal dynamics of intracellular signaling. *Developmental Cell* 4: 295-305.

73. **Mumm JS, Schroeter EH, Saxena MT, Griesemer A, Tian X, Pan DJ, Ray WJ, Kopan R (2000**) A ligand-induced extracellular cleavage regulates gamma-secretase-like proteolytic activation of Notch1. *Mol Cell* 5: 197-206.

74. **Nagai T, Sawano A, Park ES, Miyawaki A (2001**) Circularly permuted green fluorescent proteins engineered to sense Ca^{2+}. *PNAS* 98: 3197-3202.

75. **Nagai T, Yamada S, Tominaga T, Ichikawa M, Miyawaki A (2004**) Expanded dynamic range of fluorescent indicators for Ca^{2+} by circularly permuted yellow fluorescent proteins. *PNAS* 101: 10554-10559.

76. **Nakai J, Ohkura M, Imoto K (2001**) A high signal-to-noise Ca^{2+} probe composed of a single green fluorescent protein. *Nat Biotechnol* 19: 137-141.

77. **Ng M, Roorda RD, Lima SQ, Zemelman BV, Morcillo P, Miesenbock G (2002**) Transmission of olfactory information between three populations of neurons in the antennal lobe of the fly. *Neuron* 36: 463-474.

78. **Nicholson-Tomishima K, Ryan TA (2004**) Kinetic efficiency of endocytosis at mammalian CNS synapses requires synaptotagmin I. *Proc Natl Acad Sci U S A* 101: 16648-16652.

79. **Ohkura M, Matsuzaki M, Kasai H, Imoto K, Nakai J (2005**) Genetically encoded bright Ca^{2+} probe applicable for dynamic Ca^{2+} imaging of dendritic spines. *Anal Chem* 77: 5861-5869.

80. **Ormo M, Cubitt AB, Kallio K, Gross LA, Tsien RY, Remington SJ (1996**) Crystal structure of the Aequorea victoria green fluorescent protein. *Sci* 273: 1392-1395.

81. **Palmer AE, Jin C, Reed JC, Tsien RY (2004**) Bcl-2-mediated alterations in endoplasmic reticulum Ca^{2+} analyzed with an improved genetically encoded fluorescent sensor. *PNAS* 101: 17404-17409.

82. **Patterson GH, Piston DW, Barisas BG (2000**) Forster distances between green fluorescent protein pairs. *Analytical Biochemistry* 284: 438-440.

83. **Persechini A, Lynch JA, Romoser VA (1997**) Novel fluorescent indicator proteins for monitoring free intracellular Ca^{2+}. *Cell Calcium* 22: 209-216.

84. **Petersen SA, Fetter RD, Noordemeer JN, Goodman CS, DiAntonio A (1997**) Genetic analysis of glutamate receptors in *Drosophila* reveals a retrograde signal regulating presynaptic transmitter release. *Neuron* 19: 1237-1248.

85. **Pinton P, Tsuboi T, Ainscow EK, Pozzan T, Rizzuto R, Rutter GA (2002**) Dynamics of glucose-induced membrane recruitment of protein kinase C beta II in living pancreatic islet beta -cells. *J Biol Chem* 277: 37702-37710.

86. **Pologruto TA, Yasuda R, Svoboda K (2004**) Monitoring neural activity and [Ca^{2+}] with genetically encoded Ca2+ indicators. *J Neurosci* 24: 9572-9579.

87. **Prasher DC (1995**) Using GFP to see the light. *Trends Genet* 11: 320-323.

88. **Reiff DF, Thiel PR, Schuster CM (2002**) Differential regulation of active zone density during long-term strengthening of *Drosophila* neuromuscular junctions. *J Neurosci* 22: 9399-9409.

89. **Reiff DF, Ihring A, Guerrero G, Isacoff EY, Joesch M, Nakai J, Borst A (2005)** *In vivo* performance of genetically encoded indicators of neural activity in flies. *J Neurosci* 25: 4766-4778.

90. **Romoser VA, Hinkle PM, Persechini A (1997)** Detection in living cells of Ca^{2+}-dependent changes in the fluorescence emission of an indicator composed of two green fluorescent protein variants linked by a calmodulin-binding sequence - a new class of fluorescent indicators. *J Biol Chem* 272: 13270-13274.

91. **Rudolf R, Mongillo M, Rizzuto R, Pozzan T (2003)** Looking forward to seeing calcium. *Nat Rev Mol Cell Biol* 4: 579-586.

92. **Sakai R, Repunte-Canonigo V, Raj CD, Knopfel T (2001)** Design and characterization of a DNA-encoded, voltage-sensitive fluorescent protein. *Eur J Neurosci* 13: 2314-2318.

93. **Sankaranarayanan S, Ryan TA (2000)** Real-time measurements of vesicle-SNARE recycling in synapses of the central nervous system. *Nat Cell Biol* 2: 197-204.

94. **Schulze KL, Broadie K, Perin MS, Bellen HJ (1995)** Genetic and electrophysiological studies of *Drosophila* syntaxin-1A demonstrate its role in nonneuronal secretion and neurotransmission. *Cell* 80: 311-320.

95. **Scott EK, Raabe T, Luo L (2002)** Structure of the vertical and horizontal system neurons of the lobula plate in *Drosophila*. *J Comp Neurol* 454: 470-481.

96. **Shagin DA, Barsova EV, Yanushevich YG, Fradkov AF, Lukyanov KA, Labas YA, Semenova TN, Ugalde JA, Meyers A, Nunez JM, Widder EA, Lukyanov SA, Matz MV (2004)** GFP-like proteins as ubiquitous metazoan superfamily: evolution of functional features and structural complexity. *Mol Biol Evol* 21: 841-850.

97. **Shaner NC, Campbell RE, Steinbach PA, Giepmans BNG, Palmer AE, Tsien RY (2004)** Improved monomeric red, orange and yellow fluorescent

proteins derived from Discosoma sp. red fluorescent protein. *Nat Biotechnol* 22: 1567-1572.

98. **Shimomura O, Johnson FH, Saiga Y (1962**) Extraction, purification and properties of aequorin, a bioluminescent protein from the luminous hydromedusan, Aequorea. *J Cell Comp Physiol* 59: 223-239.

99. **Shyn SI, Kerr R, Schafer WR (2003**) Serotonin and Go modulate functional states of neurons and muscles controlling C. elegans egg-laying behavior. *Curr Biol* 13: 1910-1915.

100. **Siegel MS, Isacoff EY (1997**) A genetically encoded optical probe of membrane voltage. *Neuron* 19: 735-741.

101. **Sinha SR, Wu LG, Saggau P (1997**) Presynaptic calcium dynamics and transmitter release evoked by single action potentials at mammalian central synapses. *Biophys J* 72: 637-651.

102. **Spradling AC, Rubin GM (1982**) Transposition of cloned P elements into *Drosophila* germ line chromosomes. *Sci* 218: 341-347.

103. **Spradling AC, Rubin GM (1983**) The effect of chromosomal position on the expression of the *Drosophila* xanthine dehydrogenase gene. *Cell* 34: 47-57.

104. **Stosiek C, Garaschuk O, Holthoff K, Konnerth A (2003**) *In vivo* two-photon calcium imaging of neuronal networks. *Proc Natl Acad Sci U S A* 100: 7319-7324.

105. **Svoboda K, Denk W, Kleinfeld D, Tank DW (1997**) *In vivo* dendritic calcium dynamics in neocortical pyramidal neurons. *Nature* 385: 161-165.

106. **Tank DW, Regehr WG, Delaney KR (1995**) A quantitative analysis of presynaptic calcium dynamics that contribute to short-term enhancement. *J Neurosci* 15: 7940-7952.

107. **Tank DW, Sugimori M, Connor JA, Llinas RR (1988**) Spatially resolved calcium dynamics of mammalian Purkinje cells in cerebellar slice. *Sci* 242: 773-777.

108. **Tsien RY (1998**) The green fluorescent protein. *Annu Rev Biochem* 67: 509-544.

109. **Tsien RY, Miyawaki A (1998**) Biochemical imaging: seeing the machinery of live cells. *Sci* 280: 1954-1955.

110. **Wang JW, Wong AM, Flores J, Vosshall LB, Axel R (2003**) Two-photon calcium imaging reveals an odor-evoked map of activity in the fly brain. *Cell* 112: 271-282.

111. **Wang Y, Guo HF, Pologruto TA, Hannan F, Hakker I, Svoboda K, Zhong Y (2004**) Stereotyped odor-evoked activity in the mushroom body of *Drosophila* revealed by green fluorescent protein-based Ca^{2+} imaging. *J Neurosci* 24: 6507-6514.

112. **Wilson RI, Turner GC, Laurent G (2004**) Transformation of olfactory representations in the *Drosophila* antennal lobe. *Sci* 303: 366-370.

113. **Wong AM, Wang JW, Axel R (2002**) Spatial representation of the glomerular map in the *Drosophila* protocerebrum. *Cell* 109: 229-241.

114. **Wu MN, Bellen HJ (1997**) Genetic dissection of synaptic transmission in *Drosophila*. *Curr Opin Neurobiol* 7: 624-630.

115. **Wu MN, Fergestad T, Lloyd TE, He Y, Broadie K, Bellen HJ (1999**) Syntaxin 1A interacts with multiple exocytic proteins to regulate neurotransmitter release *in vivo*. *Neuron* 23: 593-605.

116. **Yang F, Moss LG, Phillips GN (1996**) The molecular structure of green fluorescent protein. *Nat Biotech* 14: 1246-1251.

117. **Yasuda R, Nimchinsky EA, Scheuss V, Pologruto TA, Oertner TG, Sabatini BL, Svoboda K (2004**) Imaging calcium concentration dynamics in small neuronal compartments. *Sci STKE* 2004: l5.

118. **Yeh E, Gustafson K, Boulianne GL (1995**) Green fluorescent protein as a vital marker and reporter of gene expression in *Drosophila*. *PNAS* 92: 7036-7040.

119. **Yoshihara M, Littleton JT (2002**) Synaptotagmin I functions as a calcium sensor to synchronize neurotransmitter release. *Neuron* 36: 897-908.

120. **Yu D, Baird GS, Tsien RY, Davis RL (2003**) Detection of calcium transients in *Drosophila* mushroom body neurons with camgaroo reporters. *J Neurosci* 23: 64-72.

121. **Yu D, Ponomarev A, Davis RL (2004**) Altered representation of the spatial code for odors after olfactory classical conditioning; memory trace formation by synaptic recruitment. *Neuron* 42: 437-449.

122. **Zapata-Hommer O, Griesbeck O (2003**) Efficiently folding and circularly permuted variants of the Sapphire mutant of GFP. *BMC Biotechnol* 3: 5.

123. **Zhang J, Campbell RE, Ting AY, Tsien RY (2002**) Creating new fluorescent probes for cell biology. *Nat Rev Mol Cell Biol* 3: 906-918.

124. **Zito K, Parnas D, Fetter RD, Isacoff EY, Goodman CS (1999**) Watching a synapse grow: Noninvasive confocal imaging of synaptic growth in *Drosophila*. *Neuron* 22: 719-729.

Finally, yet importantly, I want to thank my parents for providing a background, which enabled me to make this PhD-thesis. I'm grateful for the efforts they put into my education, for their financial aid and their confidence in me.

Curriculum Vitae

Education:

since 2001   PhD thesis at the Max-Planck-Institute of Neurobiology, Martinsried, Germany under supervision of Prof. Dr. Alexander Borst and Dr. Dierk F. Reiff:
"Characterization and modification of genetically encoded indicators to monitor neural activity in *Drosophila melanogaster*".

2002   summer course "Neurobiology", Woods Hole, Massachusetts, USA.

2000/01   diploma thesis at the Technical University of Munich, Chair of Microbiology and the GSF Neuherberg, Institute of Biochemical Plant Pathology, Germany:
"Molecular communication between Rhizosphere Bacteria and Tomato Plants: effects of *N*-Acylhomoserine Lactones on herbal signal paths"

2000   working student at the Technical University Munich, Chair of Microbiology, Munich, Germany.

1998/99   internship at MorphoSys AG, Martinsried, Germany.

1998   working student at the Max-Planck-Institute of Biochemistry, "RNA-metabolism and neuronal diseases". Martinsried, Germany.

1998   working student at the GSF Neuherberg (Research Center for Environment and Health), Institute of Mammalian Genetics, Neuherberg, Germany.

1995 - 2001   Undergraduate studies in Biology at the Technical University of Munich, Germany.

1995   Graduation from High School: Dante-Gymnasium, Munich, Germany.

Publications:

Steidle A, Sigl K, Schuhegger R, Ihring A, Schmid M, Gantner S, Stoffels M, Riedel K, Givskov M, Hartmann A, Langebartels C, Eberl L (2001) Visualization of *N*-Acylhomoserine Lactone Mediated Cell-Cell Communication between Bacteria Colonizing the Tomato Rhizosphere. *Appl. Environ. Microbiol* 67: 5761-5770.

Reiff DF, Ihring A, Guerrero G, Isacoff EY, Joesch M, Nakai J, Borst A (2005) *In vivo* performance of genetically encoded indicators of neural activity in flies. *J Neurosci* 25: 4766-4778.

Schuhegger R, Ihring A, Gantner S, Bahnweg G, Knappe C, Vogg G, Hutzler P, Schmid M, Van Breusegem F, Eberl L, Hartmann A, Langebartels C (2006) Induction of systemic resistance in tomato by *N*-acylhomoserine lactone – producing rhizosphere bacteria. *Plant Cell Environ*, in press